THE EVOLUTIONARY STATUS OF THE HOT R CORONAE BOREALIS STARS

Donald L. Pollacco

A Thesis Submitted for the Degree of PhD
at the
University of St Andrews

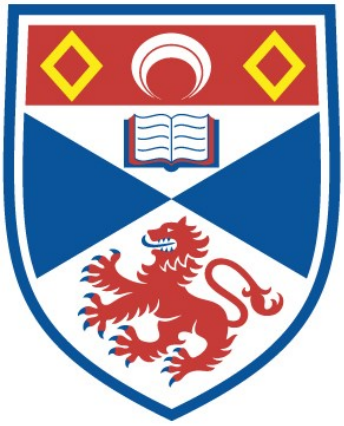

1989

THE UNIVERSITY OF ST. ANDREWS

The Evolutionary Status of the Hot R Coronae Borealis Stars

Donald L. Pollacco

Submitted for the degree of Ph. D.

Febuary, 1989.

To Diane

In submitting this thesis to the University of St. Andrews I understand that I am giving permission for it to be made available for use in accordance with the regulations of the University Library for the time being in force, subject to any copyright vested in the work not being affected thereby. I also understand that the title and abstract will be published, and that a copy of the work may be made and supplied to any *bona fide* library or research worker.

ABSTRACT

The evolutionary status of the hot R CrB stars has long remained a matter of conjecture, primarily because of the relative dearth of relevant observational material. Previously the group had been thought to occupy a position intermediate in status between the EHe and R CrB classes as they have (at least at first glance) observational properties in common with both types of object.

The photosphere of DY Cen has been quantitatively confirmed to be hydrogen-deficient and photometric variations suggest the star undergoes short period pulsations. Using a period-temperature relation applicable to hydrogen-deficient stars it would appear that this object has similar physical properties to both the EHe and R CrB stars.

Narrow band imaging of V348 Sgr has shown that the associated nebula exhibits a bipolar structure and therefore must be closely related to planetary nebulae *rather than* H II regions. Spectroscopic observations have proved that the star in its present evolutionary state is incapable of ionising the nebula. Several scenarios for this behaviour are briefly discussed. The large helium enrichment found in the nebula indicates that processed material must have been ejected during the last major episode of mass loss. Evidence is presented that suggests a strong hydrogen abundance gradient exists within the nebula.

A novel technique has been developed for determining reddening distances. Its main advantage over other similar methods is that both early and late-type stars may be used to establish the reddening-distance relationship. With more development this technique may prove to be an important tool in distance determinations for objects such as planetary nebulae etc. This technique was used to derive a distance of (4.7 ± 1.0)kpc for V348 Sgr. Using the core-mass relation for hydrogen-deficient stars implies that both V348 Sgr and MV Sgr are lower mass and luminosity objects than EHe and R CrB stars.

The evidence presented in this thesis indicates that the hot R CrB group is *not* a homogeneous one. DY Cen is much more luminous and massive than the other members. The mass and luminosity of V348 Sgr and MV Sgr are consistent with the scenario that both have recently suffered a thermal pulse (causing re-ignition of a helium burning shell) and are currently looping back to the R CrB domain of the HR diagram.

I Donald Pollacco hereby certify that this thesis has been composed by myself, that it is a record of my own work and that it has not been accepted in partial or complete fulfilment of any other degree or professional qualification.

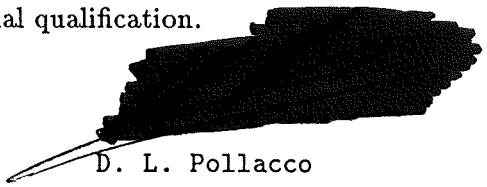

D. L. Pollacco

I was admitted to the Faculty of Science of the University of St. Andrews under Ordinance General No. 12 on 1st October 1985 and as a candidate for the degree of Ph.D. on 1st October 1986.

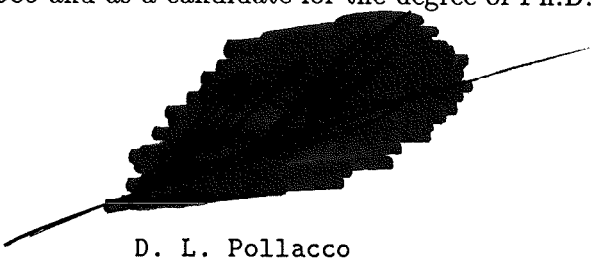

D. L. Pollacco

I hereby certify that the candidate has fulfilled the conditions of the Resolution and Regulations appropriate to the Degree of Ph.D.

P. W. Hill

Acknowledgments

I would like to thank my supervisor Dr. P. W. Hill for his constant enthusiasm for this project — at times much greater than my own. It was his continuous encouragement that forced us to enter the new fields required by this thesis.

I also owe a debt, much greater than this thesis, to Diane, my constant companion throughout the duration of this work, without whom this thesis would never have materialized. Fortunately my mood imitation of the V348 light curve failed (mostly) to dampen her companionship — although like V348 I must have been impossible to reach on so many occasions. She must bear as much responsibility for this thesis as myself.

How do I thank all the people (astronomers and non-astronomers) that have influenced this work (many of whom will not realise it!). Although acknowledgement here cannot repay that debt: Kevin, Steve, Helen, Graham L., Aileen, Chris, Graham W., Andy, Paul, Al, Roger S., Ron, Fran, Frank, Mags, Simon, Tony, Robin Clegg, Patrick Harrington, Donald Osterbrock, Dave Kilkenny, Michael Feast, Ian Skillen, Peter Mack, Ron and Joan (from Sutherland), and all the staff at the Victoria Cafe (and Peter), thank you. I would like to thank Peter H., my mentor and a source of much inspiration over many years past and hopefully many to come.

A special thanks is saved for Steve, Fran and Frank who laboriously read part or all of the original manuscript making comments (if you saw the original version of this thesis you would realise that this was a non-trivial task!).

I would like to express my sincere gratitude to the staffs of the University Observatory, the Observatorio del Roque de los Muchachos, the Anglo Australian Observatory, European Southern Observatory (Garching) and especially the South African Astronomical Observatory, all of whom have given me much assistance during observing runs.

I would like to thank the Science and Engineering Research Council for financial support in the form of a postgraduate studentship and PATT, SAAO and ESO for extremely generous allocations of telescope time. Use of the computing facilities of the University of St. Andrews and Starlink (thanks Roger) are gratefully acknowledged.

Lastly, but definitely not least I'd like to thank Clive whose fundamental understanding of many of the techniques used in this thesis have proved invaluable.

Contents

List of Figures

List of Tables

Chapter 1

What are hot R Coronae Borealis Stars?

1.1 Classical R Coronae Borealis stars

The R Coronae Borealis (R CrB) stars are cool hydrogen-deficient supergiants that undergo irregular drops in apparent brightness (upto 9^m) reaching minimum within a few weeks. The recovery to maximum may take a year or longer. While at maximum most are known to be slightly variable. However, it is only in the case of RY Sgr where the variation is large ($\sim 0^m.5$) that observations by amateurs and professional astronomers have been able to show the light variations of the star are cyclic with a period of around 38 days. The stellar radial velocity has been found to be periodic on the same timescale. The star is thought to be pulsating radially.

During the decline to minimum the stellar continuum is seen to be highly reddened and the spectrum is dominated by emission lines thought to be chromospheric in origin. Post minima the emission spectrum gradually disappears and the stellar continuum strengthens.

At near IR (around J) wavelengths the spectrum is dominated by the stellar flux and accordingly pulsates in unison with the optical variation. The deep minima are

also apparent. At longer wavelengths (around L) the emission is dominated by a circumstellar shell heated by the stellar radiation field (Feast *et al.* , 1977) and therefore does display the synchronous emission variations along with the pulsation cycle. The amplitude of this variation is small and the emission is dominated by re-emission from the heated dust. The L band photometry also exhibits a long term (1 500 day) variation (Menzies, 1986). At this wavelength the characteristic deep minima are not apparent.

Two models have been proposed to account for this behaviour:

(i) *the orbiting dust cloud model* of O'Keefe (1939) in which the minima are thought to be due to orbiting dust clouds eclipsing the star.

(ii) *the directional ejection of material*, as expanded on by Feast (1986; and references therein). Material ejected from the star condenses into dust and if orientated in the observer's line of sight causes the photosphere to be obscured. At this point the stellar continuum is heavily reddened, and the chromospheric spectrum visible. This model requires that the IR emission of the ejected material is small compared with the shell emission.

Clearly (i) is not consistent with the current observational material as it would be expected to produce symmetrical minima. Model (ii) (*the consortium of puffs model*) shows good agreement with the observed phenomena. However, many aspects of the model remain mysterious primarily because of the long pulsation periods involved and the randomness of the deep minima.

Spectroscopically similar to the R CrB stars, the hydrogen-deficient carbon (HdC: Warner, 1967) stars do not have IR excesses (Walker, 1986) and are not known to suffer R CrB type minima. They do appear to be photometrically variable over a long timescale (Kilkenny, 1988).

1.2 Extreme hydrogen-deficient Helium stars

The Extreme hydrogen-deficient Helium (EHe) stars are hotter than R CrB stars and do not show the deep minima associated with the latter. Spectroscopically these stars are

remarkable in that the Balmer hydrogen lines are always absent or very weak, while the He I lines are strong. EHe stars have been found to be slightly variable with amplitudes of just a few hundredth of a magnitude. In some cases the variations have been found to be caused by radial pulsation, while the hotter stars appear to be pulsating in non-radial modes (Saio and Jeffery, 1987). However, due to the observational difficulties in acquiring accurate photometric data on small amplitude variations with relatively long periods (a few hours to a few weeks) the nature of the pulsation has only been determined for a small number of objects. These objects do not show IR excesses (ie no circumstellar material) although in a few cases very weak emission lines have been detected (*the emission line EHe stars*).

1.3 The hot R Coronae Borealis stars

This is a small class of (3) objects that are thought to share physical and observational properties with both the R CrB and EHe stars. Observationally they all display the characteristic R CrB type minima and as far as is known they all have hydrogen-deficient atmospheres. The presence of chromospheric or wind lines emission lines in their spectra suggests that they are still losing large amounts of material. In the case of V348 Sgr, the star is known to be surrounded by a small low excitation nebula, signifying that an extended period of mass loss has occurred. IUE colour temperatures indicate that the three stars have surface temperatures of between 10 000–20 000 K. All three stars have been detected in the IR and have been found to have IR excesses.

1.3.1 DY Cen

This star was discovered by Hoffleit (1930) and classified as an R CrB star on the basis of its light behaviour over a thirty year period. Rao (1986) has reported Herbig to have found the object to display strong C II absorption lines and weak Balmer emission in its spectrum and Feast (1986a) has estimated its spectral type as early A. Kilkenny (1986) has found hydrogen absorption lines to be easily detectable. DY Cen is known to have a weak IR excess (Glass, 1978).

1.3.2 MV Sgr

This object was again discovered by Hoffleit (1959) and classified as an R CrB star from its light curve. Herbig (1964) first recognized MV Sgr as having a hot photosphere and drew comparisons between it and the EHe stars, noting the complete absence of hydrogen absorption lines. Herbig also noted the large number of weak emission lines arising from metals, eg iron. From low dispersion IUE spectra Drilling *et al.* (1984a) has estimated a surface temperature of around 15 400 K for MV Sgr. This star was found to be a strong IR source by Feast and Glass (1974).

1.3.3 V348 Sgr

Classified as being of the R CrB type by Hoffleit (1958), V348 Sgr has been the source of much controversy. Whereas the other hot R CrB stars rarely display minima V348 Sgr varies on a short timescale. It is thought to have a surface temperature of around 20 000 K (Schönberner and Heber, 1986), but this estimate is crucially dependent on the value of reddening adopted. This object is thought to be associated with a small low excitation nebula (Herbig, 1958) of unknown nature (is it a compact H II region or related to planetary nebulae?). The unpredictability of the star has made high resolution spectroscopic observations difficult and only Houziaux (1968) has obtained a suitable spectrogram. This suggested the stellar photosphere was carbon rich and hydrogen-deficient. Other observers (notably Dahari and Osterbrock, 1985) have obtained spectra of the star throughout its light curve, but since these spectra were only of low resolution were unable to comment on the underlying photospheric spectrum.

Figure 1.1 shows the positions of the group within the HR diagram.

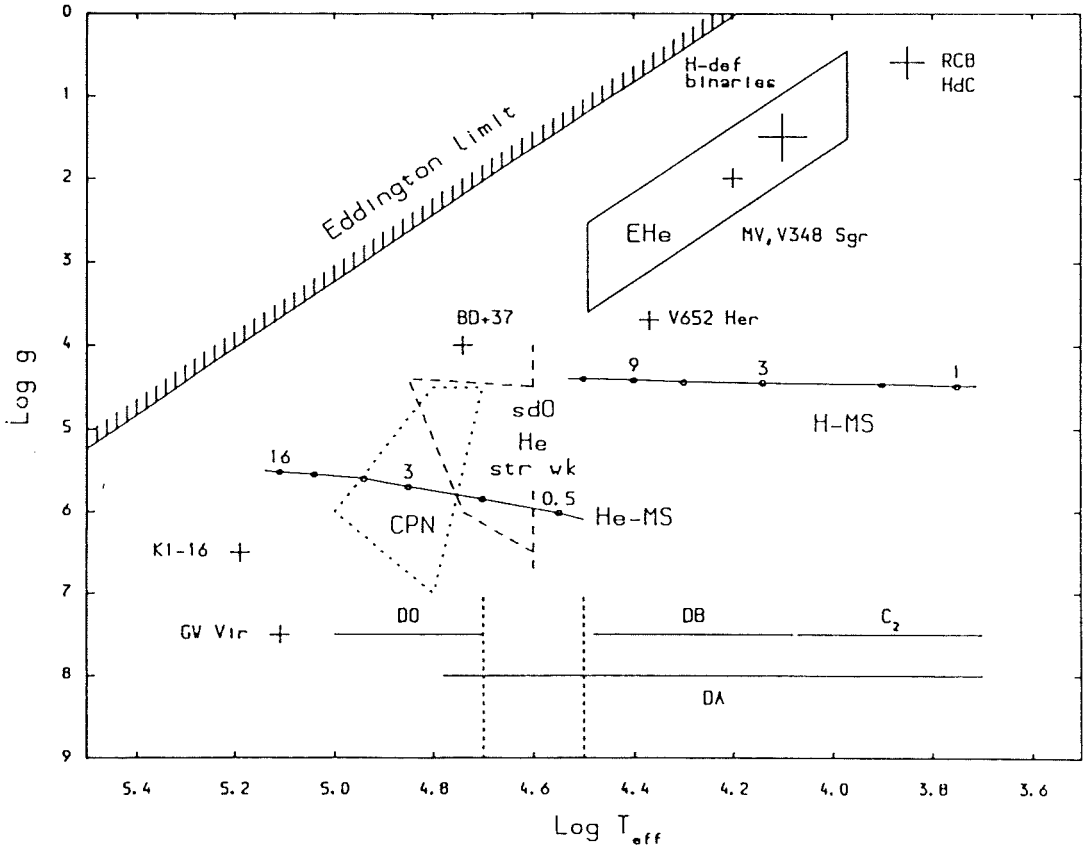

Figure 1.1: HR diagram showing the relative positions of the hot R CrB, EHe and R CrB groups (from Hill, 1986).

1.4 Previous speculation on the evolutionary status of the hot R CrB stars

Because of the close resemblance between EHe and R CrB stars, the hot R CrB stars have for many years been thought to occupy an evolutionary path between the two groups (Schönberner, 1977).

Schönberner's (1977) evolutionary tracks for hydrogen-deficient stars evolve from the R CrB to the EHe star domains of the HR diagram with a timescale that was found to be strongly dependent on the stellar mass (for stars with $M \sim 1\ M_{\odot}$ the timescale is a few thousand years). Evidence was found by Kilkenny (1982) who showed that the pulsation period for RY Sgr was decreasing at a rate ($\dot{P} = -0.011$ days/yr) that clearly implied the star was contracting, reaching the EHe configuration within 3 000 years via the hot R CrB star region. However, there remain several points difficult to interpret within this framework

(i) While the R CrB stars are known to have large IR excesses (indicating considerable quantities of circumstellar material) the EHe stars do not. It is difficult to imagine a scenario whereby the circumstellar material is removed from the R CrB star leaving the exposed EHe star within the required evolutionary timescale.

(ii) It appears that the EHe stars form a continuous temperature sequence above that of the R CrB stars.

(iii) The hot R CrB stars have surface temperatures above many EHe stars but still have large quantities of circumstellar material.

These facts led Drilling *et al.* (1984b) to suggest that two evolutionary tracks may be operative

(i) the R CrB stars are evolving to higher temperatures whereupon they resemble the hot R CrB stars,

(ii) the HdC stars are merely cool EHe stars. The direction of evolution is not clear.

all the observational constraints. At present detailed evolutionary calculations have not yet been performed, but it does at least in principle offer a different perspective to the problem.

1.4.1 The evolutionary status of V348 Sgr

The paucity of observational material has led many workers to propose several different evolutionary scenarios for this object. Webster and Glass (1974) studied the spectra of V348 Sgr and concluded that along with CPD–56°8032, He 2–113 and M4–18 they formed a cool extension to the Wolf-Rayet carbon sequence (WC) of stars. Dahari and Osterbrock (1985) regarded V348 Sgr as a giant star stripped of its outer layers. Until photospheric abundances are known for this object and its luminosity and distance determined, these ideas are tantamount to nothing more than speculation.

1.5 The origin of hydrogen-deficient stars

All theories dealing with the origin of hydrogen-deficient stars must be able to account for the following observational constraints:

(i) they appear to be single, highly evolved stars,

(ii) their kinematical properties place them amongst an old population,

(iii) those few objects that have had photospheric analyses made show strong indications of significant quantities of processed material.

The first ideas concentrated on mixing processes (eg *deep envelope mixing on the AGB*— Paczynski, 1971) but this floundered as relatively high stellar masses were required. Later, the idea of a white dwarf suffering a *last thermal pulse* emerged (Renzini, 1979 and Iben *et al.* , 1983). Although approximately correct abundances resulted, the evolutionary timescales involved were short compared with those determined observationally[1] requiring just tens of years for a M $\sim$ 0.9 $M_{\odot}$ star to evolve through the R CrB region. However, they did note that the evolutionary timescale is strongly dependent on the stellar mass.

It was Webbink (1984) who first proposed the revolutionary new scenario of *coalescing white dwarfs.* At first glance this idea may sound somewhat esoteric, but it does satisfy

[1]The physical appearance of R CrB itself is known not to have changed appreciably over the last 300 years.

1.6 References

1. Dahari, O. and Osterbrock, D.E., 1985. *Astrophys. J.*, **277**, 648
2. Drilling, J.S., Schönberner, D., Heber, U. and Lynas-Gray, A.E., 1984a. *Astrophys. J.*, **278**, 224
3. Drilling, J.S., Landolt, A.U. and Schönberner, D., 1984b. *Astrophys. J.*, **279**, 748
4. Feast, M.W., 1986. *In IAU Coll. No.* **87**, *Hydrogen-Deficient Stars and Related Objects*, p.151, eds. Hunger, K., Schönberner D. and Rao, N. Kameswara., Reidel
5. Feast, M.W., 1986a. *In IAU Coll. No.* **87**, *Hydrogen-Deficient Stars and Related Objects*, p.21, eds. Hunger, K., Schönberner D. and Rao, N. Kameswara., Reidel
6. Feast, M.W., Catchpole, R.M., Lloyd Evans, T., Robertson, B.S.C., Dean, J.F., and Bywater, R.A., 1977. *Mon. Not. R. astr. Soc.*, **178**, 415
7. Glass, I.S., 1978. *Mon. Not. R. astr. Soc.*, **185**, 23
8. Herbig, G.H., 1964. *Astrophys. J.*, **140**, 1317
9. Herbig, G.H., 1958. *Astrophys. J.*, **127**, 312
10. Hill, P.W., 1986. *In IAU Coll. No.* **87**, *Hydrogen-Deficient Stars and Related Objects*, p.489, eds. Hunger, K., Schönberner D. and Rao, N. Kameswara., Reidel
11. Hoffleit, D., 1959. *Astronomical J.*, **64**, 241
12. Hoffleit, D., 1958. *Astronomical J.*, **63**, 78
13. Hoffleit, D., 1930. *Harvard Bull.*, **874**, 1
14. Houziaux, L., 1968. *Bull. Astron. Inst. Czechoslowakia*, **19**, 265
15. Iben, I. Jr., Kaler, J.B., Truran, J.W. and Renzini, A., 1984. *Astrophys. J.*, **264**, 605
16. Kilkenny, D., 1988. Submitted to *Mon. Not. R. astr. Soc.*
17. Kilkenny, D., 1986. *Private communication*
18. Kilkenny, D., 1982. *Mon. Not. R. astr. Soc.*, **200**, 1019
19. Menzies, J.W., 1986. *In IAU Coll. No.* **87**, *Hydrogen-Deficient Stars and Related Objects*, p.207, eds. Hunger, K., Schönberner D. and Rao, N. Kameswara., Reidel

20. O'Keefe, J. A., 1939. *Astrophys. J.*, **90**, 294

21. Paczynski, B., 1971. *Acta Astron.*, **21**, 1

22. Rao, N. K., 1986. *In IAU Coll. No.* **87**, *Hydrogen-Deficient Stars and Related Objects,* p.21, eds. Hunger, K., Schönberner D. and Rao, N. Kameswara., Reidel

23. Renzini, A., 1979. In *Stars and Stellar Systems*, p.135, Ed. Westerland, B. E. (Reidel)

24. Renzini, A., 1981. In *Effects of Mass loss on Stellar Evolution*, p.319, Eds. Chiosi, C. and Stalio, R. (Reidel)

25. Saio, H. and Jeffery, C. S., 1988. *Astrophys. J.*, **328**, 714

26. Schönberner, D., 1977. *Astr. Astrophys.*, **57**, 437

27. Schönberner, D. and Heber, U., 1986. *In IAU Coll. No.* **87**, *Hydrogen-Deficient Stars and Related Objects,* p.217, eds. Hunger, K., Schönberner D. and Rao, N. Kameswara., Reidel

28. Walker, H. J., 1986. *In IAU Coll. No.* **87**, *Hydrogen-Deficient Stars and Related Objects,* p.407, eds. Hunger, K., Schönberner D. and Rao, N. Kameswara., Reidel

29. Warner, B., 1967. *Mon. Not. R. astr. Soc.*, **137**, 119

30. Webbink, R. F., 1984. *Astrophys. J.*, **277**, 355

31. Webster, B. L. and Glass, I. S., 1974. *Mon. Not. R. astr. Soc.*, **166**, 491

Chapter 2

Photometric observations of DY Cen

2.1 Introduction

Although DY Cen is the brightest of the hot R CrB stars its photometric behaviour was unknown at the outset of this study. Kilkenny (1986) had suspected it as being variable but was unable to provide enough data to confirm this. Subsequent photometry by Tadhunter and Pollacco (unpublished) has verified this. Bearing in mind the intermediate nature of this object between the R CrB and EHe stars it was decided to determine if the variations were regular and if they showed similarities to variations found in the latter two groups.

2.2 Observations

DY Cen was observed at SAAO using the 0.5 m telescope and dedicated Modular photometer from the 19^{th} May to the 8^{th} June 1987. During this period the photomultiplier tube was fitted with a red sensitive Hamamatsu R943–02 tube (serial number EA1516), which was operated at an EHT of 1700V and cooled to −15°C. The dark count and beta source sensitivity were found to be remarkably constant (to a few percent). Johnson

filters were employed throughout the run.

At maximum brightness DY Cen reaches 12^{th} magnitude. This is near the observational limit for the 0.5 m telescope and consequently long integrations were required to reach a reasonable signal to noise ratio (S/N). Extreme care was exercised while positioning the star in the photometer aperture. Each observation consisted of a sequence of measurements of comparison (C), variable (V) and check (CK) stars as follows:

C, V, C, V, CK, V, C

The faintness of the star makes it imperative to determine regularly the sky brightness especially during periods when the sky brightness may fluctuate rapidly, for example, during the rising or setting of the moon. For this reason, sky readings were obtained after each DY Cen measurement. The sky position was chosen after examining the SERC Schmidt Survey plate (IIIa–J emulsion) for the area, thus enabling a region devoid of stars to be used. The comparison star and check stars used in this program were:

HD 116562 (C) and HD 116700 (CK)

Both stars are substantially brighter than DY Cen each being about $9^{\mathrm{m}}.5$.

E–Region photometric standard stars (see Menzies, Banfield and Laing, 1980) were also observed so as to:

(i) place the variable and comparison stars on an absolute calibration,

(ii) determine the extinction coefficients on the particular night of observation,

(iii) check the colour equations for the system (which are known to be remarkably stable over many observing seasons).

On a completely clear night (ie 100% clear) 15–20 standards were observed.

As previously mentioned the faintness of the star necessitated long integrations, thus, to reach a theoretical accuracy of 5 millimags (ie > 50 000 cts.), integrations of 120 secs

with the B filter and 100 secs with the V filter were required. To reach a corresponding accuracy in the sky measurements, integrations of around 60 and 50 seconds with the B and V filters, respectively, were required. The faintness of the star in the U band made measurement in this waveband impractical. The sequence outlined above was found to require approximately 45 minutes for completion.

After carefully scrutinizing the raw data (especially the sky measurements and checking the repeatability of the star measurements within each sequence), the data was reduced with the SAAO standard photometry package by J. Westerhuys.

2.3 Results

Table 2.1 shows the average values for V and $B-V$ (after subtracting the corresponding comparison star values) for DY Cen and HD 116700.

Figure 2.1 shows the differential V magnitudes for V — C and CK — C measurements. In order to maintain the clarity of the diagram a constant (3.15) has been subtracted from all differential magnitudes relating to V — C.

As can be seen, the scatter in the V — C observations is much larger than that of the CK — C star values. There are three possible interpretations for this:

(i) the star had recently suffered an R CrB type minimum,

(ii) the star undergoes long period variations with an amplitude of $0^{\mathrm{m}}.4$.

(iii) the variation is a result of the loss of photometric accuracy brought about by the faintness of the star.

It is unlikely that (iii) is correct, as suitable precautions were taken in the observational technique; also, sequences were rejected when the scatter in the DY Cen measurements were found to exceed $0^{\mathrm{m}}.015$. A search of recent literature and especially the Bulletins of the Variable Star Section of the Royal Society of New Zealand (published on a monthly basis), indicated that the star had not suffered a minimum, and had essentially been at maximum for at least a year either side of the observation period. For this reason we can

Table 2.1: Mean differential V and $B-V$ magnitudes for each measurement sequence.

HJD + 2446000	V (V — C)	$B-V$ (V — C)	V (CK — C)	$B-V$ (CK — C)
935.3192	3.512	0.067	0.067	-0.064
935.3724	3.511	0.089	0.071	-0.060
936.2563	3.507	0.068	0.073	-0.067
936.2903	3.510	0.068	0.071	-0.058
936.3233	3.509	0.071	0.073	-0.064
936.3546	3.513	0.070	0.077	-0.066
936.4276	3.510	0.066	0.076	-0.058
936.4590	3.521	0.068	0.074	-0.061
936.4888	3.498	0.095	0.073	-0.061
940.4748	3.482	0.054	0.069	-0.062
940.5050	3.485	0.057	0.071	-0.063
941.2936	3.451	0.054	0.081	-0.063
942.2643	3.372	0.045	0.058	-0.059
942.2939	3.367	0.051	0.056	-0.061
942.3233	3.372	0.046	0.061	-0.066
942.3535	3.374	0.051	0.056	-0.062
942.3831	3.374	0.048	0.063	-0.066
942.4523	3.374	0.047	0.064	-0.068
942.4810	3.376	0.050	0.067	-0.067
942.5052	3.375	0.048	0.066	-0.063
943.2370	3.334	0.051	0.067	-0.061
943.2662	3.333	0.046	0.066	-0.062
943.2952	3.336	0.046	0.061	-0.057
943.3243	3.332	0.050	0.067	-0.062
943.3533	3.328	0.057	0.068	-0.062
943.4297	3.332	0.051	0.070	-0.064
943.4586	3.328	0.061	0.071	-0.058
943.4871	3.329	0.056	0.068	-0.060
945.3491	3.381	0.050	0.065	-0.063
945.3848	3.397	0.040	0.071	-0.065
945.4146	3.377	0.055	0.069	-0.061
946.3478	3.322	0.059	0.060	-0.061
946.3762	3.333	0.046	0.068	-0.064
946.4044	3.329	0.050	0.068	-0.063
946.4775	3.313	0.055	0.064	-0.061
947.2485	3.290	0.045	0.067	-0.066
947.2775	3.283	0.048	0.064	-0.069
947.3060	3.284	0.048	0.059	-0.061
947.3345	3.282	0.044	0.064	-0.063
947.3588	3.279	0.049	0.061	-0.066
947.4366	3.283	0.043	0.060	-0.060
947.4614	3.275	0.053	0.065	-0.066
949.2499	3.351	0.042	0.084	-0.076
949.4739	3.330	0.060	0.069	-0.068
952.2341	3.341	0.034	0.063	-0.065
952.2713	3.343	0.035	0.066	-0.061
952.3483	3.341	0.037	0.066	-0.064
952.3770	3.327	0.047	0.064	-0.069
952.4438	3.330	0.027	0.065	-0.062
952.4722	3.304	0.033	0.063	-0.061
954.2303	3.310	0.044	0.065	-0.061
954.2601	3.312	0.046	0.068	-0.064
954.2903	3.318	0.049	0.067	-0.063
954.3203	3.327	0.037	0.068	-0.064
954.3494	3.327	0.042	0.068	-0.064
954.3785	3.330	0.047	0.069	-0.060
954.4074	3.327	0.050	0.069	-0.062
954.4365	3.333	0.054	0.073	-0.069
955.2440	3.357	0.037	0.068	-0.065
955.2747	3.353	0.042	0.066	-0.065
955.3052	3.361	0.044	0.064	-0.061

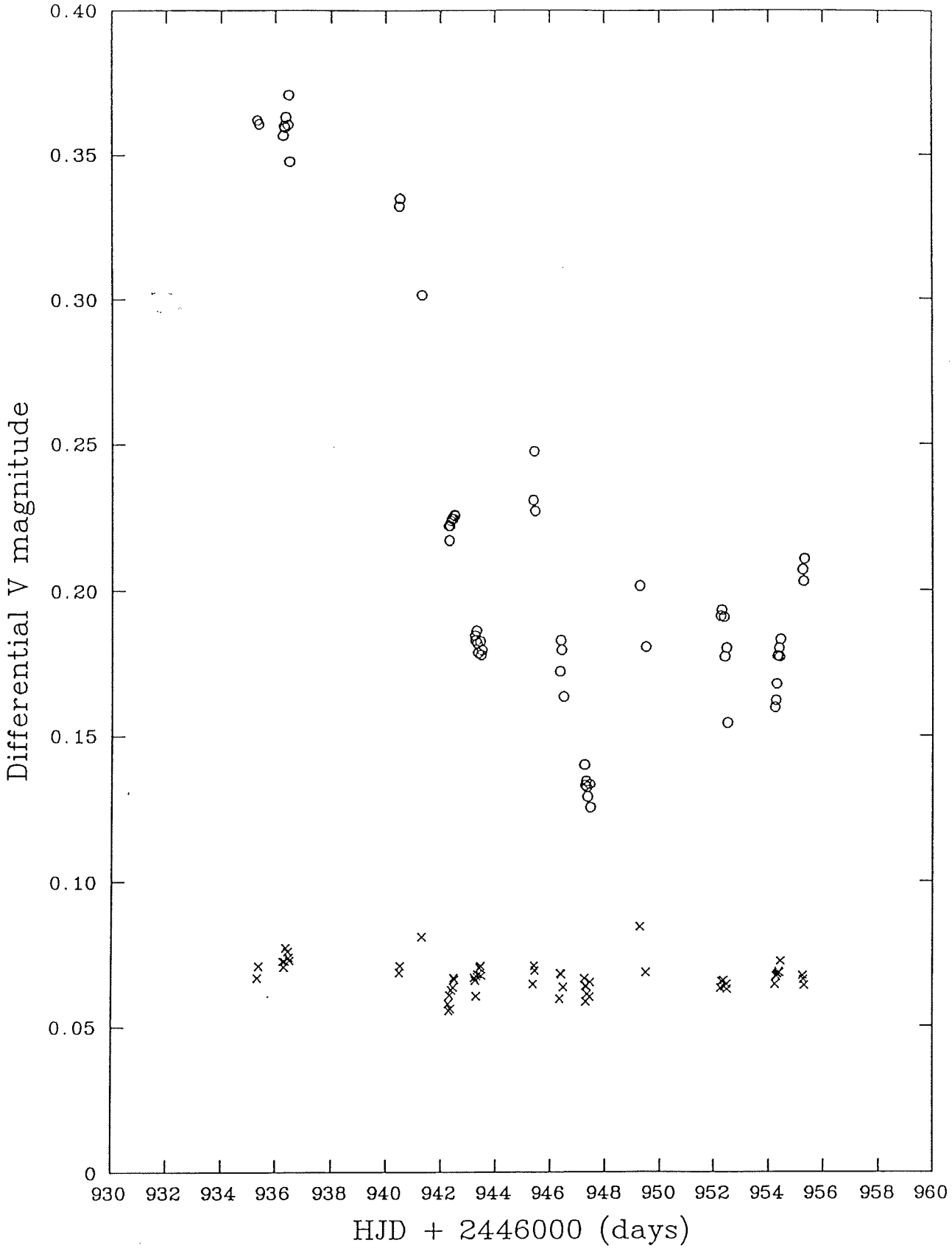

Figure 2.1: V plotted against HJD (o for V — C, x for CK — C).

also discount (i). Therefore it appears that (ii) is the most reasonable interpretation. We shall assume this to be the case but return to this point later (see Section 2.6).

The variation in the colour index $B - V$ is shown plotted in Figure 2.2. It can be seen that there is a long term trend (with an amplitude of about $0^{m}.05$); however, the scatter is of the same order as the CK — C observations. Therefore it is difficult to gain any information regarding the presence of short period variations, but we can tentatively place upper limits on their amplitude (about $0^{m}.02$).

For the sake of completeness Table 2.2 shows the V magnitude and $B - V$ colours for C, V and CK.

Table 2.2: Magnitudes and colours for comparison and check stars.

Star	V	$B - V$	No. of obs.
HD 116562 (C)	9.416 ± 0.013	0.274 ± 0.005	183
HD 116700 (CK)	9.483 ± 0.011	0.211 ± 0.006	61
DY Cen (V)	12.784 ± 0.071	0.326 ± 0.015	180

2.4 Analysis

The data were analysed with the Fourier transform package, *PULSAR* (Skillen, 1985). The short time base of the observations (with respect to the long period suspected above) rendered determination of any periods greater than around 11 days unreliable. However, in the first instance, it was assumed that the long period variation was a simple sinusoidal oscillation repeating every 40 days (as is common with the cooler R CrB stars, see Section (2.5)). The observations were therefore *pre-whitened* by the equivalent frequency (Figure 2.3) and Fourier transforms of the resulting data taken. The classical power spectrum (Deeming, 1975) of the data is shown in Figure 2.4.

The most significant peaks in the power spectrum were found to correspond to the following frequencies:

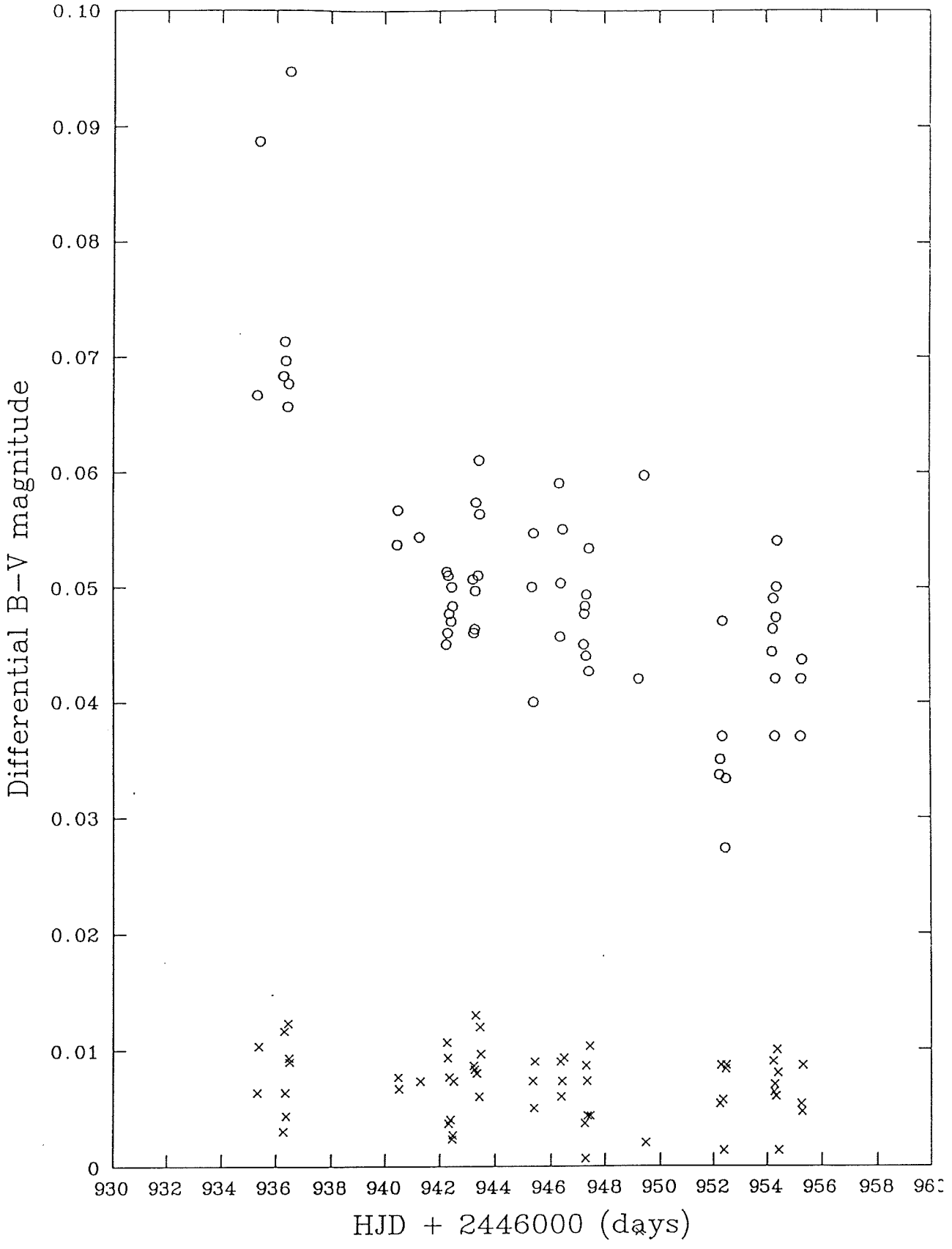

Figure 2.2: $B - V$ (symbols as before) plotted against HJD.

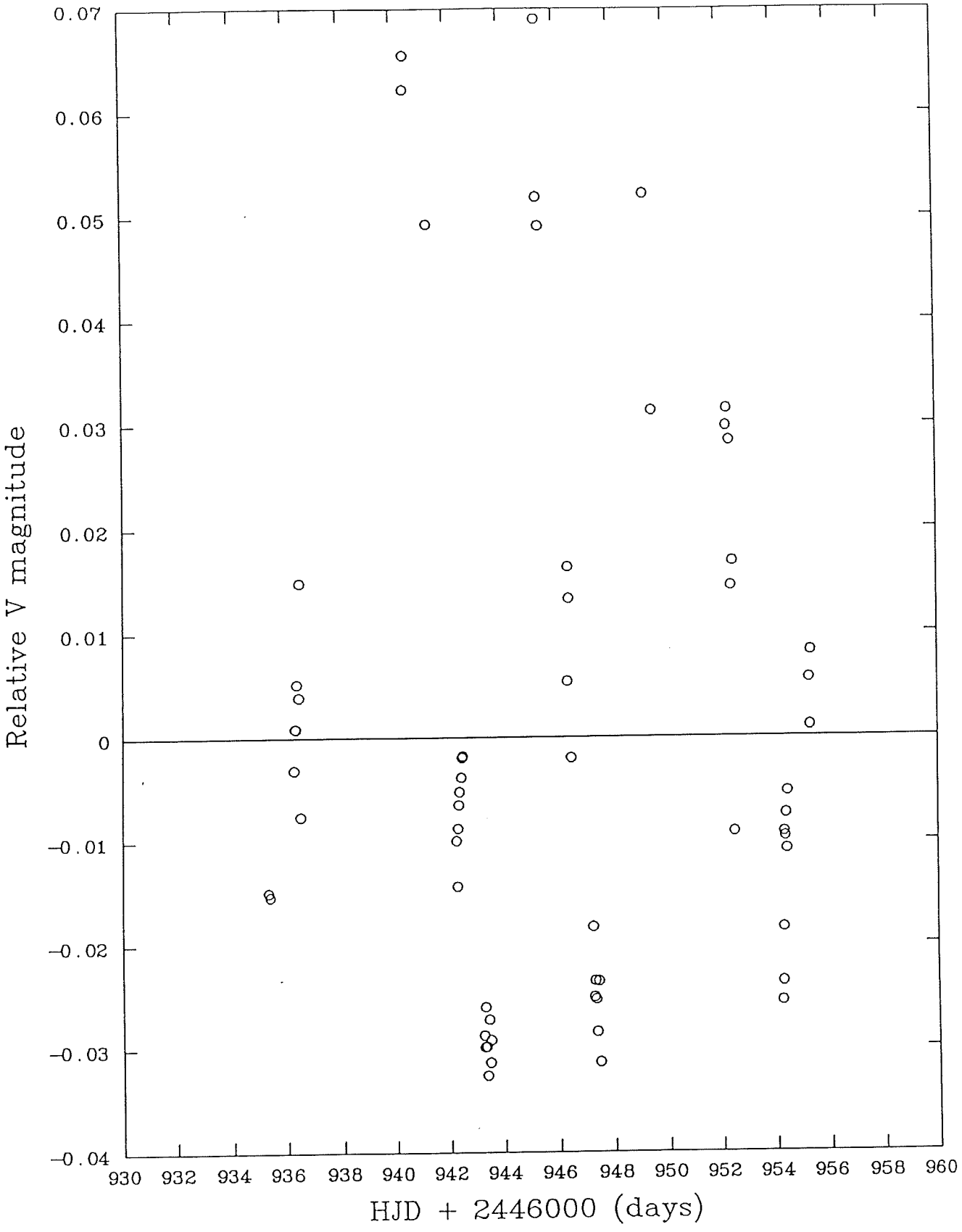

Figure 2.3: Data pre-whitened by 40 day period.

(i) 0.089 c day^{-1} (11.2 days)

(ii) 0.182 c day^{-1} (5.5 days)

(iii) 0.260 c day^{-1} (3.8 days)

It is likely that (i) is merely an overtone of (ii). The power window for the period shows that there are no significant peaks caused by the observational sampling (ie the relative power in the peaks is a factor of 100 or so less than the peaks in the data power spectrum—even when the peaks between the spectra coincide).

To check the validity of the above results a series of tests were applied:

Test 1. To ensure that the data were not biased by the choice of pre-whitening frequency, different values ranging from 25 days to 120 days were applied (generally in 5 day intervals). As before the resulting data were analysed using the *PULSAR* package. The frequencies determined above were again recovered, but the power within each frequency was found to be loosely correlated to the choice of pre-whitening frequency.

Test 2. It is important to gain a qualitative estimate of the noise power in the data and to ensure that the frequencies obtained are significant. To achieve this aim, *PULSAR* was used to randomize all the magnitude values on the time axis, and then obtain the resulting power spectrum (Figure 2.5) . As can be seen from Figure 2.4, the peak power (from the power spectrum of the data pre-whitened by 40 day period) is approximately a factor of 10—20 greater than the noise power.

Test 3. To check the coherence of the results the data were split into two equal segments and a separate fourier analysis attempted. No significant difference was found (see Figure 2.6) between the two data sets. The power spectrum of the data obtained between HJD 2446935–2446943 is less resolved than that in the second data string. A cursory glance at Figure 2.1 shows that at this time the long term variation was changing most rapidly and therefore the pre-whitening frequency used could have a critical effect on the subsequent analysis.

Test 4. The primary assumption of all fourier techniques is that the variation to be modelled *can be fitted by a finite number of sine curves.* However, with suitable

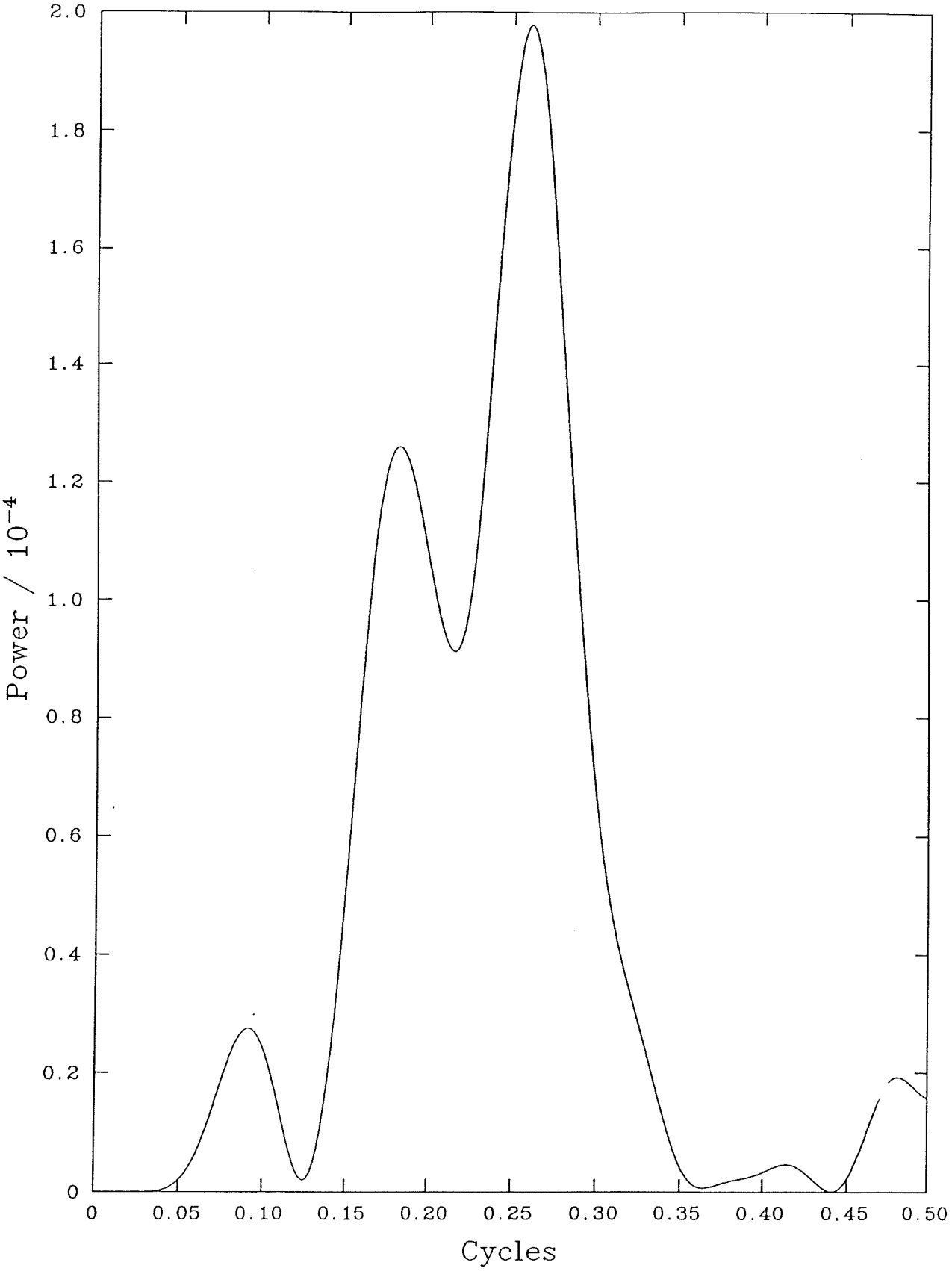

Figure 2.4: Power spectrum of pre-whitened data.

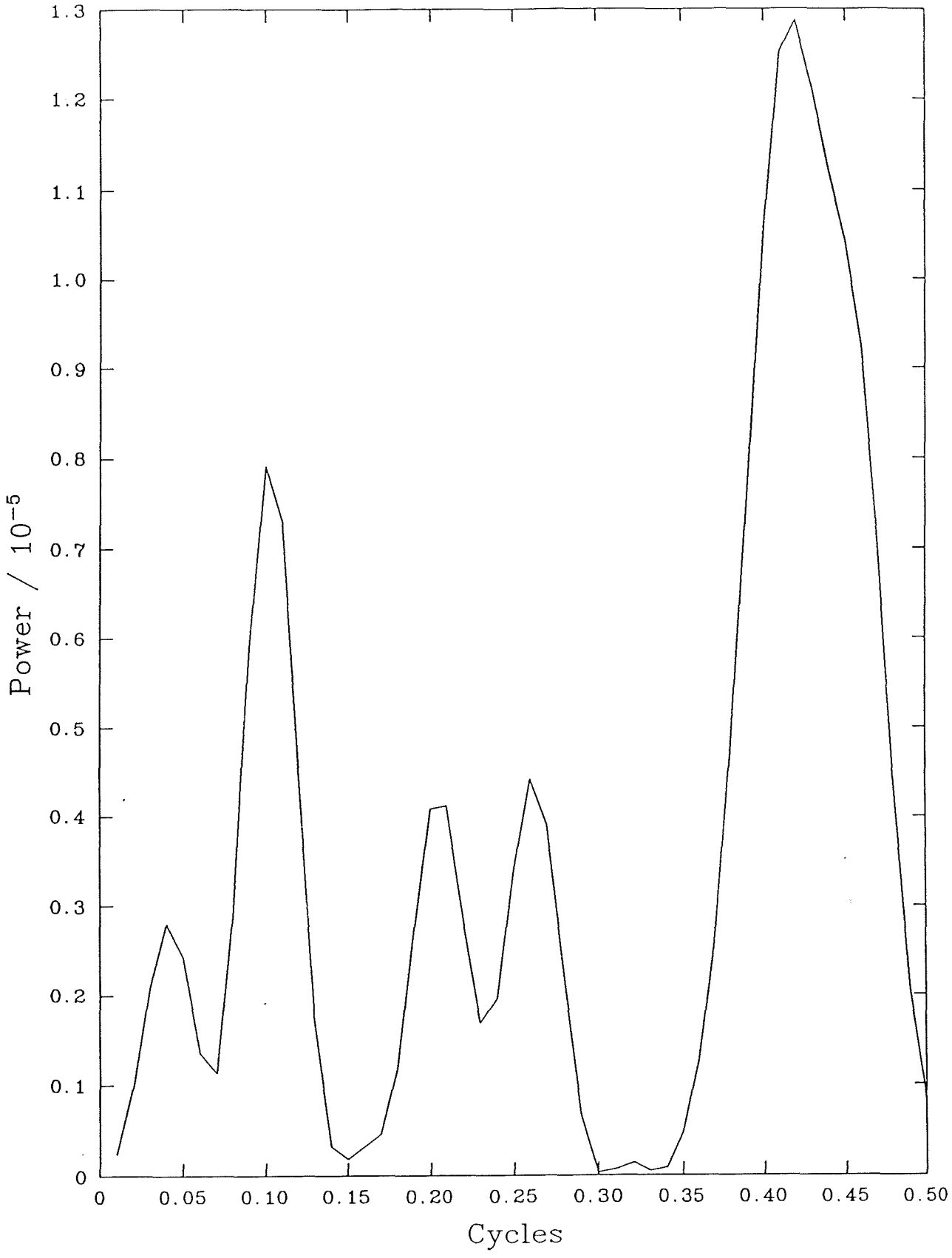

Figure 2.5: Power spectrum of randomized data.

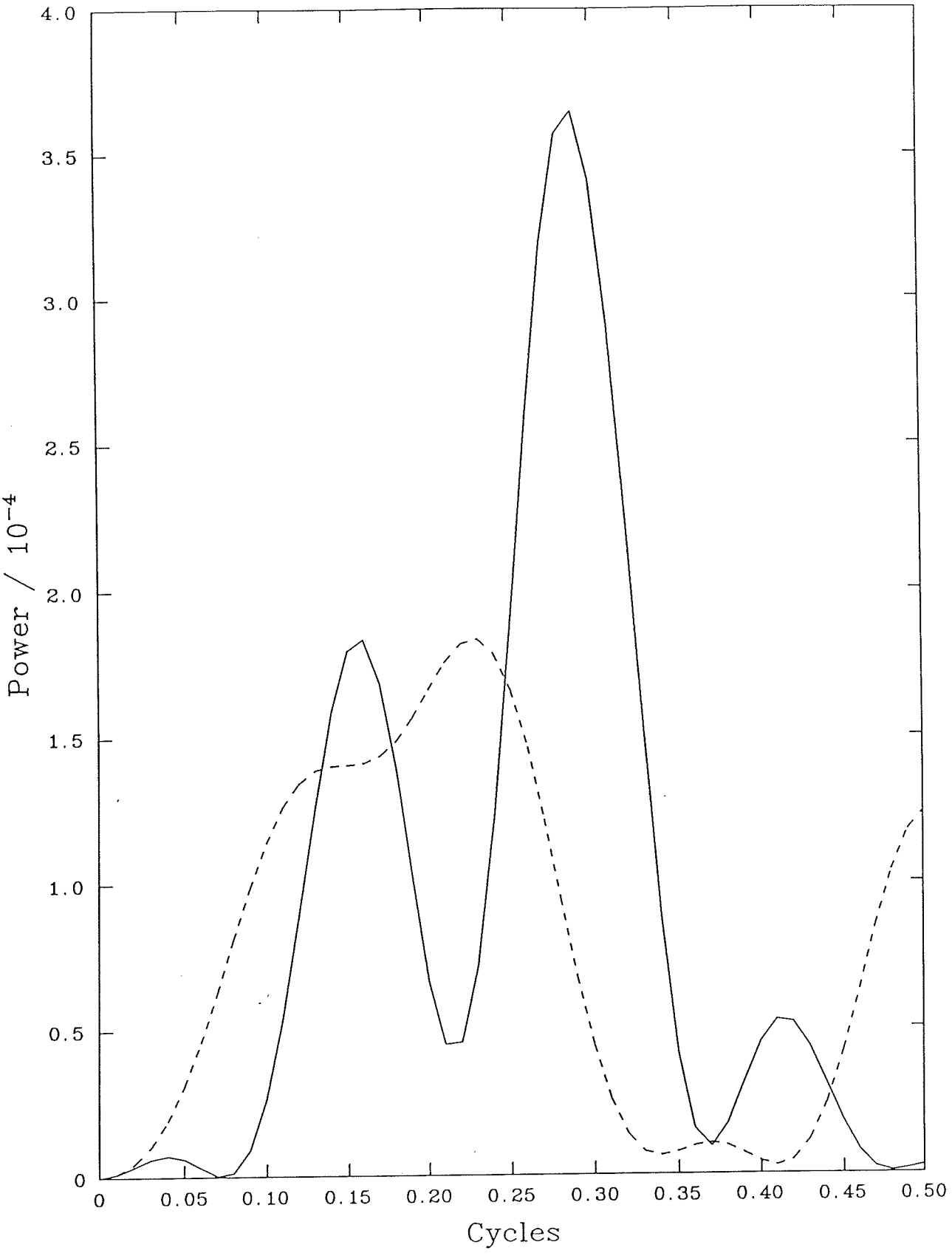

Figure 2.6: Power spectra of split data (- - for HJD 2446935–2446943, and --- for HJD 2446945–2446955).

conditions, variations may occur where this type of assumption is no longer valid, such as *floppy* periods (ie periods that are not perfectly reproducible from one cycle to the next), or those where the amplitude changes very rapidly within a small part of the period. In cases such as these misleading results could be inferred, so to check their authenticity it is advantageous to apply a independent technique that does not make this assumption. Dworetsky (1983) has described a specialized autocorrelation technique (Lafler and Kinman, 1965)—the so-called *String* method—which was coded in St. Andrews by Dr. P. W. Hill and adapted by the author for this particular case. The strength of this method lies in its simplicity, as it merely sweeps a range of frequencies through a data string and then performs a least squares analysis on the results of the phasing. As Dworetsky (1983) points out, information can also be obtained from the data regarding the shape of the variation (the string-length, L).

When the string method was applied to the DY Cen data, it was still found necessary to remove the long term trend so that the short term variations became more apparent (as before, the technique is not sensitive to the value of the pre-whitening frequency). The deepest minima shown in Figure 2.7 demonstrate that the frequencies found by fourier techniques are also detectable by an autocorrelation method. The average string-length was found to be 1.627, thus indicating a close resemblance to a *saw-tooth* shaped light curve.

Figure 2.8 shows the data phased over the 3.8 day period (the dominant frequency). As can be seen, the phase coverage is rather sparse (especially over the latter half of the cycle) and there are a number of extraneous points. However, this figure does demonstrate well the saw-tooth appearance of the light curve.

It should be remembered that other helium stars, notably BD-1°3438 (Jeffery *et al.* , 1986) display *floppy* periods. In these cases it is better to adopt an average period for the variation. Data covering many cycles are required to establish average periods.

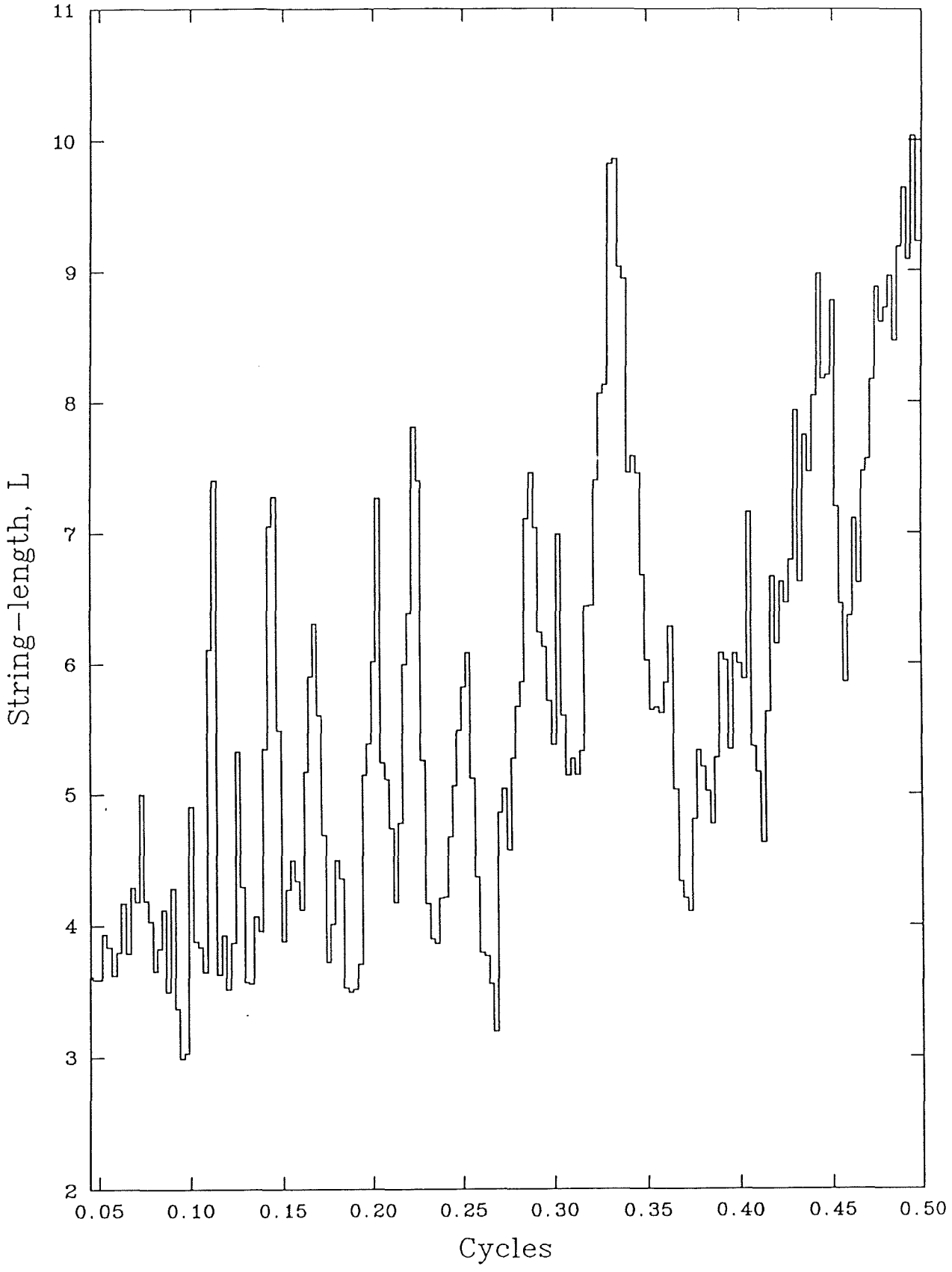

Figure 2.7: Identification of frequencies using the *String* method.

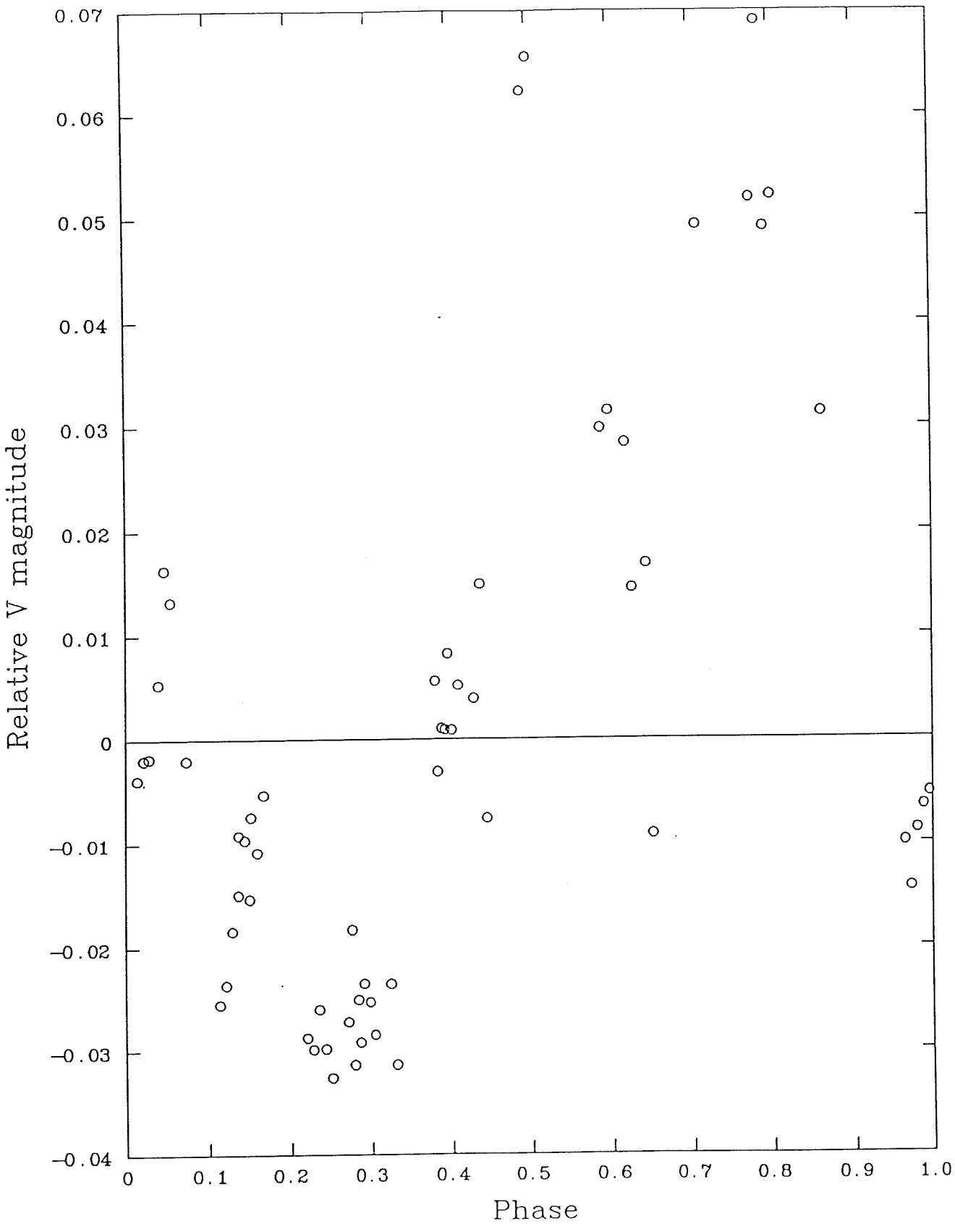

Figure 2.8: Data phased over 3.8 day period.

2.5 Discussion

The cooler R CrB stars are thought to vary in magnitude with periods ranging from about 38–120 days (Feast, 1986a). However, only regarding RY Sgr (and possibly R CrB itself), where the star is bright and the amplitude large, have variations been observed over many cycles and the periods consequently well determined (Alexander *et al.* , 1972). Many of the fainter stars are also thought to be variable (Bateson, 1978) but the floppiness, length and small amplitude of the variations have rendered observations difficult. It must be said that it is difficult to understand why RY Sgr and R CrB appear similar in so many respects but are very different as regards their amplitude of variation. Colour and radial-velocity variations suggest (for RY Sgr at least) that the variations are due to radial pulsation.

It has been suggested that the pulsation periods of the cool R CrB stars are related to their surface temperatures (cf. *period—temperature relation*, Wood, 1976). The cool end of the relation is defined by S Aps which is thought to have a surface temperature of 4 000 K and a pulsation period of about 120 days (Waters, 1966). The hotter end is better defined with a number of stars *suspected* of having periods near 40 days and displaying G-type spectra. The relation is reported to extend to the hotter helium stars which have periods of a few days (but still retain the floppiness of the R CrB star periods). However, Feast (1986a) believes that it is possible that all R CrB stars are at essentially the same temperature and that they pulsate with periods near 40 days, their spectral differences being ascribed to abundance variations. Corroborative evidence is given by Kilkenny (1983) who has re-determined a period of 40 days for S Aps (this period is thought to be the star's fundamental mode with the previous period a harmonic).

Saio and Jeffery (1988) have studied linear nonadiabatic pulsation in luminous hydrogen-deficient stars and shown that given a stellar surface temperature (T_{eff}) and an estimate of the pulsation period, a pulsation mass may be determined. Good results rely on an accurate estimate of T_{eff} (usually determined from UV continuum fluxes) which at present is not available for DY Cen; however, Feast (1986b) has estimated a spectral type of around A (type) from the inspection of medium-resolution spectra. (The

ionization of the spectra of DY Cen presented in Chapter 3 suggests a temperature of 14 000($\pm$ 1 500) K).

To continue any further we must make certain assumptions:

(i) DY Cen is a EHe star with a T_{eff} of 14 000 K, and

(ii) it undergoes radial pulsations with a period (π) of between 3.8–5.5 days.

Figure 2.9 shows the position of DY Cen on the log π – log T_{eff} diagram.

From Saio and Jeffery and the quantities above we can determine that M $\sim$ 0.71–0.78 $M_{\odot}$. Using a mass–luminosity relation applicable to helium stars (Jeffery, 1988 and Saio, 1988) then log ($L/L_{\odot}$) $\sim$ 4.10–4.25. It is important to remember that these relations are only valid if the envelope mass is negligible when compared to the core mass. At M $\sim$ 0.7 $M_{\odot}$ the envelope is probably $\sim$ 5% of the stellar mass. At lower stellar masses the relative mass of the envelope increases. Thus for DY Cen the mass obtained can serve only as a lower limit, but its proximity to the cut-off limit suggests that this result may only be in error by a small amount.

At present no attempt has been made to produce an atmospheric model for DY Cen, therefore it is instructive to determine an approximate value of log ($g/g_{\odot}$). Using the mass and luminosity obtained we find log ($g/g_{\odot}$)$\sim$ 1.61–1.75. Figure 2.10 shows the position of DY Cen in the log g – log T_{eff} plane.

The photometric mass of the star appears marginally lower than those obtained for other helium stars (cf. $M_p \sim$ 0.8–0.9 $M_{\odot}$, Saio and Jeffery, 1988). However, BD-9°4395 has a spectroscopically-determined mass of 0.68 $M_{\odot}$ while its photometric variations are complex and thought to be caused by non-radial oscillations. This star is also hotter ($T_{eff} \sim$ 23 000 K) than DY Cen but does show some similarity in its emission line spectrum (Jeffery, 1986).

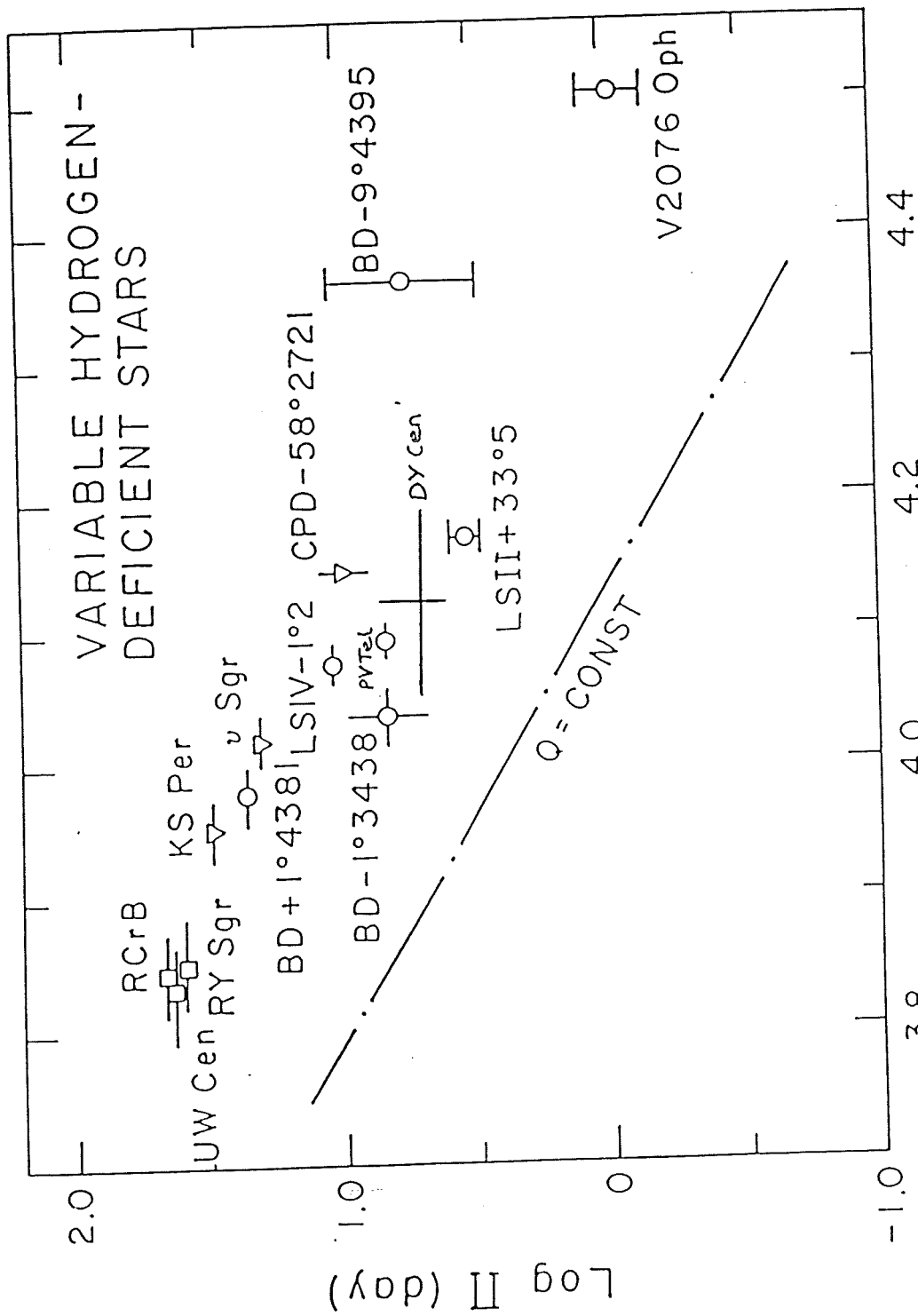

Figure 2.9: The position of DY Cen in the log π – log T_{eff} plane (Saio and Jeffery, 1988).

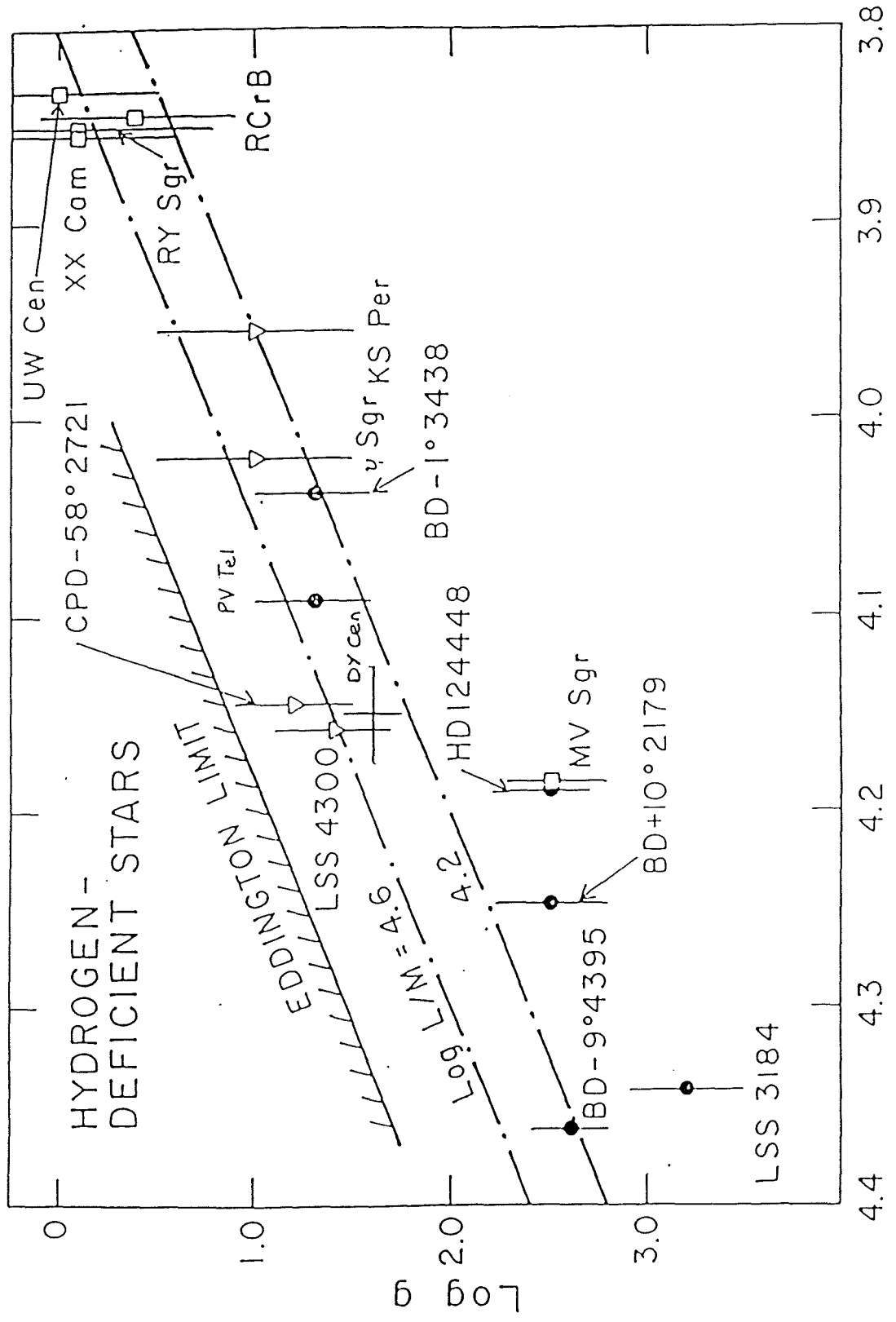

Figure 2.10: The position of DY Cen on the log g – log T_{eff} plane (Saio and Jeffery, 1988).

2.6 A note on the long term variation

Obviously with such a short time base it is impossible to determine anything qualitative about the long term variation reported earlier. However, it is worth speculating as to its significance. Bateson (1975, 1978) has reported a periodic variation based on visual measurements. He finds a 120 and/or 55 day periods. It is interesting to note that this is similar to other reported R CrB star periods. If these variations are real then they will be impossible to interpret within the framework of the Saio and Jeffery period–temperature relation. This may indicate that other factors such as chemical composition may play an important role in R CrB star pulsations.

2.7 Summary

DY Cen appears to undergo short period variations (3.8–5.5 day) superimposed on a much longer period variation (> 25 days). Provided DY Cen is an EHe star and its variations may be interpreted as radial pulsations, then a luminosity of $L \sim 13\,000$–$18\,000\ L_\odot$ *and a mass of* $M \sim 0.71$–$0.78\ M_\odot$ *are implied.*

2.8 References

1. Alexander, J.B., Andrews, P.J., Catchpole, R.M., Feast, M.W., Lloyd-Evans, T., Menzies, J.W., Wisse, P.M., and Wisse, M., 1972. *Mon. Not. R. astr. Soc.*, **158**, 305
2. Bateson, F., 1975. *Pub. of the Variable Star Section of the R. astr. Soc. N. Zealand*, **3**, 1
3. Bateson, F., 1978. *Pub. of the Variable Star Section of the R. astr. Soc. N. Zealand*, **6**, 39
4. Deeming, T.J., 1975. *Astrophys. and Space Sci. 36*, 137
5. Dworetsky, M.M., 1983. *Mon. Not. R. astr. Soc.*, **203**, 917
6. Feast, M.W., 1986a. *In IAU Coll. No.* **87**, *Hydrogen-Deficient Stars and Related Objects*, p.151, eds. Hunger, K., Schönberner D. and Rao, N. Kameswara., Reidel
7. Feast, M.W., 1986b. *In IAU Coll. No.* **87**, *Hydrogen-Deficient Stars and Related Objects*, p.21, eds. Hunger, K., Schönberner D. and Rao, N. Kameswara., Reidel
8. Jeffery, C.S., Hill, P.W., and Morrison, K., 1986. *In IAU Coll. No.* **87**, *Hydrogen-Deficient Stars and Related Objects*, p.95, eds. Hunger, K., Schönberner D. and Rao, N. Kameswara., Reidel
9. Jeffery, C.S., 1987. *In IAU Coll. No.* **87**, *Hydrogen-Deficient Stars and Related Objects*, p.81, eds. Hunger, K., Schönberner D. and Rao, N. Kameswara., Reidel
10. Jeffery, C.S., 1988. *Mon. Not. R. astr. Soc.*, **235**, 1287
11. Kilkenny, D., 1983. *Mon. Not. R. astr. Soc.*, **205**, 907
12. Kilkenny, D., 1986. *Private Communication*
13. Menzies, J.W., Banfield, R.W., and Laing, J.D., 1980. *SAAO Circ.*, **1**, 149
14. Saio, H., 1988. *Mon. Not. R. astr. Soc.*, **235**, 203
15. Saio, H. and Jeffery, C.S., 1988. *Astrophys. J.*, **328**, 714
16. Skillen, I., 1985. *Ph.D. Thesis*, St. Andrews University
17. Waters, B.H.J., 1966. *R. astr. Soc. N. Zealand Circ.*, No 119
18. Wood, P.R., 1976. *Mon. Not. R. astr. Soc.*, **174**, 531

Chapter 3

Spectroscopic observations of DY Cen

3.1 Introduction

DY Cen was classified as a R CrB star from its photometric light curve (Hoffleit, 1930), and low resolution spectrograms. Previously available spectra (Kilkenny, 1986) do not show any emission lines in the blue part of the spectrum. As the two other hot R CrB stars both appear to have strong emission lines at nearly all phases of their light curves, DY Cen allows the best opportunity to obtain reliable photospheric abundances for the group.

3.2 Observations

In response to a service request, DY Cen was observed at the AAT on the 13^{th} March, 1988. The seeing during the observations was bad, with around 5–10 arcseconds being recorded in the telescope log. The 25 cm camera was used with the *IPCS* as the detector. The 1200V grating enabled a wavelength coverage of about 1 000Å, at a resolution of 1.5Å. Neutral density filters were used to keep the count rate below detector saturation. Suitable wavelength calibration was accomplished using a copper-argon discharge lamp,

with an arc observation taken either side of the DY Cen observations. No flat field was taken as experience has shown that IPCS data does not require flat-fielding with relatively short integrations.

Two wavelength regions were observed. The first, centred at λ3700Å, covered the hydrogen (Balmer) and helium series limits; this spectrum is of reasonable quality allowing line identifications, equivalent widths and also radial velocities to be determined. The second was centred at λ4600Å, but unfortunately only the strongest features are discernable as the seeing had deteriorated by this point and only 300 cts were collected in the continuum. However, line identifications were possible.

3.3 Reductions and results

The spectra were reduced using Starlink's FIGARO suite of programs. Briefly, this consisted of:

(i) extraction of star and sky from the 2-d frame,

(ii) subtraction of scaled sky from star spectrum,

(iii) wavelength calibration using corresponding arc frames,

(iv) conversion of this scale to a linear relationship (*scrunching*),

(v) normalisation of the spectrum to the average continuum value in 100Å bins.

For both spectra, 52 arc lines were identified. Subsequently a 5^{th} order polynomial fit was made resulting in an rms error of less than 0.1Å. Figures 3.1 and 3.2, respectively, show the spectra.

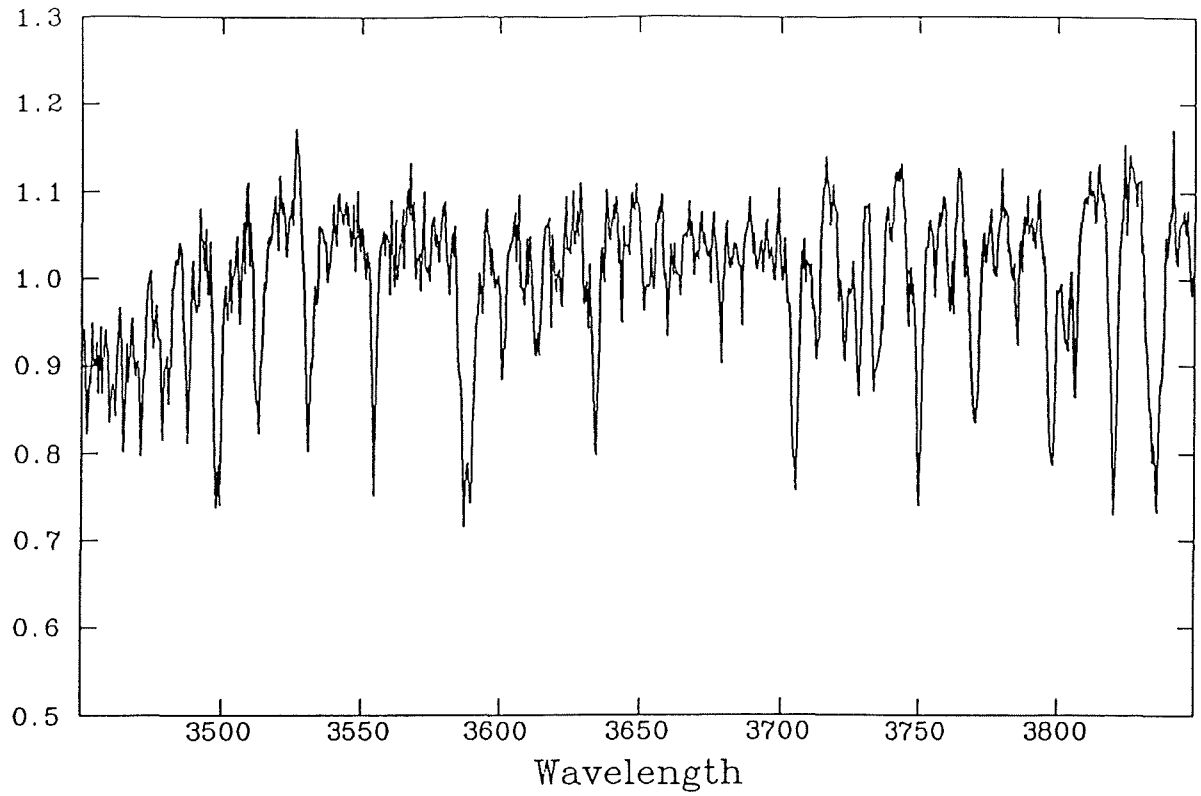

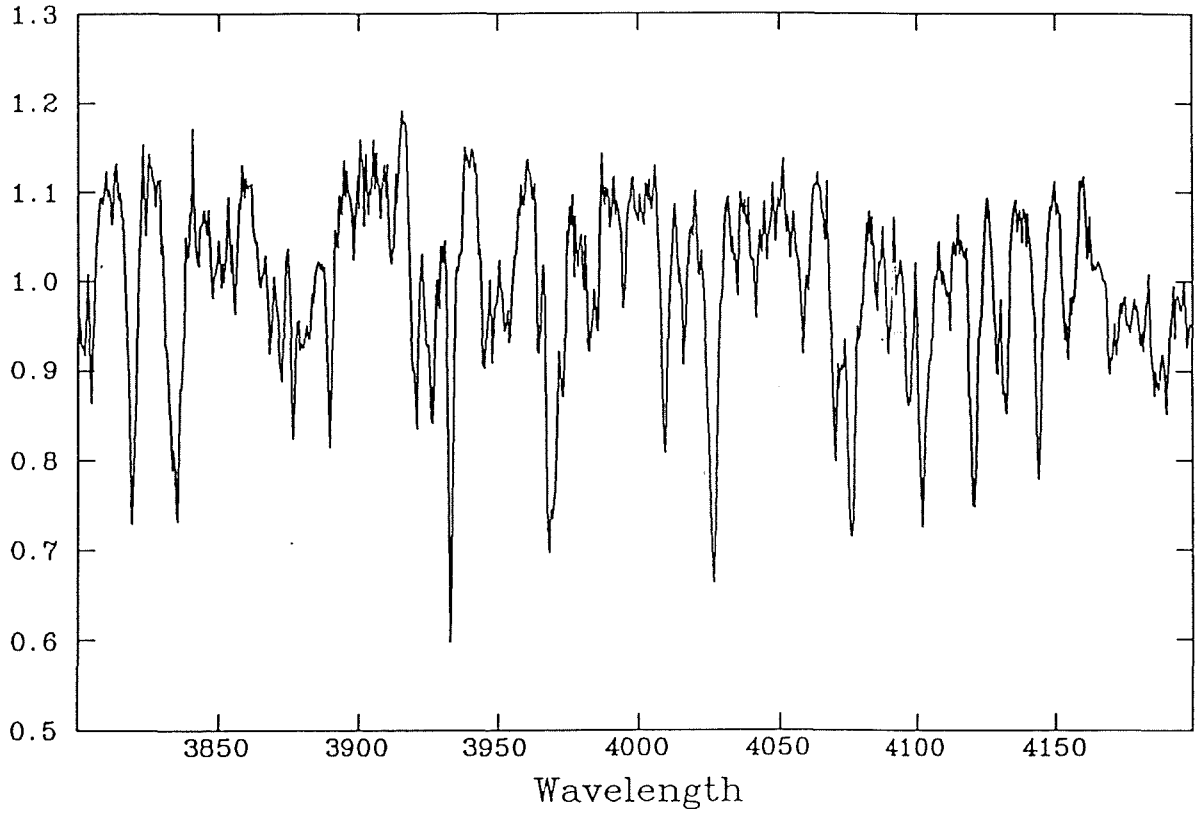

Figure 3.1: Spectrum centred at $\lambda 3700\text{Å}$.

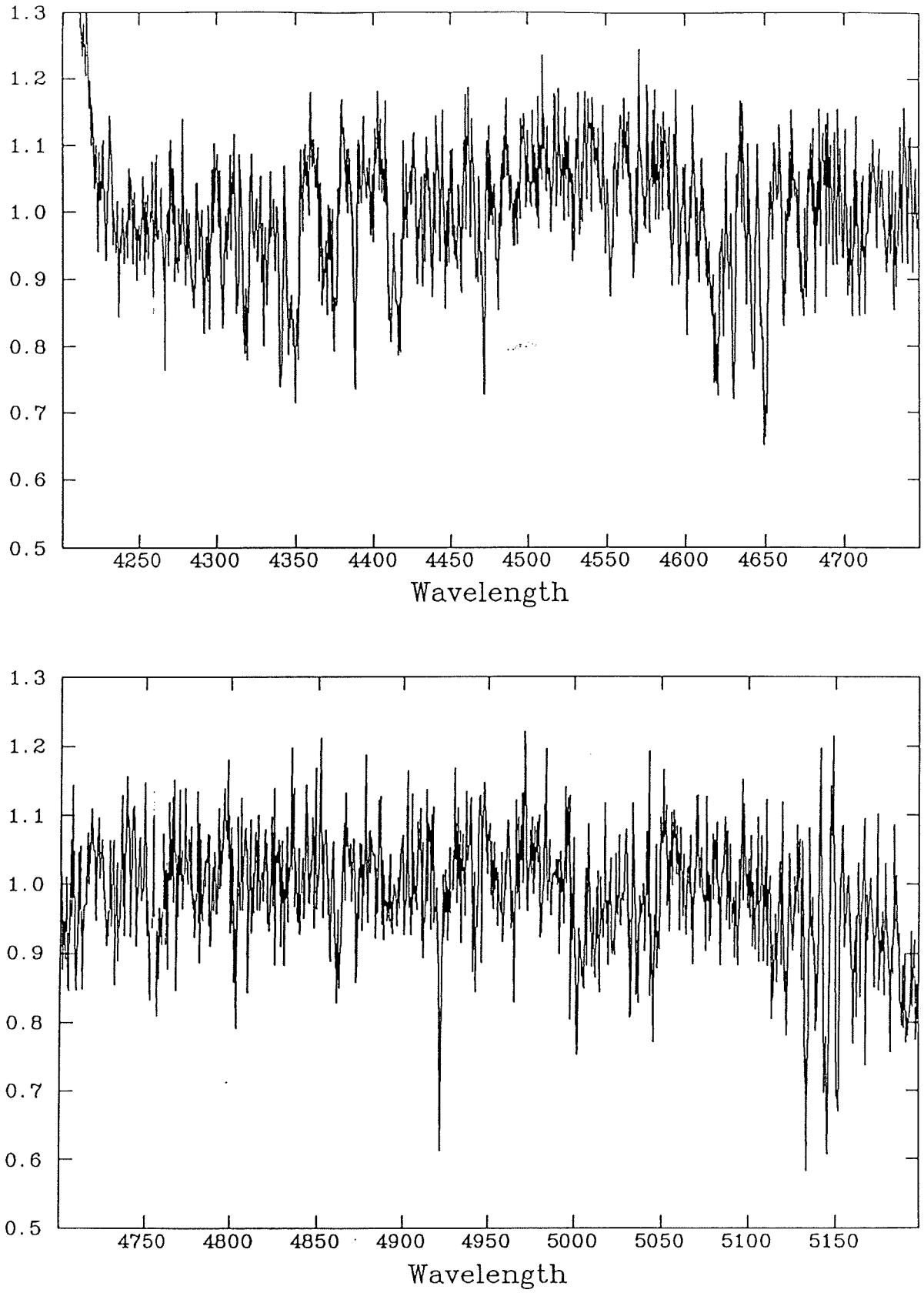

Figure 3.2: Spectrum centred at λ4600Å.

Table 3.1 shows the measured wavelengths, equivalent width measurements and line identifications (Heber,1983 and Lynas-Gray *et al.* , 1981) for most of the absorption lines shown in Figure 3.1. The Q column gives an indication of the effect of blending on the lines; those lines marked with an alphabetical character are blended with others marked by the same character. A *ct* in this column indicates that an accurate representation of the stellar continuum was not possible and equivalent width measurements were not attempted.

For those lines that are unblended and for which the continuum was reasonably well defined a radial velocity was determined using *REDUCE* (Hill, *et al.* 1982), see Table 3.2. A correction of $+17.6\,\mathrm{km\,s^{-1}}$ was also required to account for the effects of the earth's motion at the time of the observations.

The radial velocity after all corrections have been applied was found to be $(15.1 \pm 2.5)\,\mathrm{km\,s^{-1}}$.

As previously mentioned the spectrum centred at λ4600Å had a very low S/N ratio, and was only useful for determining line identifications. Table 3.3 shows the results of this investigation.

Table 3.1: Line identifications and equivalent widths for spectrum centred at λ3700Å.

Lambda (Å)	Q	EW (Å)	ID	Lambda (Å)	Q	EW (Å)	ID
3453.2	ct		He I	3920.9	i	0.717	C II (4)
3479.2	ct		He I (43)	3926.3	i	0.910	He I (58)
3481.6	ct			3933.1		1.193	Ca II (1)
3488.0	ct		He I (42)	3944.9	j		C II (32,31)
3497.3	ct		O II (7), He I (40)	3947.8	j		C II (32,31)
3499.3	ct		He I (40), O II (7)	3952.2	j	1.672	C II (32,31)
3513.0	ct		He I (38)	3954.2	j		C II (32,31), N II (6)
3530.6		0.773	He I (36)	3964.4	k		He I (5)
3554.6		0.731	He I (34)	3968.3	k	2.420	Ca II (1), C II (37,38), Hϵ
3587.4	a	1.966	He I (31)	3973.2	k		C II (37,38)
3589.9	a		C II (23)	3982.5	l	0.658	?S III (8)
3600.6		0.528	He I (30), Al III (1)	3985.5	l		?S III (8)
3612.8	b	0.589	Al III (1)	3994.4		0.237	N II (12)
3613.8	b		He I (6)	4009.4		0.812	He I (55)
3634.4		0.998	He I (28)	4015.8		0.557	?Ni II (12)
3643.7	c	0.182	?Ne II (5), Cr II (1)	4026.6		1.844	He I (18)
3678.8		0.387		4034.9	m	0.253	S II (59), N II (39)
3705.2		1.061	He I (25)	4041.7		0.297	N II (39)
3712.6	d	0.481	Al III (4), Ne II (5), O II (3)	4053.6	n	0.553	N II (39)
3722.8	d	0.594	S III (6), Ne II (5), O II (3)	4058.0	n		N II (39)
3727.3	d	0.522	Ne II (5), O II (3)	4069.7	o	2.602	N II (38), C II (36)
3733.1	d	0.873	He I (24)	4075.4	o		C II (36), S III (3.01)
3745.8	e	0.247	He I	4084.7		0.300	N II (38), O II (10)
3749.8	e	1.032	S III (1), O II (3), ?H 12	4089.1		0.451	Si IV (1)
3756.1		0.190	He I (66)	4092.3	p		
3761.5		0.351		4096.4		0.872	N II (38)
3770.8		1.053	He I (65), N II (4), ?H 11	4102.0		1.614	Hδ
3785.5		0.284	He I (64)	4112.1	q		N II (44)
3798.2	f	1.141	?Si III (3), H 10	4120.6		1.240	He I (16)
3803.1	f	0.532		4128.7	r		S III (3)
3806.0	f	0.492	He I (63)	4131.1	r	1.088	S III (3)
3819.7		1.129	He I (22)	4132.3	r		N II (43)
3833.9	g	1.977	He I (62)	4143.6		1.030	He I (53)
3835.4	g		C II (13), H 9	4152.9	s	0.653	S II (44), O II (19)
3842.7		0.160	N II (30)	4154.5	s		S II (44), O II (19)
3847.6		0.275	N II (30)	4169.4	ct		He I (52)
3855.3		0.230		4171.4	ct		N II (43)
3867.6	h	0.419	He I (20)	4175.5	ct		N II (42)
3872.0	h	0.666	He I (60)	4180.7	ct		N II (50)
3875.9	h	0.707	C II (33)	4185.6	ct		
3889.1		0.750	He I (2), H 8	4189.6	ct		S II (44)
3898.4		0.096		4196.9	ct		N II (49)
3911.6		0.142	O II (17)	4209.0	ct		

Table 3.2: Radial velocities for unblended lines.

Lambda† (Å)	Ion	Shift (Å)	RV Kms^{-1}	err Kms^{-1}
3530.487	He I	-0.011	-0.96	3.71
3554.394	He I	-0.235	-19.81	2.71
3634.235	He I	0.057	4.73	1.69
3705.003	He I	-0.241	-19.49	2.86
3712.750	O II	-0.069	-5.61	5.33
3797.900	H10	-0.116	-9.17	0.75
3819.606	He I	0.081	6.36	2.63
3876.188	C II	-0.009	-0.70	2.33
3876.409	C II	-0.254	-19.62	0.31
3964.727	He I	-0.050	-3.79	1.17
3973.263	O II	-0.090	-6.79	1.28
4009.270	He I	0.073	5.45	1.39
4026.140	He I	0.197	14.65	2.04
4069.636	O II	0.086	6.35	0.59
4120.812	He I	-0.099	-7.18	1.34
4143.759	He I	0.146	10.54	2.15

† all rest wavelengths taken from Petrie (1953).

3.4 Discussion

Unfortunately the spectra are not of sufficient quality to allow a surface abundance analysis. However, it is possible to determine a hydrogen abundance (Hunger, 1975) in a very approximate way by comparing the ratio of the equivalent widths of He I λ4026Å with Hδ (or He I λ4471Å with Hγ). This leads to $n_H / n_{He} \sim 0.9$, which is high for an EHe star and actually places DY Cen amongst the intermediate hydrogen-deficient Helium stars. There are several reasons for believing that this value represents a upper limit:

(i) the relation is mainly defined for the hotter hydrogen-deficient stars,

(ii) diagnostic lines used may be blended with lines from other ionic species,

(iii) Feast (1986) has suggested a spectral type of around A. At this implied temperature the hydrogen absorption cross section is greatest, and so even a trace amount of hydrogen will lead to detectable lines, and

(iv) by comparing the spectra with the intermediate stars it is obvious that these stars display reasonably normal hydrogen lines and it is the helium lines that are enhanced (Hunger, 1975). In DY Cen the hydrogen lines are greatly reduced in intensity.

Thus a more realistic estimate of the hydrogen abundance in this star will only be obtainable as higher resolution and higher signal to noise spectra become available.

The spectra do allow us to estimate the ionization in the photosphere and hence to estimate the surface temperature. Figure 3.3 shows the blue spectrum of DY Cen compared to other helium stars (comparison spectra taken from Jeffery *et al.* , 1987) The resolution of this spectrum was degraded to match that of the helium stars.

The helium stars are roughly arranged in a temperature sequence; ranging from 9 000 K for LSIV -14°109 to 31 600 K for HD 160641. It is important to note that the individual spectra are not flux calibrated and vary in quality so comparison of line depths is not useful. However, the spectra serve as a guide as to the absorption lines to expect at different temperatures. Overall the most similar comparison spectrum is that of LSE 78

Table 3.3: Lines ID from spectrum centered at λ4600Å.

Lambda (Å)	ID	Lambda (Å)	ID
4237	N II (48)	4681	S II (8)
4267	C II (6)	4704	N II (68)
4285	C II (45), S III (4)	4707	?
4292	C II (41,42)	4709	N II (25,68)
4304	C II (12.02)	4713	He I (12)
4313	C II (28)	4728	C II (48)
4319	C II (28), O II (2)	4732	Fe II (43)
4341	Hγ	4753	O II (24)
4346	O II (2)	4757	?
4350	O II (2)	4779	N II (29)
4367	O II (2)	4788	N II (29)
4374	C II (45,46)	4803	C II (17.08)
4388	He I (51)	4810	N II (20)
4411	C II (40,39)	4822	?
4416	O II (5)	4831	?
4429	N II (55)	4840	?
4432	N II (55)	4857	O II (29)
4438	He I (38)	4861	Hβ
4447	N II (15)	4872	O II (57)
4453	O II (5)	4911	?
4456	?S II (43)	4922	He I (48)
4467	?O II (87,94)	4942	S II (7)
4471	He I (14)	4958	?C II (25)
4480	Al III (8)	4965	C II (25)
4491	O II (86)	4981	?
4515	Fe II (37)	5002	N II (4)
4529	N II (59)	5005	N II (6,19)
4533	S II (47)	5011	N II (64)
4553	Si III (2), S II (40,48)	5015	He I (4)
4567	Si III (2)	5022	N II (64)
4574	Si III (2)	5032	S II (7), C II (17)
4591	O II (15), S II (47)	5036	C II (17), Fe II (36)
4596	O II (15)	5045	C II (35), N II (4)
4601	N II (5)	5114	C II (51)
4608	N II (5)	5122	C II (12)
4619	C II (50), Si III (13)	5133	C II (16)
4630	C II (49)	5138	C II (16)
4642	O II (1)	5145	C II (16)
4650	O II (1), C III (1)	5151	C II (16)
4661	O II (1)	5160	O II (32)
4674	O II (1), N II (1)	5182	?N II (70)

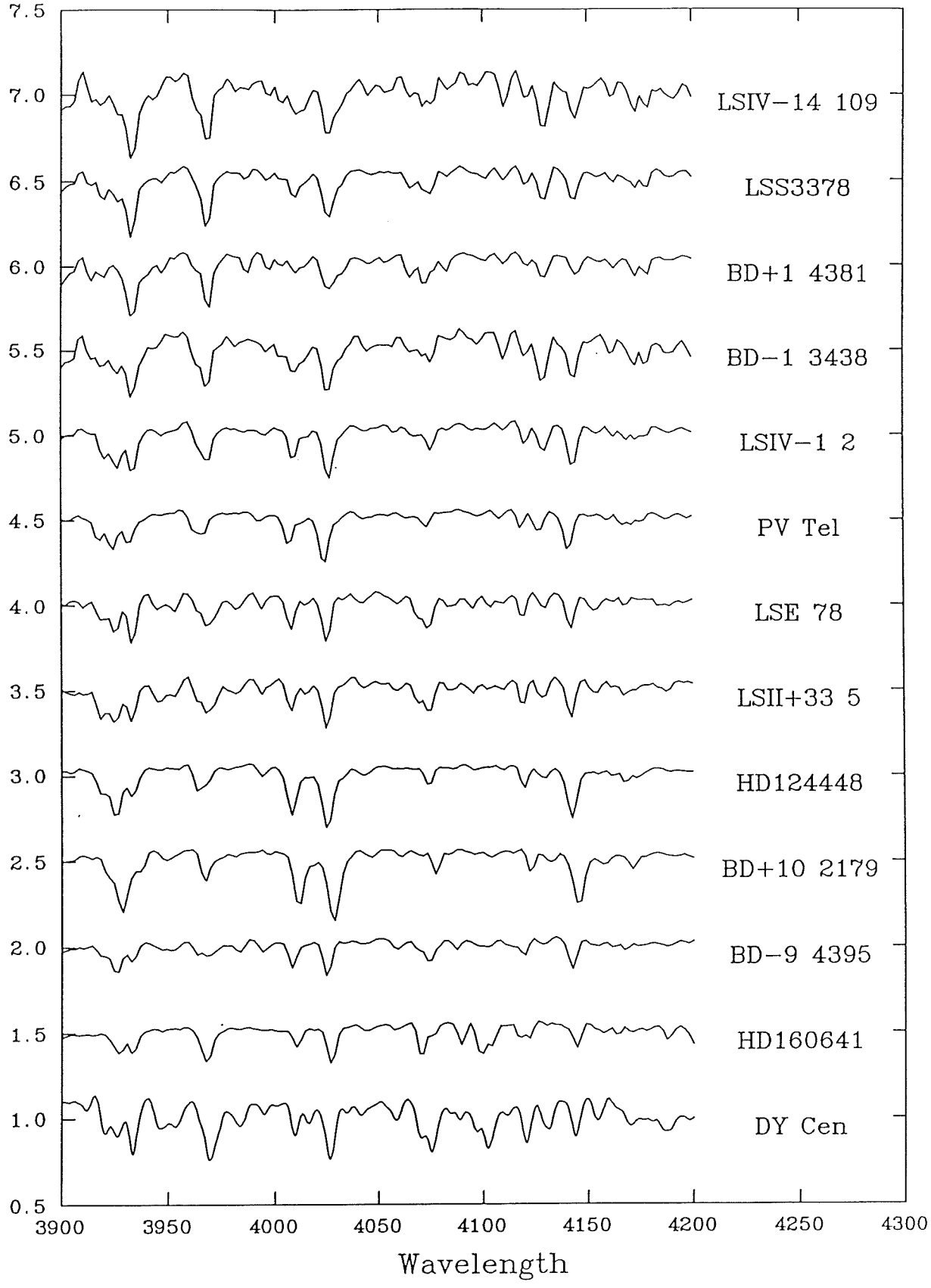

Figure 3.3: Comparison spectra for DY Cen

($T_{eff} \sim 14\,000$ K, Drilling *et al.* , 1984). The range of ionic species found in both AAT spectra are also consistent with this result.

The spectra also suggest that the surface gravity may be small; other EHe stars of high gravity have gravity-broadened wings in their helium lines. Although blending of lines in DY Cen is a major problem, at this resolution this does not appear to be the case. This re-enforces the comparison with some of the emission line EHe stars (such as LSE 78), which also have unbroadened wings and are hence thought to be low surface gravity objects. A low surface gravity was also inferred from the photometry (see Chapter 2).

3.5 Summary

DY Cen appears to be a carbon rich supergiant. A lower limit in n_H / n_{He} *of* $\sim$ *0.9 has been obtained. The photospheric ionization suggests a temperature of* $T_{eff} = (14\,000 \pm 1\,500)\,K$. *The heliocentric radial velocity was found to be* $(15.1 \pm 2.5)\,km\,s^{-1}$.

3.6 References

1. Drilling, J.S., Schönberner, D., Heber, U., and Lynas-Grey, A.E., 1984. *Astrophys. J.*, **278**, 224
2. Feast, M.W., 1986. *In IAU Coll. No.* **87**, *Hydrogen-Deficient Stars and Related Objects,* p.21, eds. Hunger, K., Schönberner D. and Rao, N.Kameswara., Reidel
3. Heber, U., 1983. *Astr. Astrophys.*, **118**, 39
4. Hill, G., Fisher, W.A., and Poeckert, R., 1982. *Pub. Dom. Astrophys. Obs.*, **16**, 43
5. Hoffleit, D., 1930. *Harvard Bull.*, **874**, 1
6. Hunger, K., 1975. In *Problems in Stellar Atmospheres and Envelopes*, p. 57, Eds. Baschek, B., Kegel, W.H. and Traving, G. (Springer-Verlag)
7. Jeffery, C.S., Drilling, J.S. and Heber, U., 1987. *Mon. Not. R. astr. Soc.*, **226**, 317
8. Kilkenny, 1986, *Private communication*
9. Lynas-Gray, A.E., Walker, H.J., Hill, P.W. and Kaufman, J.P., 1981. *Astr. Astrophys. Suppl. Ser.*, **44**, 349
10. Petrie, R.M., 1953. *Pub. Dom. Astrophys. Obs.*, **9**, 297

Chapter 4

V348 Sagittarii—imaging

4.1 Introduction

For a number of years V348 Sgr has been known to be surrounded by a small nebula (Herbig, 1957). With the Palomar Red Survey plates, Herbig found the nebula to have a diameter of about 8–10″, while plates taken with the variable at minimum light indicated the presence of an inner shell (diameter about 1″). The Palomar Survey plates also suggested that a small nebula about 4′ away may also be related to the system. As no other images have been presented in the literature, it was felt to be of great importance to obtain:

(i) broadband images taken by a large telescope situated in the southern hemisphere, allowing the nature of Herbig's *unusual* nebula to be determined, and

(ii) narrow band images using interference filters. These would enable the ionization structure and morphology of the nebula surrounding V348 Sgr to be qualitatively studied.

Both of these projects were attempted and successfully completed.

4.2 Broadband imaging

4.2.1 Observations

In response to a service request Dr. D. Malin obtained a prime focus plate of V348 Sgr and the neighbouring nebula with the AAT (plate number 2493) on 6^{th} June, 1986. A red sensitive IIIa-F emulsion was used with a Schott RG630 filter, effectively isolating the red region of the spectrum, including some strong nebula emission lines. The emulsion was hypersensitised and exposed for 90 minutes. Although the seeing was only about 2″ during the exposure the star images look *softer* than normal suggesting the telescope may have been slightly out of focus. The central part of the plate was then scanned with the COSMOS measuring machine at ROE.

4.2.2 Results

Despite the possible focus error the image obtained is of superb quality and at the time was by far the best image of V348 Sgr available. During the exposure the star was very faint and is only barely discernable (if at all) within the central part of the nebula. This image is shown in Plate 4.1.

Unfortunately the neighbouring nebula was not digitised by COSMOS; however a polaroid of the region was obtained and plainly shows the *unusual* nebula to merely be a nearly edge-on spiral galaxy. Herbig (1957) obtained a weak spectrum of this object and found it to be a continuum source which, bearing in mind the nature of the object, is to be expected.

Figure 4.1 shows a contour plot of the V348 Sgr image (obtained using FIGARO). The image is full of intricate details. However, without a corresponding continuum image (ie one taken with a filter blocking any nebula emission), it is extremely difficult to ascertain if some of the features in the nebula are indeed real or just chance alignments of faint stars (the limiting magnitude of the plate is far beyond that of the Palomar Sky Survey). Due to the relatively small dynamic range of the photographic plate the brightest stars (those brighter than about 17^m) are saturated—including V348 Sgr.

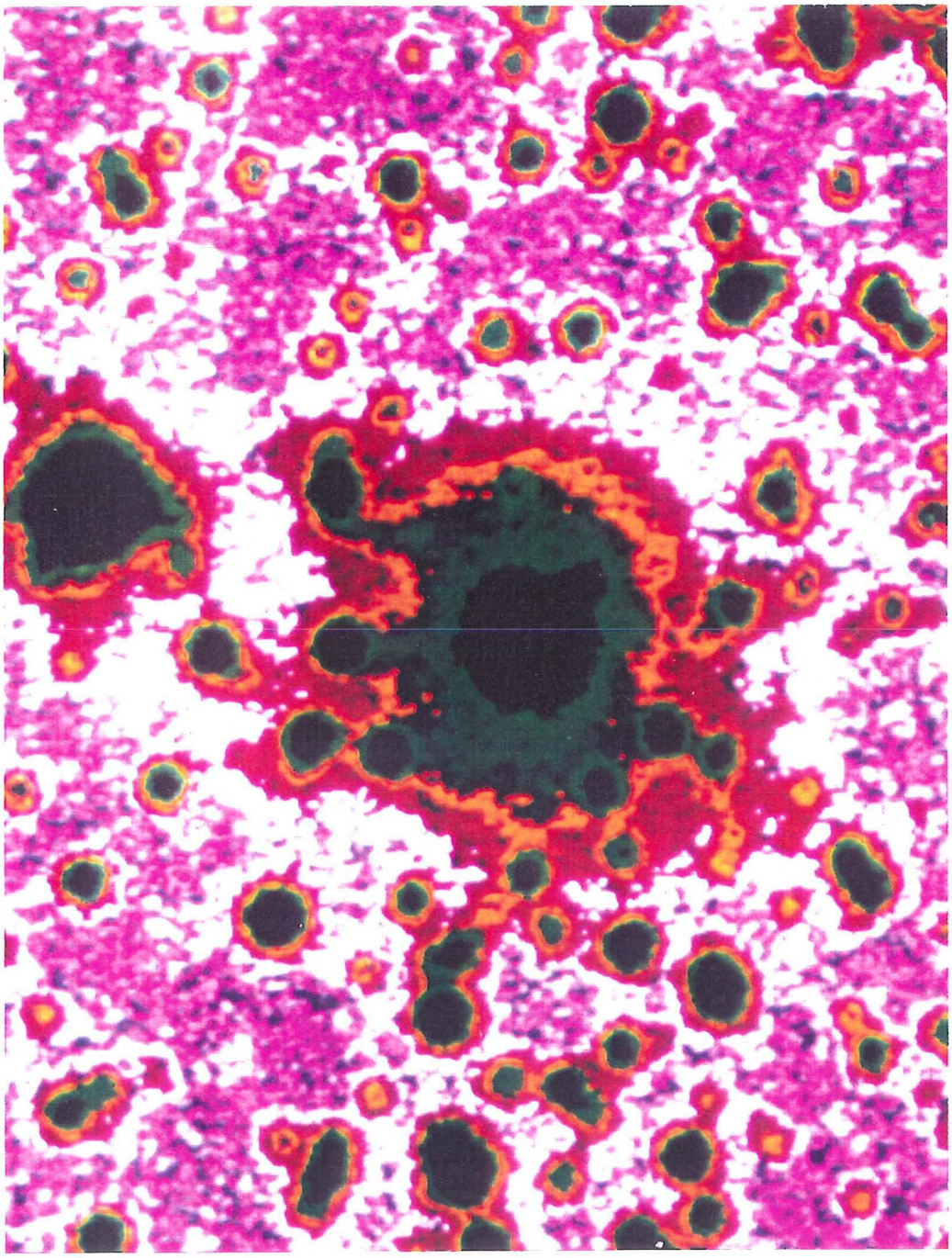

Plate 4.1: False colour representation of the AAT service plate of V348 Sgr.

Also the seeing/focus problem has washed out details within the inner nebula.

The bright star (coordinates x=30, y=135—star 12 in Heck *et al.* 's (1985) photometric sequence for V348 Sgr) also appears to be immersed in nebulosity (confirmed by spectroscopy as an extension of the V348 Sgr nebula, see Chapter 5). With suitable scaling it can be seen that the nebula easily fills the whole of the area shown. Radial filaments (seen on the contour plot) are also visible.

4.3 Narrow-band imaging

In order to examine the ionization structure within the nebula envelope it is necessary to image with narrow band filters centered on the strongest emission lines. As the nebula surrounding V348 Sgr was previously known to be of low excitation then the strongest lines were expected to be the Balmer recombination lines and the *forbidden* lines of [NII] and [OII]. Two dark nights with the 2.2 m telescope were awarded by ESO for a project to obtain narrow band images of all the hot R CrB stars. ESO also offered the Remote Observing Facility to the project, enabling operation of the telescope from Garching, West Germany. Although we had originally planned to use a coated GEC chip, the pre-flash lights in the camera head were not operational, so an RCA chip was used (ESO CCD number 5). The choice of CCD influenced which lines were to be observed. Thus the [OII] λ3726Å line could not be observed (the RCA response is very low at this wavelength), while at [NII] λ6584Å and Hα, the quantum efficiency is around 75%. See Table 4.1 for the actual filter numbers and descriptions.

Table 4.1: ESO filter numbers used

Emission line	ESO number	Central wavelength Å	FWHM Å
Hα	507	6566	15
[NII] 6584Å	50	6595	23
Continuum	438	6632	69

During the observing period (13/14th July, 1988) bad weather and technical problems

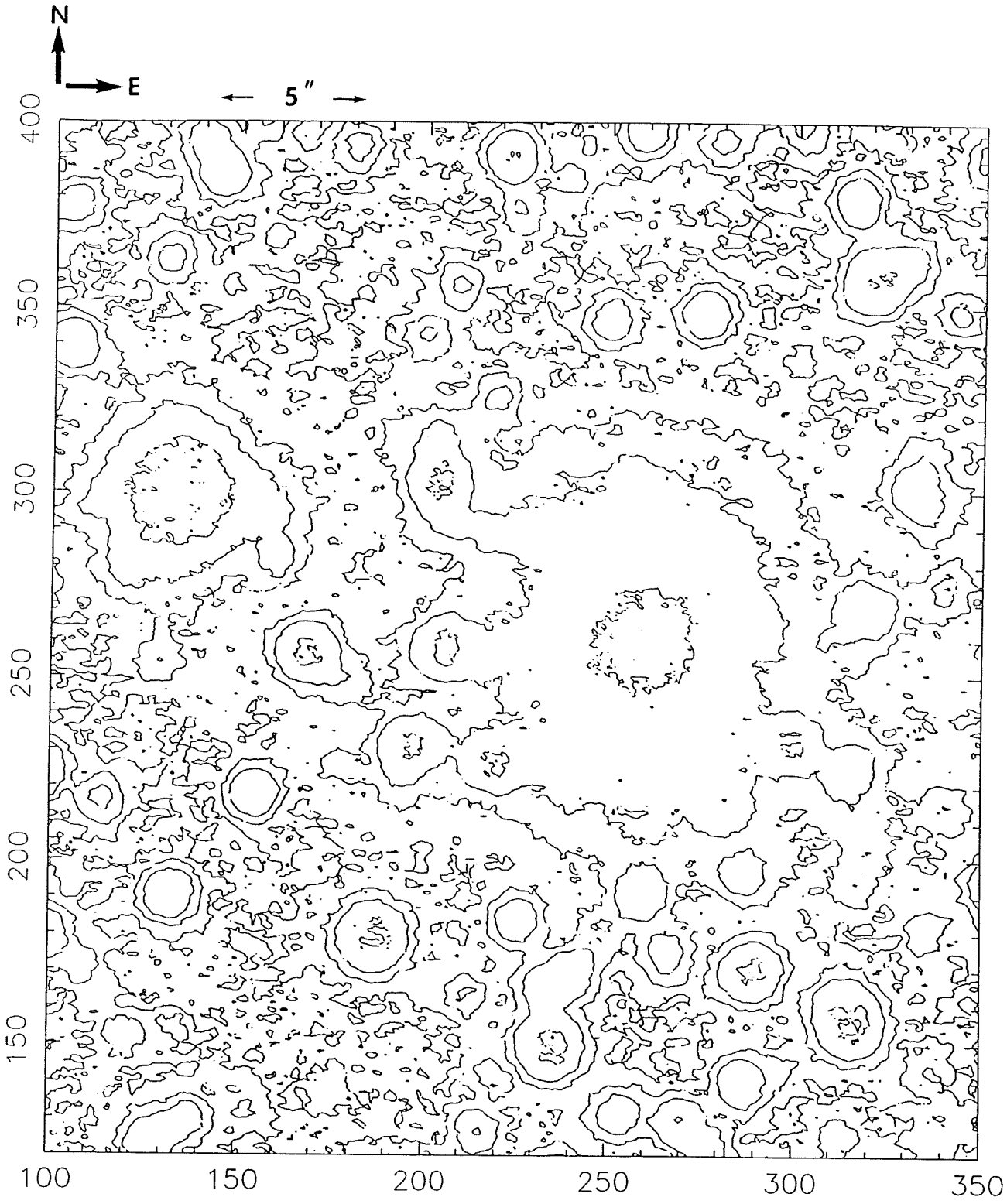

Figure 4.1: Contour plot of the AAT service plate. Ten intensity levels are equally spaced between the background and the brightest point in the image.

hampered the run. However, during a brief clear spell some observations were possible. As the observation period was not photometric only relative calibration of the frames was possible.

4.3.1 Reduction of CCD frames

During the observing session, flat-fields were obtained through all the filters used in this study. One of the drawbacks of remote observing is that real time control of the telescope is difficult, therefore flat-fields were acquired using a uniformly-illuminated board mounted within the dome (the use of dome flat-fields as opposed to those obtained on the twilight sky is a contentious issue). For each filter, three flat-fields were taken and subsequently were averaged and normalised to produce a single flat-field for each filter with good photon statistics. Plate 4.2 shows a typical flat-field image. The object images were then divided by the corresponding flat-field to remove the pixel to pixel variations in quantum efficiency of the detector.

As absolute flux calibration was not possible, it was thought acceptable to remove the additive effects of bias voltage and *hot* pixels (those with much higher than average transfer efficiency), by subtracting a suitably scaled continuum image (due to seeing and focus errors, the shape of the point spread functions were found to be slightly different for each filter so that proper subtraction of the whole stellar image was not possible). As the continuum filter was very close in wavelength to the nebular lines, approximate line ratios could be determined.

During the observing period the seeing was measured in the 3.6m dome and found to be $\sim 1.3''$ (the 3.6m telescope suffers a certain amount of *dome seeing*, and so the true seeing was likely to be $\sim 1''$). This was confirmed by inspecting the actual stellar images when the CCD was read out. A total integration of 5400 sec was obtained at Hα and likewise a 3600 sec integration at [NII] λ6584Å and a further 1200 sec with the continuum filter.

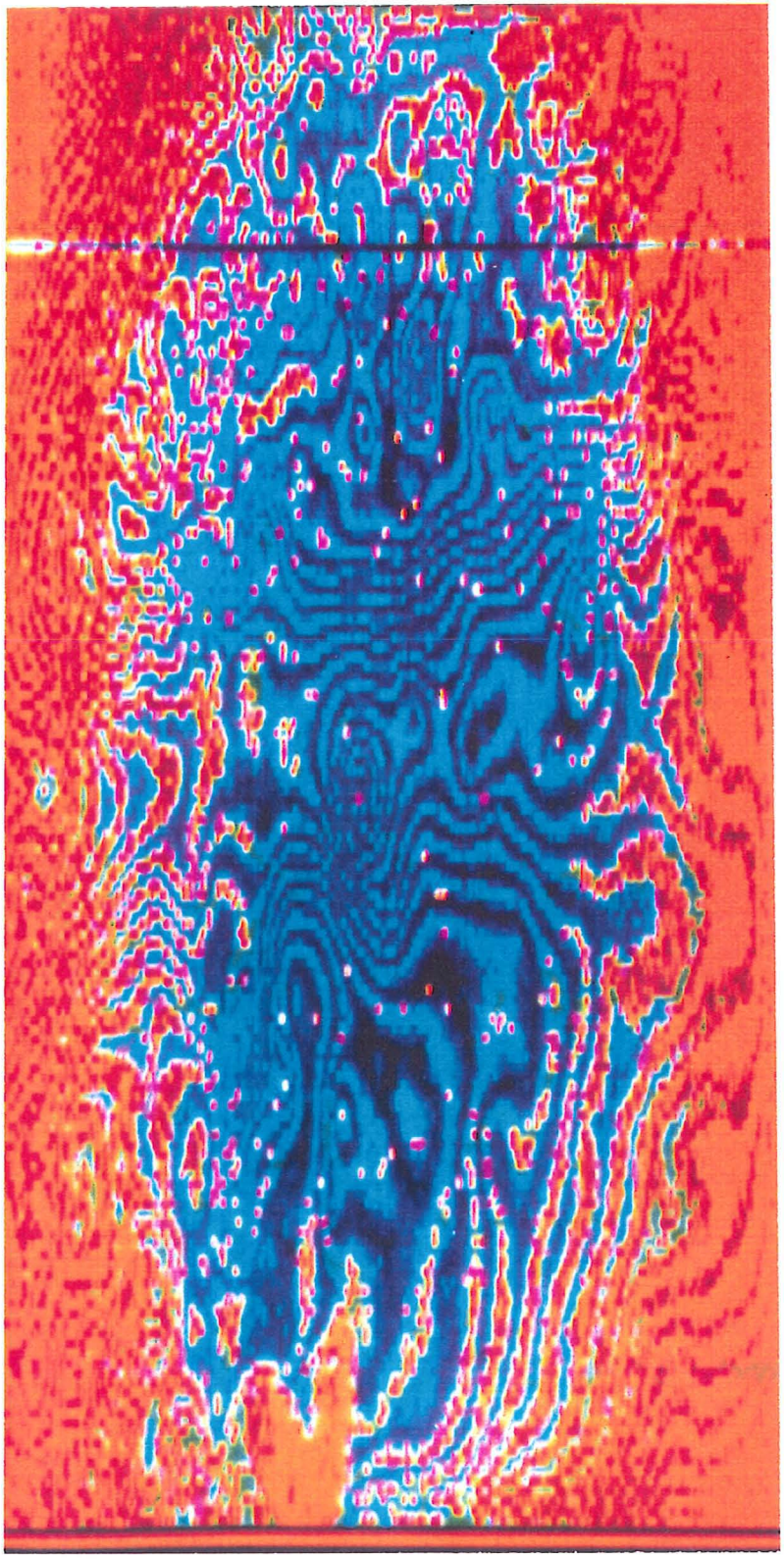

Plate 4.2: Example of a dome flat field.

4.3.2 Results

Plates 4.3–4.5 show the Hα, [NII] λ6584Å and continuum false colour images and Figures 4.2–4.6 the corresponding contour plots and also the continuum subtracted versions (in each case there are 15 contours equally spaced between the background and the highest level). In each case the nebula can be seen to extend some 33″ east—west, and 30″ north—south.

4.4 Discussion

From the above plates and contour maps a number of points are apparent:

(i) there is a striking difference in morphology between the recombination and forbidden line images,

(ii) the Hα image displays a relatively high intensity elliptical region centered on V348 Sgr with possible bipolar structure,

(iii) the [NII] λ6584Å image displays a very sharp rise in intensity towards the central part of the nebula. The elliptical structure clearly visible in the Hα image is not seen,

(iv) on both the Hα and [NII] λ6584Å images the nebulosity is seen to extend north-east towards Heck *et al.* 's star 12 (as suspected from the AAT service plate),

(v) the continuum image suggests that there is a small amount of nebula contamination. Although the nebula is of low excitation, He I lines are detectable (see Chapter 5) and the continuum filter used has been found to have 5% transmission at the He I λ6678Å line.

According to the Khromov and Kohoutek (1968) classification scheme for planetary nebulae, the brightness distribution suggests the nebula is similar to type 1, (ie *a round or ring-like structure of relatively uniform brightness*), or type 3 (ie *a nebula with two (or more) brightness maxima symmetrically placed with respect to the nebular centre*).

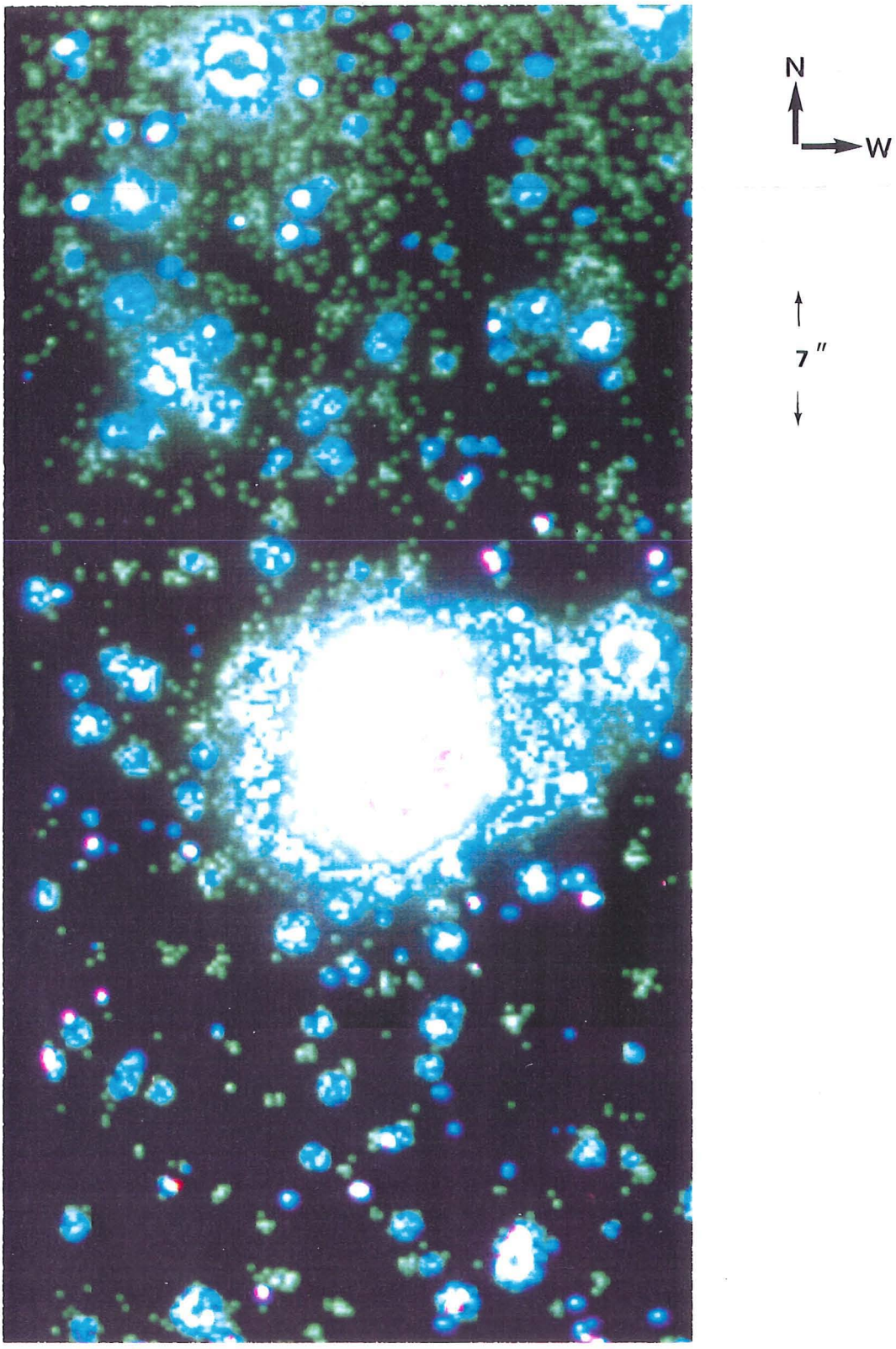

Plate 4.3: Hα image of V348 Sgr.

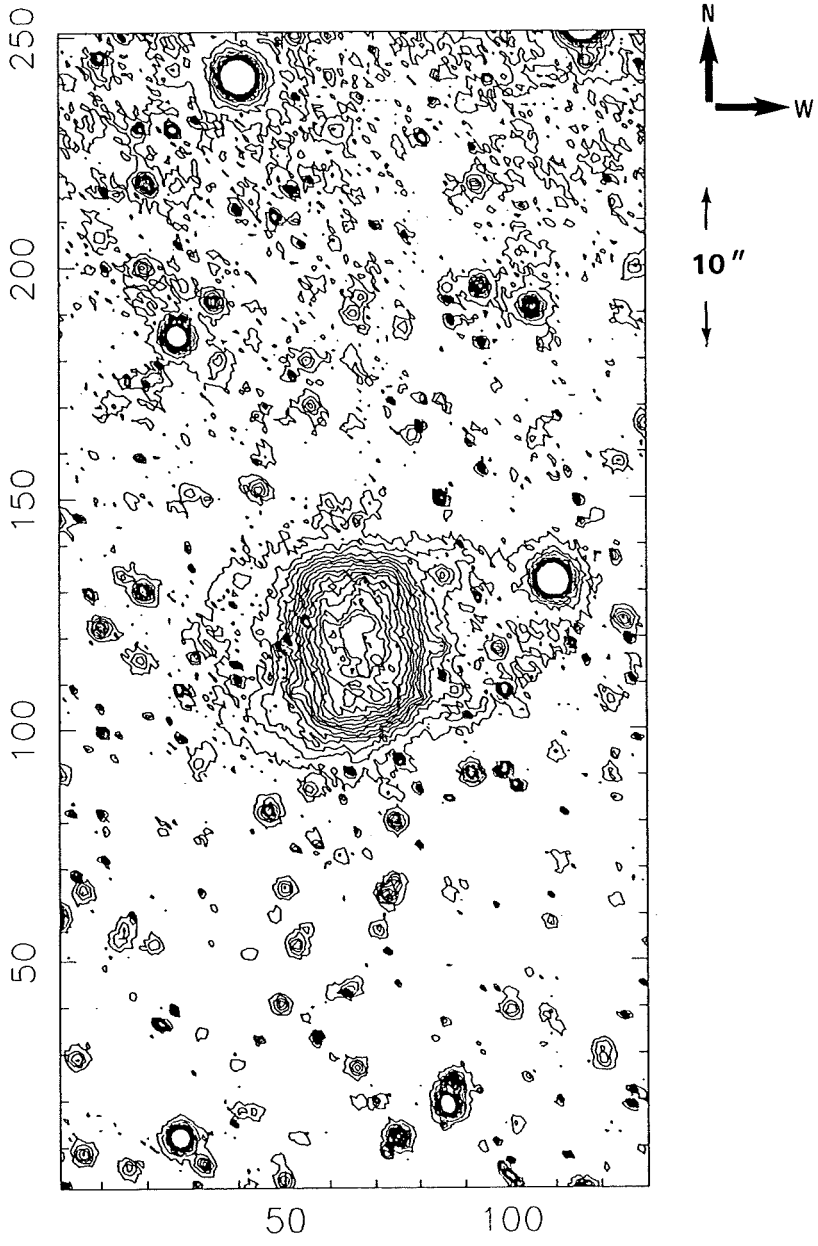

Figure 4.2: Contour plot of Plate 4.3.

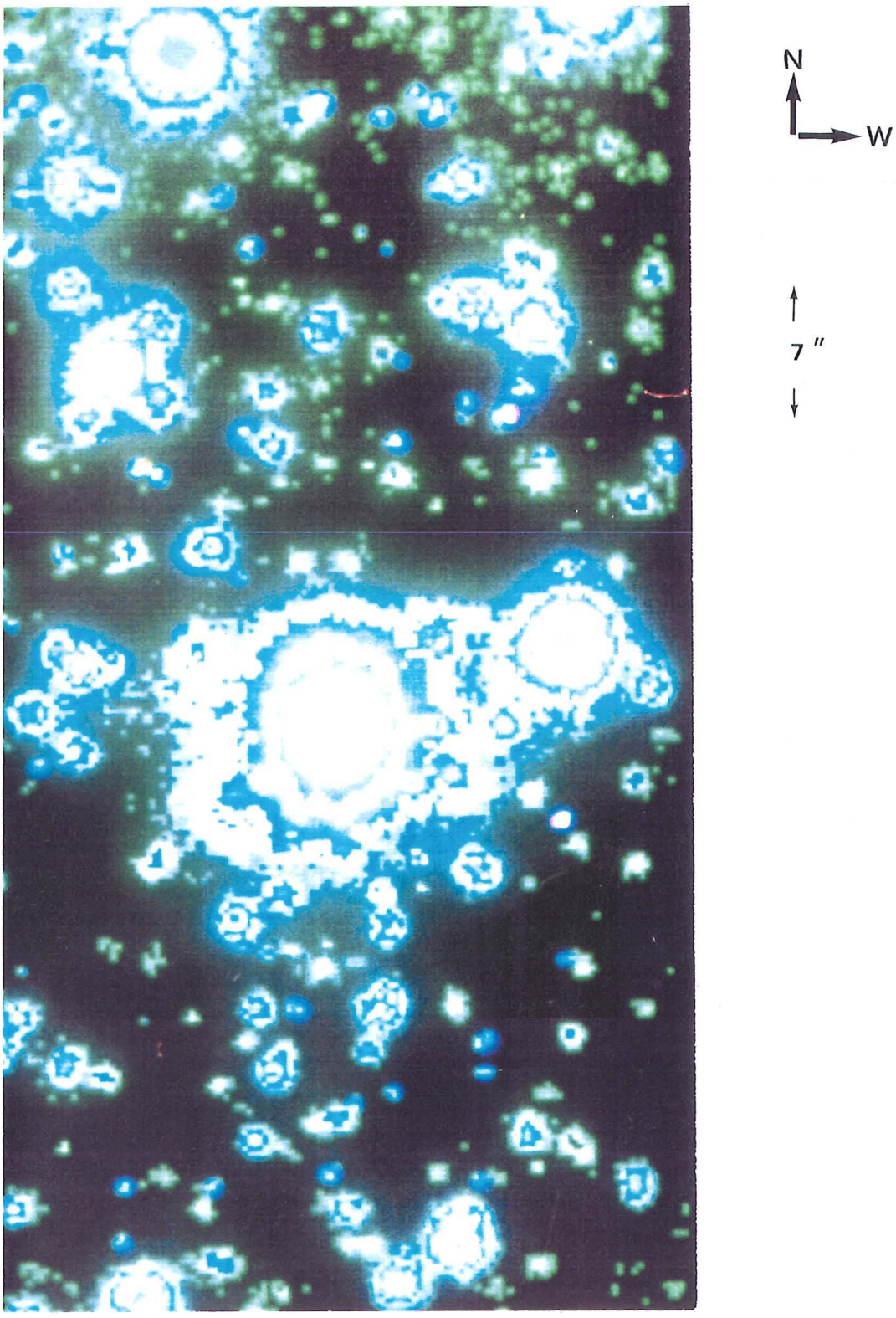

Plate 4.4: [NII] λ6584Å image of V348 Sgr.

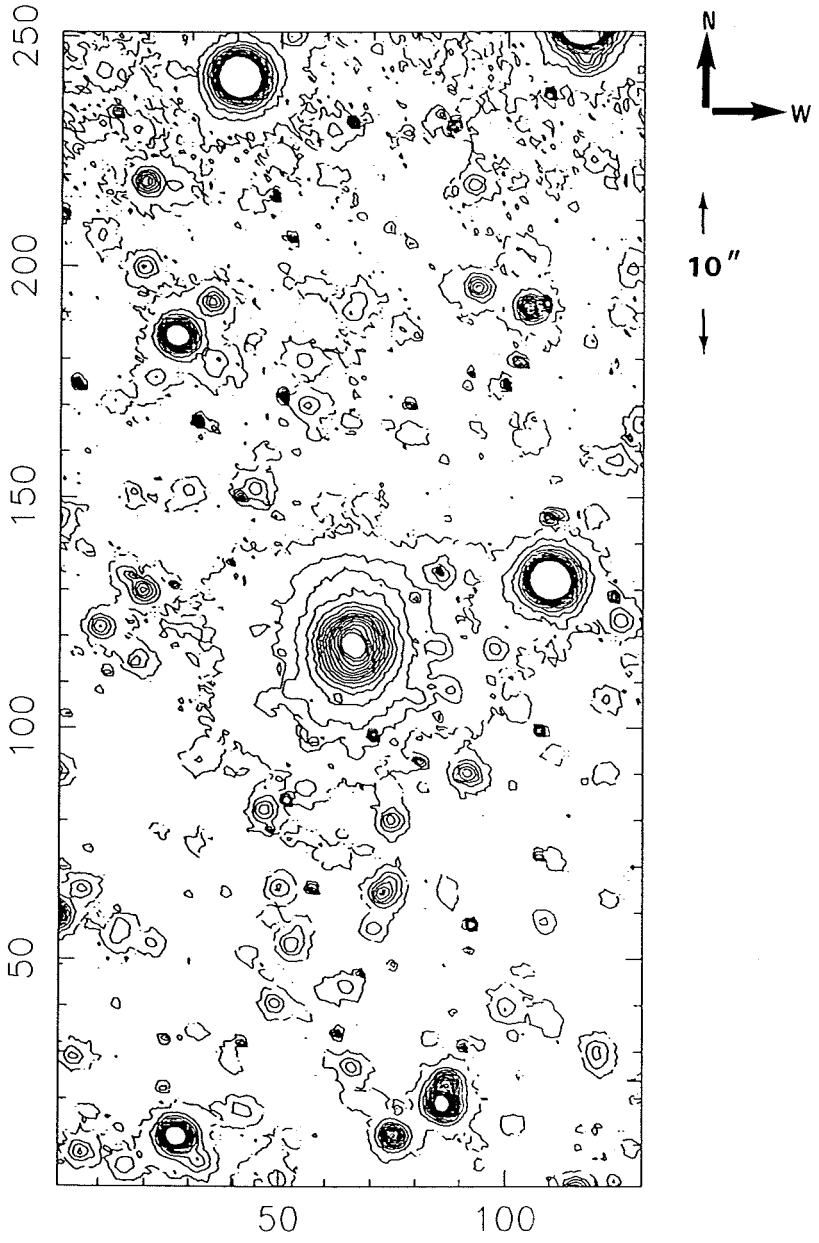

Figure 4.3: Contour plot of Plate 4.4.

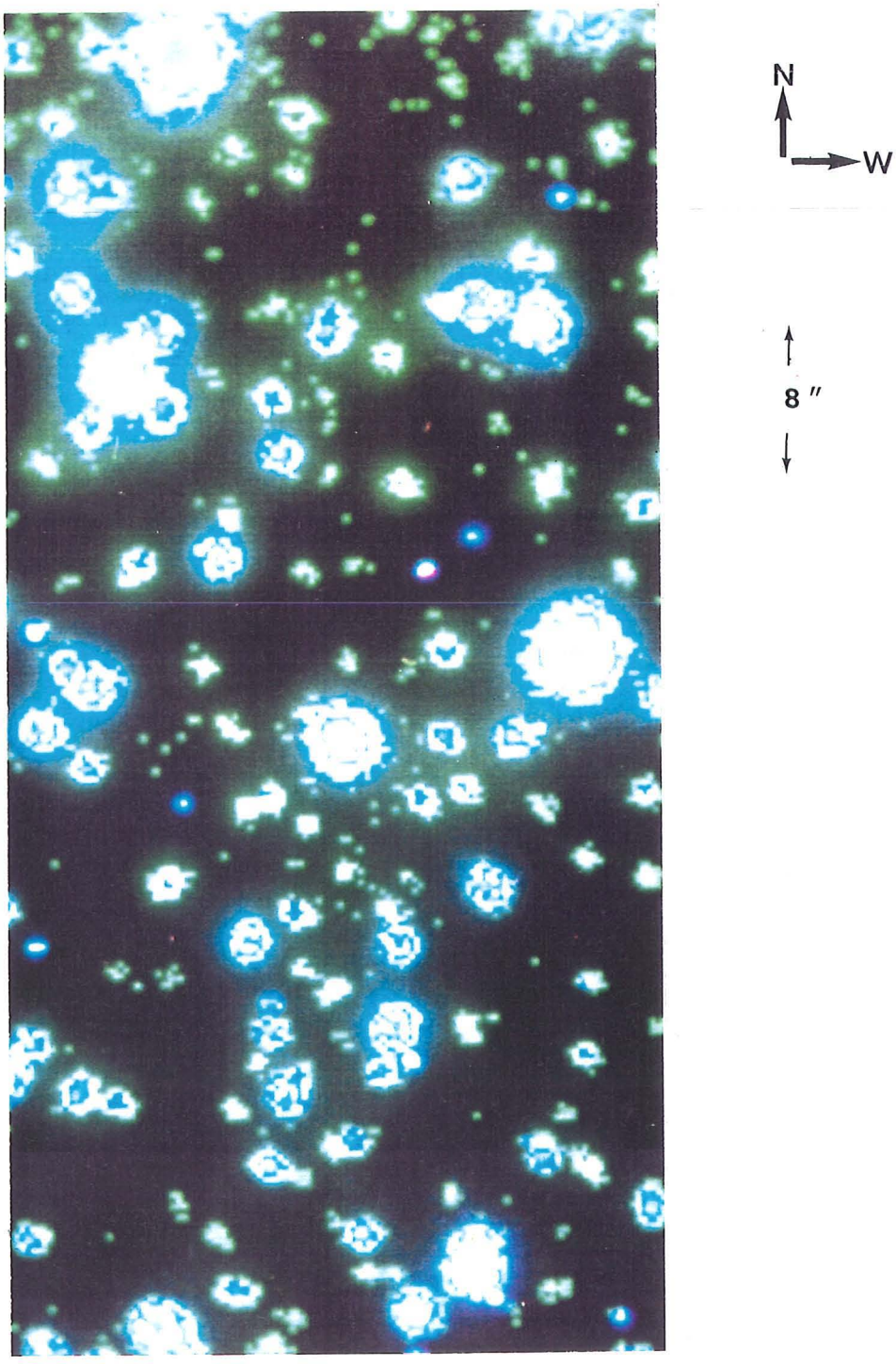

Plate 4.5: Continuum image of V348 Sgr.

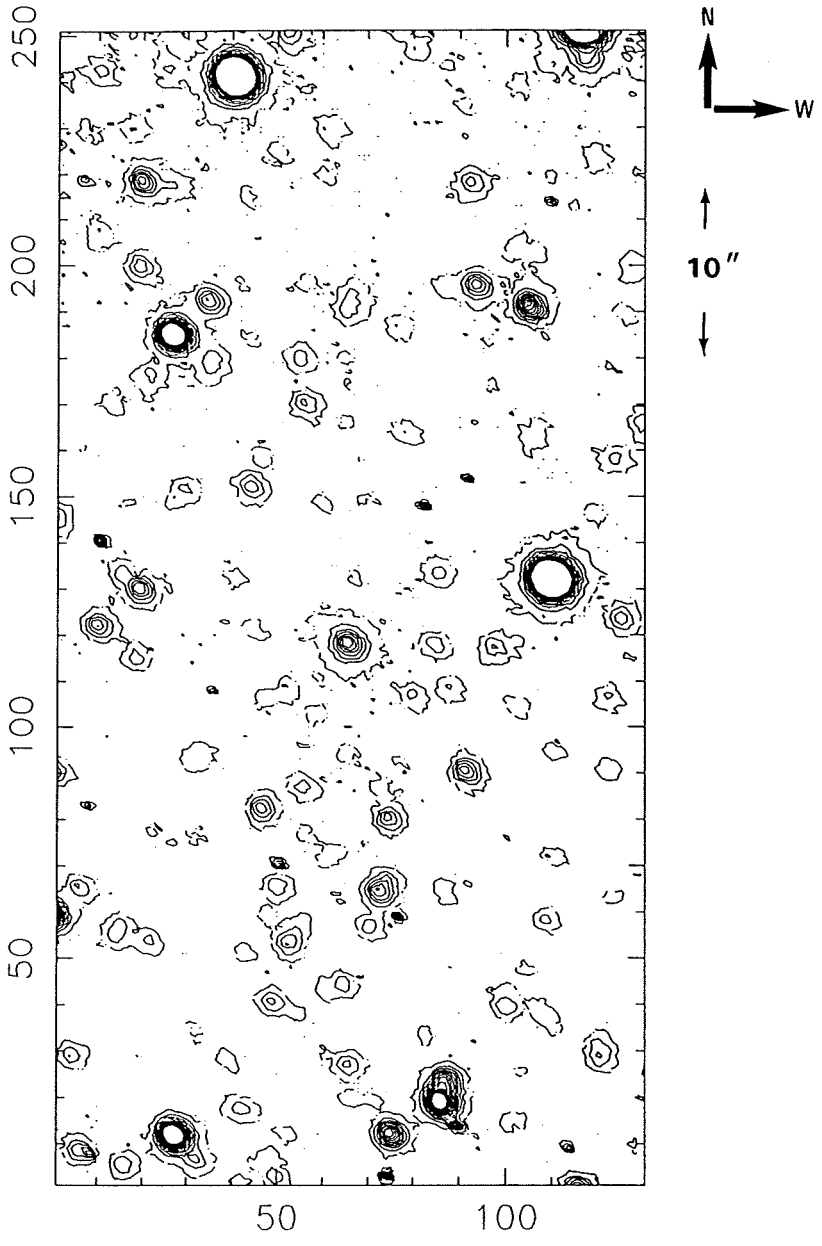

Figure 4.4: Contour plot of Plate 4.5.

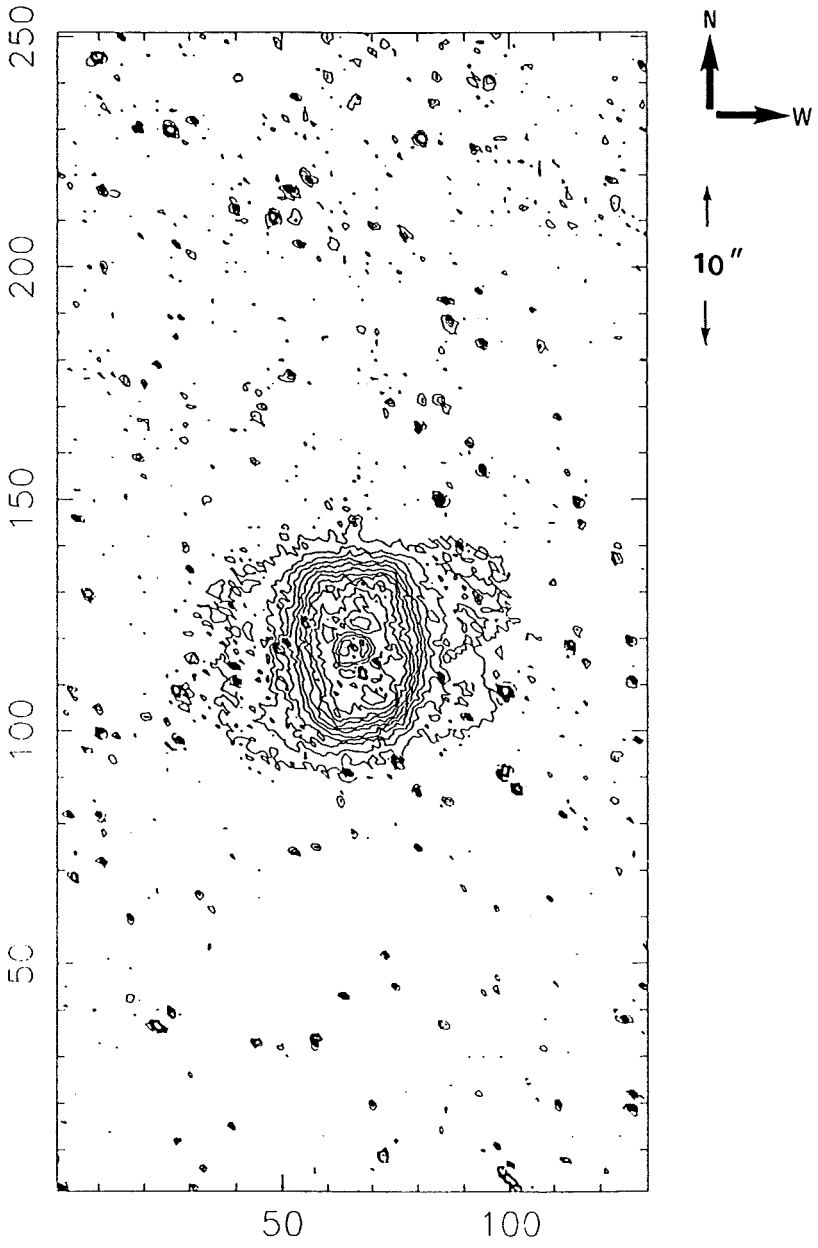

Figure 4.5: Contour plot of Hα—scaled continuum image.

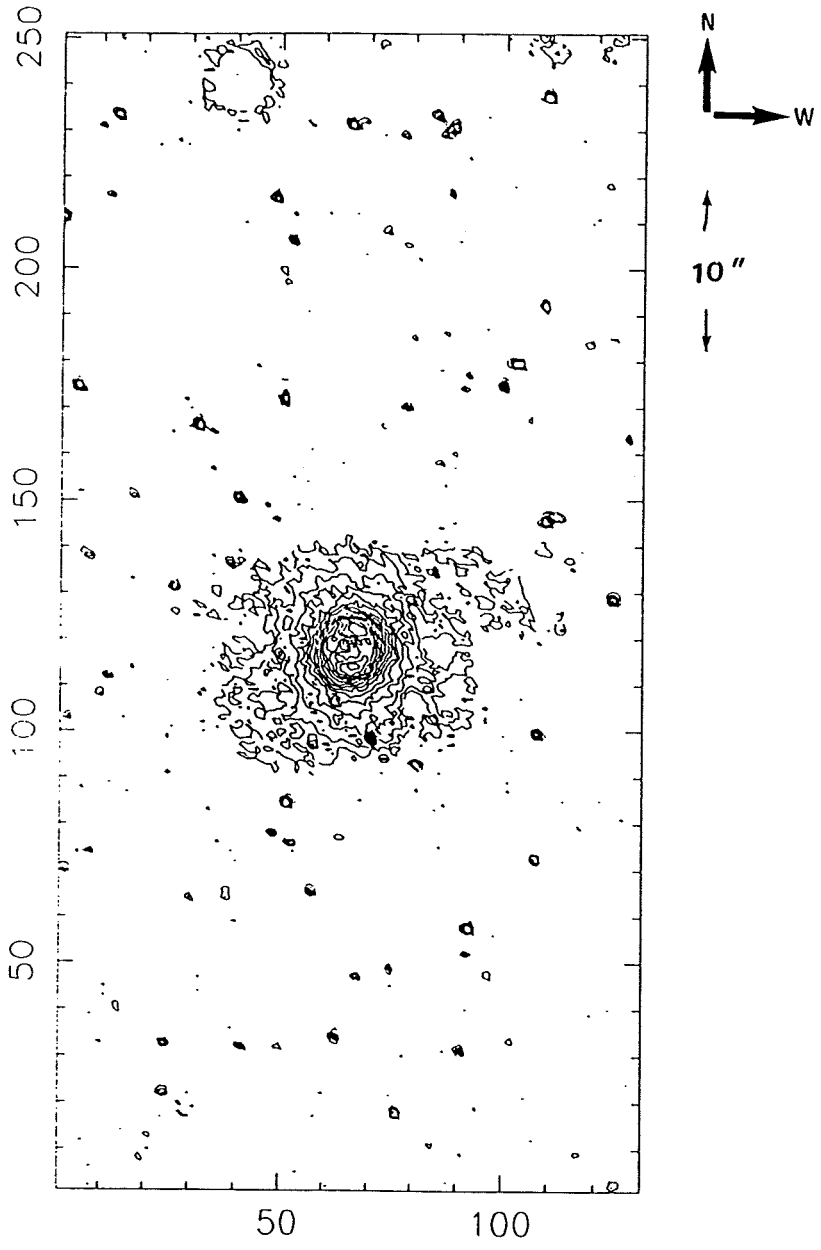

Figure 4.6: Contour plot of [NII] λ6584Å—scaled continuum image.

The continuum subtracted images are useful for determining approximate line ratios over the image, also the ratio of Hα to [NII] λ6584Å were used to demonstrate the striking morphology difference, shown in Plate 4.6 and contour plot, Figure 4.7.

As the Balmer recombination and the [NII] lines are of similar excitation it is reasonable to assume that they both originate from the same region in the nebula, in fact many planetary nebulae do indeed show similar images in these lines (Pottasch, 1984; herafter PN, p.124). Thus assuming a constant density model for the nebula it is difficult to understand the morphology differences. These images are consistent with the recent ejection of nitrogen rich material from the stellar surface demonstrating the highly evolved nature of the star. The data presented in Chapter 5 also suggest there is a strong abundance gradient within the nebula.

4.4.1 Could the nebula be a H II region ?

The nebula classification scheme discussed above is very unlikely to be applicable to H II regions—which tend to be far more irregular in structure. Moreover, this kind of morphology is more easily understood in terms of a directional ejection mechanism (although its exact nature remains a mystery).

The most simple and probably successful model to explain these structures comprises a toroid viewed at an angle, so that the brightness/density maxima are aligned along the line of sight with the thickest part of the toroid (which is dependent on the orientation of the toroid; PN, p.133).

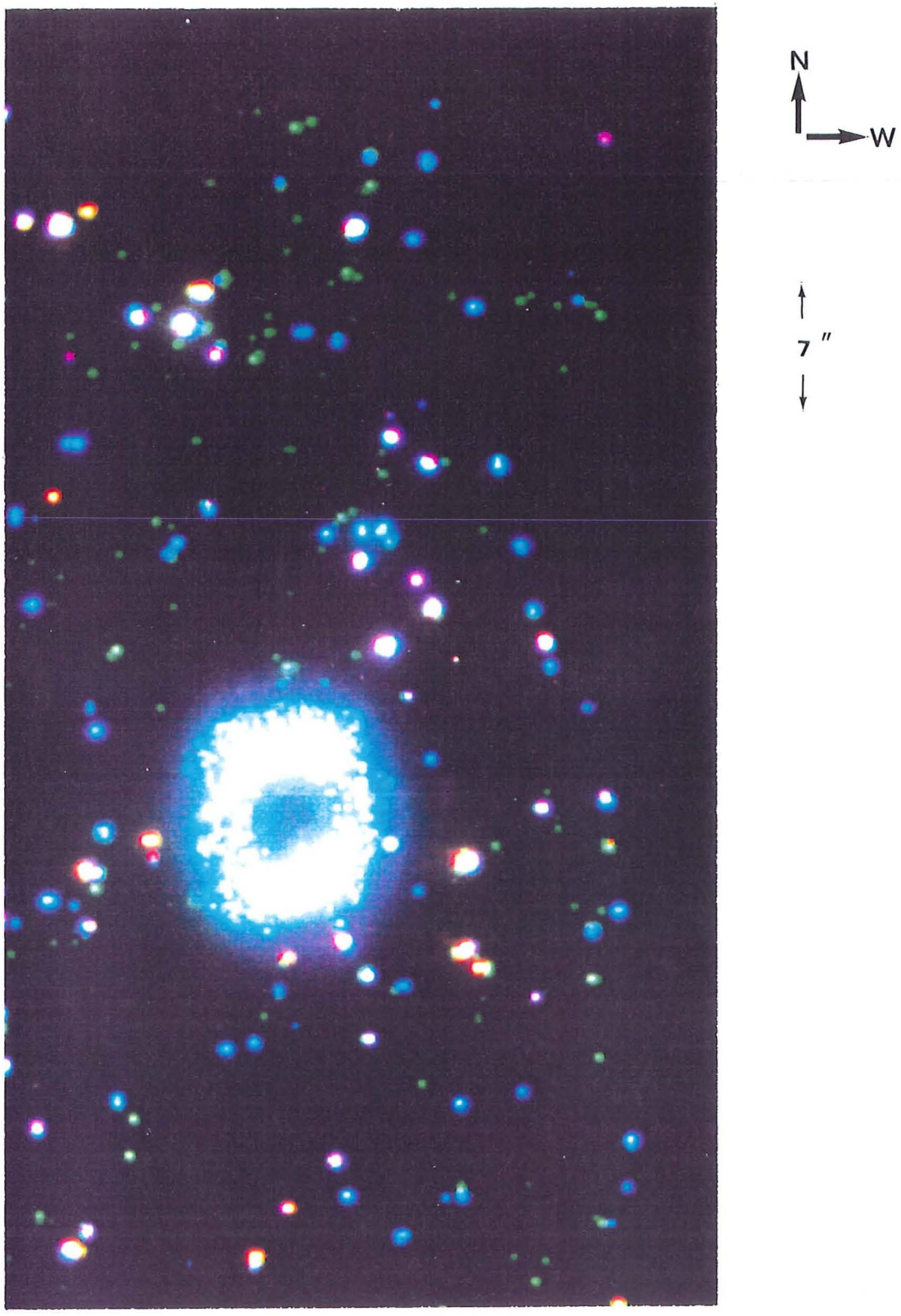

Plate 4.6: The ratio of Hα to [NII] λ6584Å images (both continuum subtracted).

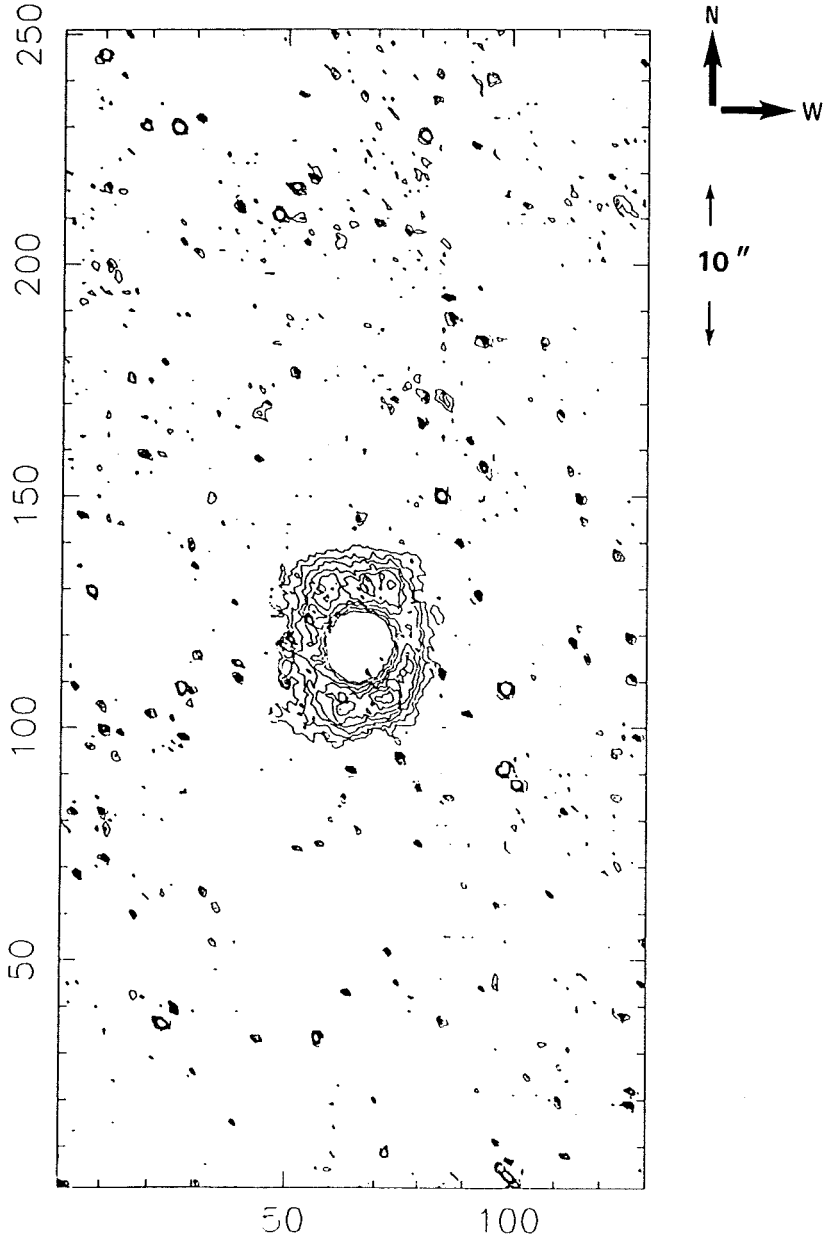

Figure 4.7: Contour plot of Plate 4.6.

4.5 Summary

V348 Sgr is surrounded by an elliptical nebula (33″ × 30″). The brightness distribution within the nebula shows a close resemblance to some bipolar planetary nebulae, hinting that at some epoch in the recent past the nebula was ejected from the stellar surface. It is difficult to understand how a compact H II region could have this structure. Morphology differences between the recombination and forbidden images suggest that significant abundance gradients exist within the nebula.

4.6 References

1. Heck, A., Houziaux, L., Manfroid, J., Jones, D.H.P. and Andrews, P.J., 1985. *Astr. Astrophys. Suppl. Ser.*, **61**, 375

2. Herbig, G., 1957. *Astrophys. J.*, **127**, 312

3. Khromov, G.S. and Kohoutek, L., 1968. In *IAU Symp.* No. **34**, p. 227 (Reidel, Dordrecht)

4. Pottasch, S.R., 1984. In *Planetary Nebulae: A Study of Late Stages in Stellar Evolution*, (Reidel, Dordrecht) (**PN**)

Chapter 5

V348 Sagittarii—long-slit spectroscopy

5.1 Introduction

As discussed in Chapter 4, V348 Sgr has been known for many years to be surrounded by a low excitation nebula. Webster and Glass (1974) and Schönberner (1986) have each stated that V348 Sgr may be of great relevance to our understanding of the later stages of stellar evolution. It is perhaps surprising then, that before this project long-slit spectra had not been published for this object. Dahari and Osterbrock (1985) (hereafter DO) have described aperture spectra of this object taken at different phases of its light curve, but were unable to deconvolve comprehensively the nebula and wind emissions (they were unaware of the large extent of the nebula). They also found that the large zenith distance incurred by observing V348 Sgr from the northern hemisphere resulted in an inaccurate flux calibration, with the blue spectrum seriously depleted by absorption in the atmosphere.

Thus it was felt imperative to obtain spatially-resolved spectra in order to understand more fully the evolutionary status of this star. The aims of this project were:

(i) to determine whether the star in its present state could ionize the nebula,

(ii) to use standard planetary nebula techniques to obtain the physical parameters of the nebula,

(iii) to obtain the abundances in the nebula and hence compare them to the values found by DO for the wind line region (DO call this a chromosphere),

(iv) to compare the nebular reddening, as deduced from the Balmer Decrement with that already determined from observations of the λ2200Å feature, and

(v) observations taken at high spectral resolution would enable a kinematical model for the nebula to be produced.

This work was carried out in collaboration with Dr. C. N. Tadhunter and Dr. P. W. Hill.

5.2 Observations

The RGO spectrograph with the Image Photon Counting System (IPCS: Boksenburg and Burgess 1973) and a GEC CCD as detectors, were used at the f/8 focus of the 3.9 m Anglo–Australian Telescope to obtain long-slit spectra of V348 Sgr. By using the IPCS with the 25 cm camera, the visual spectrum could be covered with one grating setting (250B grating) with resolution adequate to resolve some of the important emission line diagnostics such as the density sensitive [SII] $\lambda\lambda$6717/31Å lines. This configuration also allowed greater accuracy in the flux calibration as distortions within the IPCS make matching of line fluxes between adjacent wavelength regions somewhat unreliable (as would be required with a higher resolution and hence a lower spectral coverage format). The IPCS was used with 2044 frame lines (spectral direction) and 66 line increments (spatial direction). Of this a format of 2040 x 52 was used for data recording. This format produces a slit length of $\sim$ 120″, and by using an x resolution of $\times$4, a pixel size in the spatial direction of $\sim$ 0.6″ was achieved. As the seeing for both nights was never better than $\sim$ 2″ there was no danger of under sampling the seeing disc.

The observations of V348 Sgr on the night of 16^{th} July 1987 were as follows:

(i) three slit positions were chosen with the spatial directions east—west, orientated 4″ north, central and 4″ south of the star. The spectrograph slit was widened

to 4″ to accommodate as much of the nebula as possible. The three integrations totalled 3 000 secs,

(ii) integrations totalling 11 830 secs were secured at position angle (PA) $158^{0}.2$, centred on the star. This PA was chosen to ensure minimum contamination from faint stars within the slit area as suggested from an inspection of the AAT plate (see Chapter 4), and

(iii) the slit was orientated along PA $88^{0}.2$ for 1 800 secs.

During the period of the observations V348 Sgr was known to be recovering from a recent deep minimum (Feast and Pollacco, 1987) and was measured on the AAT TV monitor to have a magnitude of around $16^{m}.5$. Several observations of the standard stars GD 190 (Oke, 1974) and LTT 7379 (Stone and Baldwin 1983) were obtained at differing airmasses during the course of the night. By careful use of neutral density filters the count rates for these stars were kept well below saturation levels for the IPCS. Arc calibration frames were generally taken before and after each star observation (note, the nature of these observations does not require high accuracy in wavelength calibration). After cloud interrupted the observations a flat-field was obtained with the same instrument set up (but different grating angle).

On the second night, observations of V348 Sgr were taken with the CCD (and 250B grating) and will be discussed elsewhere (with hindsight it would have been advantageous to continue the IPCS observations). Due to time limitations, observations were not attempted with a higher resolution grating.

5.3 Reduction procedure

After flat-fielding all the frames (using FIGARO routines) the following reduction procedure was employed.

5.3.1 Wavelength calibration

The arc spectra were calibrated with their associated wavelengths by reference to Schinckel *et al.* (1982). Spurious strong lines were detected suggesting that the arc lamps were contaminated by an unidentified source. However, after much effort suitable identifications were found for about 40 unblended lines allowing an rms error in the wavelength fit of less than 2.5Å (with a 5^{th} order polynomial). After cross-correlating all the arc spectra obtained over the course of the night, the maximum shift was found to be less than 0.5 pixels. The arc spectra were then 2–dimensionally calibrated and the wavelength calibration copied to the object spectra. Reasonable agreement was found between the measured and laboratory wavelengths for some of the night sky lines identified in the 2–d spectra.

5.3.2 Atmospheric extinction and neutral density filter corrections

For all object spectra a correction for atmospheric extinction was applied following the technique suggested in the FIGARO user manual. The only frames requiring a correction for neutral density filters were those taken of the flux standards and the technique suggested in the FIGARO user manual was applied.

5.3.3 Flux calibration

Again, the technique suggested by the FIGARO user manual was used to flux calibrate the standard stars. Figure 5.1 shows the final flux calibration curve obtained, this was then *grown* into a 2–dimensional flux calibration image and applied to the object frames. As a safeguard, flux calibrated spectra of LTT 7379 obtained at different airmasses during the night were compared and the result shown in Figure 5.2. The results suggest that the final flux calibration, after all corrections had been applied, was accurate to better than 15%. The calibration is valid from $\lambda\lambda$3500–7200Å and outside this range the calibration curve suggests large errors may be present. However, as all the important emission line diagnostics lie within this range this calibration will suffice. In order to compare readily the line fluxes with those published for other objects, the images were

calibrated in ergs $cm^{-2}s^{-1}Å^{-1}$.

5.4 Results

After reduction the spectra obtained at PA $158\overset{0}{.}2$ were added together and the cross-sections containing the nebula north of the star extracted from the final 2–dimensional image, see Figure 5.3. The cross-sections south of the star were found to be contaminated by a faint stellar continuum and therefore not used in the subsequent analysis, see Figure 5.4.

As expected the nebula was found to be of very low ionization, with the ratio [OII]/[OIII] $\approx$ 45 (the usually very strong [OIII] λ5007Å line was only just detectable above the noise). However, the Balmer (up to H_8), [NII], [OII], and density sensitive [SII] lines were clearly visible. Unexpectedly, He I recombination lines were also *clearly* detectable.

The slope of the Balmer Decrement was used to deredden the spectrum to the Case B (optically thick in the Lyman lines) values as given by Brocklehurst (1971). It was found that an $E_{B-V} = 0.45 \pm 0.10$ (or $c(H\beta) = 0.66 \pm 0.15$) was required, in excellent agreement with that found by Schönberner and Heber (1986) from dereddening the λ2200Å feature in the UV. Table 5.1 lists the line ID's and their dereddened fluxes. The line fluxes were measured with the aid of the ELF routines within the DIPSO spectrum analysis package. These routines have the advantage that up to 5 blended emission lines may be fitted simultaneously, with the errors between the observed and fitted profile (total) minimized. The quoted line fluxes are accurate to $\sim$ 15–20% for the strongest unblended lines, while the error for weak blended lines maybe 50% or larger, depending on the severity of the blending. There may also be considerable uncertainty in the [OI] $\lambda\lambda$6300, 6363Å and [NII] $\lambda\lambda$5198, 5200Å lines due to possible atmospheric emission at these wavelengths.

The wide-slit observations indicated a total Hβ flux (dereddened) of $(6.75\pm2.05)\times10^{-12}$ erg $cm^{-2}s^{-1}$. This value is in fact a lower limit as some *50%* of the nebula was not covered by our slit postions. However, the correction is much lower than this would suggest as most of the line flux is conscentrated in the central regions of the nebula.

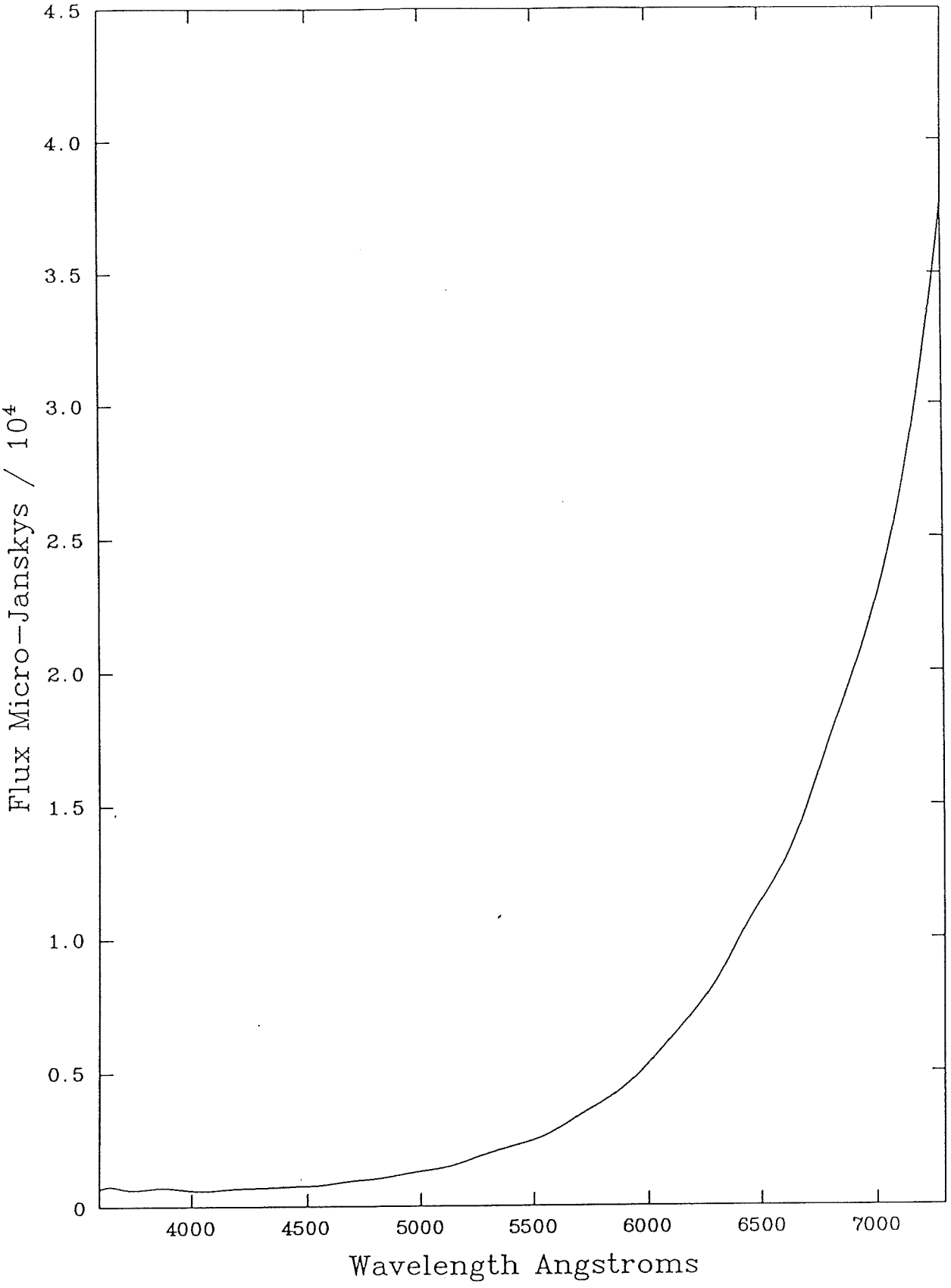

Figure 5.1: Flux calibration curve obtained from LTT 7379 observations.

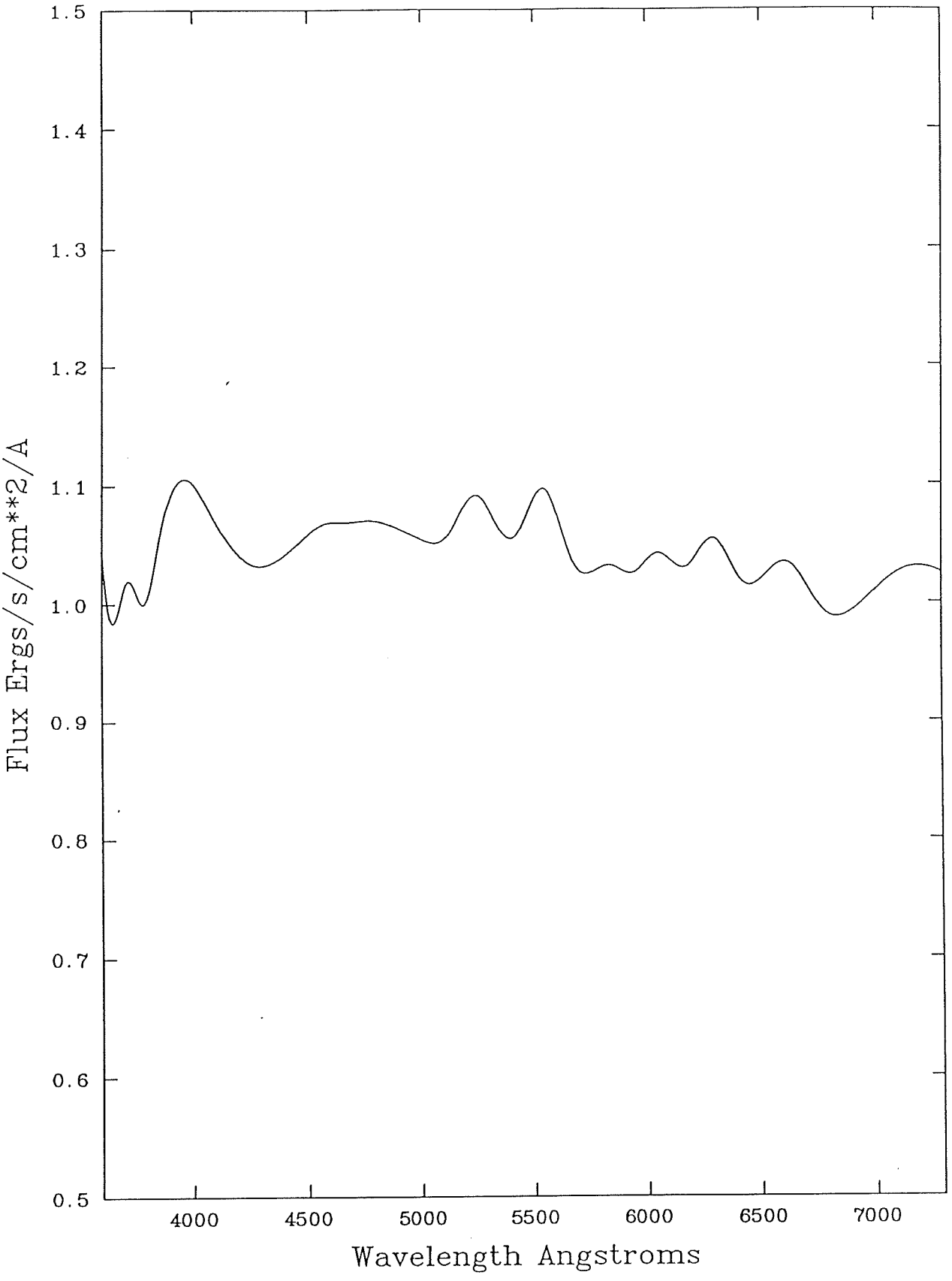

Figure 5.2: Relative calibration of LTT 7379 observations obtained at different air-masses during the night.

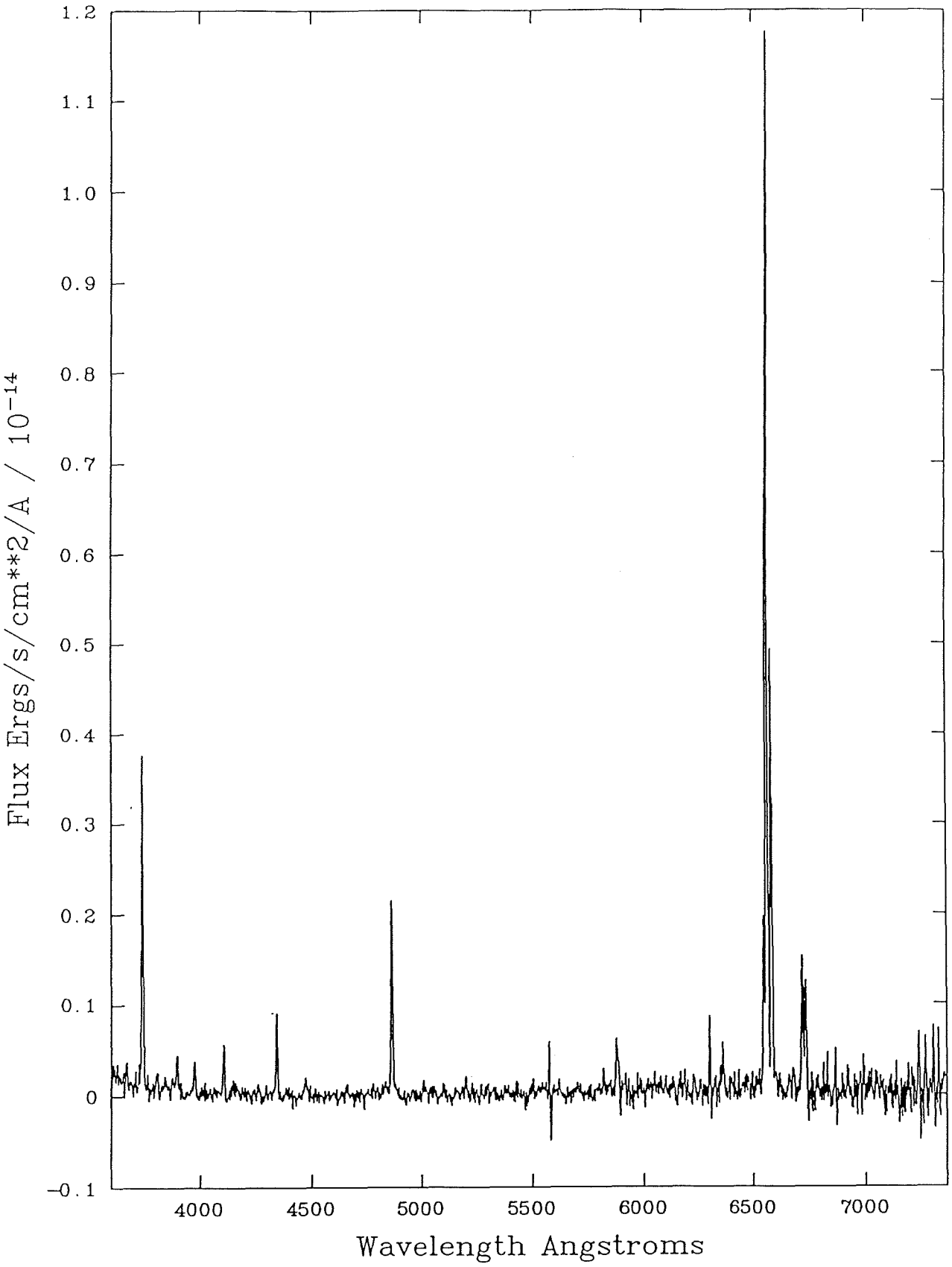

Figure 5.3: Nebula cross-sections north of the central star.

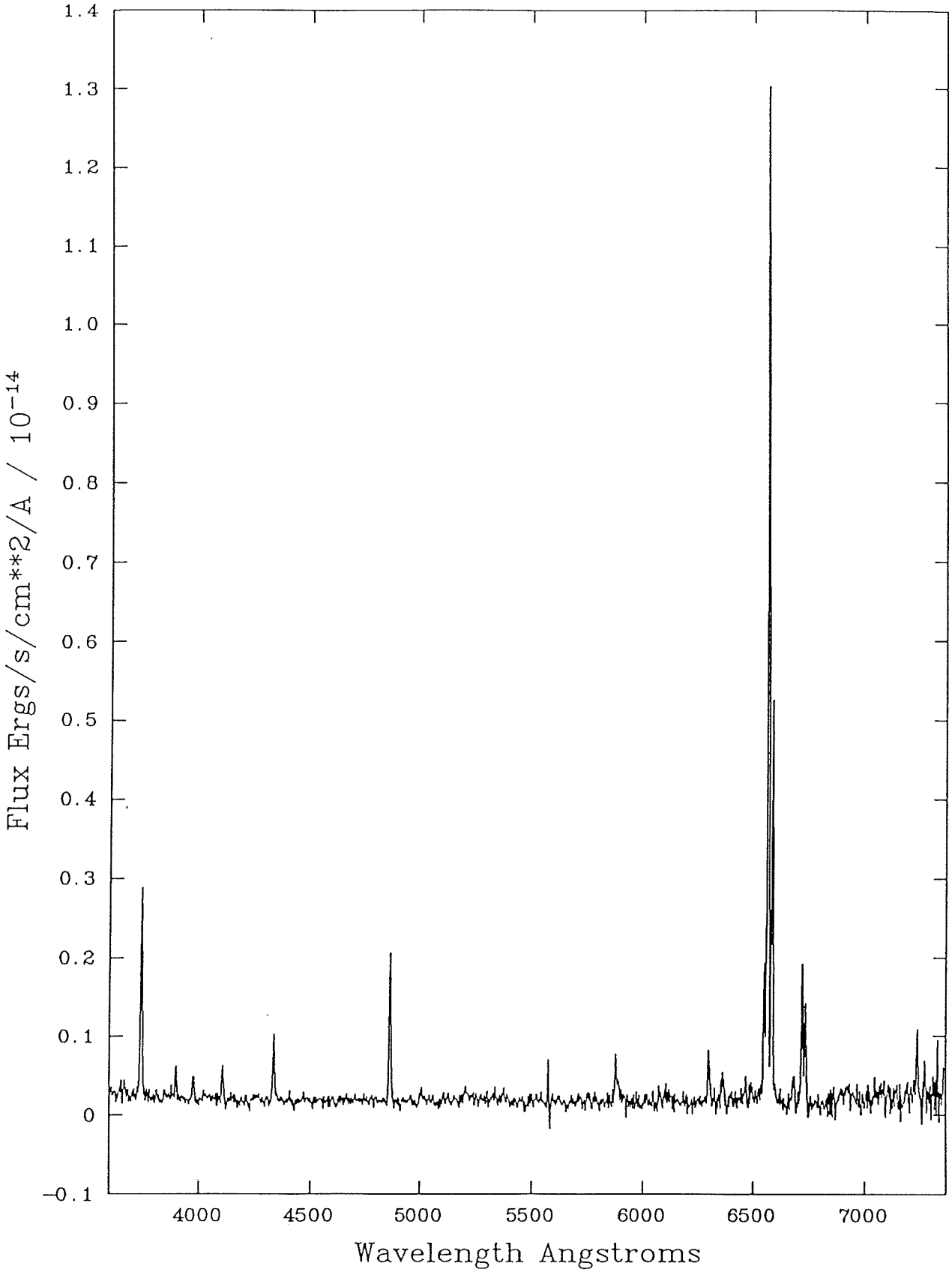

Figure 5.4: Nebula cross-sections south of the central star with a faint stellar continuum from an embedded faint star.

The spectrum obtained at PA $88^{0}.2$ showed no significant variations in line ratios compared to those in PA $158^{0}.2$, but the emission was detectable over a greater radius from the central star.

Table 5.1: Identifications and line fluxes for the nebula surrounding V348 Sgr.

Wavelength Å	ID	Dereddened Flux†
3730	[OII]	222.2
3897	H_8 + He I	23.0
3975	Hϵ	20.6
4104	Hδ	22.1
4341	Hγ	45.3
4471	He I	12.1
4862	Hβ	100.0
5008	[OIII]	5.2
5200	[NI]	5.3
5878	He I	24.7
6296	[OI]	17.0
6358	[OI]	9.1
6550	[NII]	48.5
6565	Hα	302.0
6586	[NII]	132.0
6720	[SII]	36.6
6734	[SII]	33.9

† $100 \equiv 1.03\text{x}10^{-13}$ erg $cm^{-2}s^{-1}$

5.5 The physical conditions in the nebula

In order to determine the electron temperature (T_e) of the nebula it was necessary to determine the ratio of temperature sensitive lines, such as the [OIII] $\lambda\lambda$5007/4363Å or the [NII] $\lambda\lambda$5755/6584Å lines. As can be seen from Table 5.1 the [NII] λ5755Å line was

not detected, so only an upper limit can be placed on this ratio. However, this has only a minor effect on the relative strength of the density sensitive [SII] λ6717 and λ6731Å lines, so a reliable estimate of the electron density (n_e) may still be found.

From Figure 5.3, we can estimate that a line with flux $> 0.9\%$ of Hβ would be just detectable at λ5755Å. Thus the ratio of the [NII] lines is:

$$\frac{I_{6584} + I_{6548}}{I_{5755}} > 200$$

Using Equation (5.5) of Osterbrock (1974) (hereafter AGN) an upper limit of T_e was obtained and found to be $T_e < 7000\,K$.

Atomic data for this and subsequent calculations were taken from the references given by Monk *et al.* (1988).

From the fluxes given in Table 5.1 the [SII] $\lambda\lambda$6731/6717Å ratio implies $n_e \approx 350\,cm^{-3}$. A noisy, but higher resolution spectrum obtained at the INT of the density sensitive [OII] lines suggests an n_e of $< 350\,cm^{-3}$ (see Figure 5.5), a value close to the low density limit for the ratio. This spectrum was obtained with a similar instrument set up as that used for the AAT observations except a 1200V grating was used, with the slit placed on PA $158^{0}_{.}2$. At the time of observation the star was again at an intermediate brightness.

Considering the large zenith distance of the object and lower count rate incurred, this result is reasonably consistent with the AAT observations, but may suggest that the [OII] and [SII] lines are formed in separate regions of the nebula with presumably the [OII] lines formed further from the central source. In the subsequent analysis a uniform electron density of $n_e = 350\ cm^{-3}$ was assumed.

As we are dealing only with relative line fluxes, the close proximity in wavelength between the diagnostic lines implies that the line ratios are relatively insensitive to the actual value of the reddening adopted.

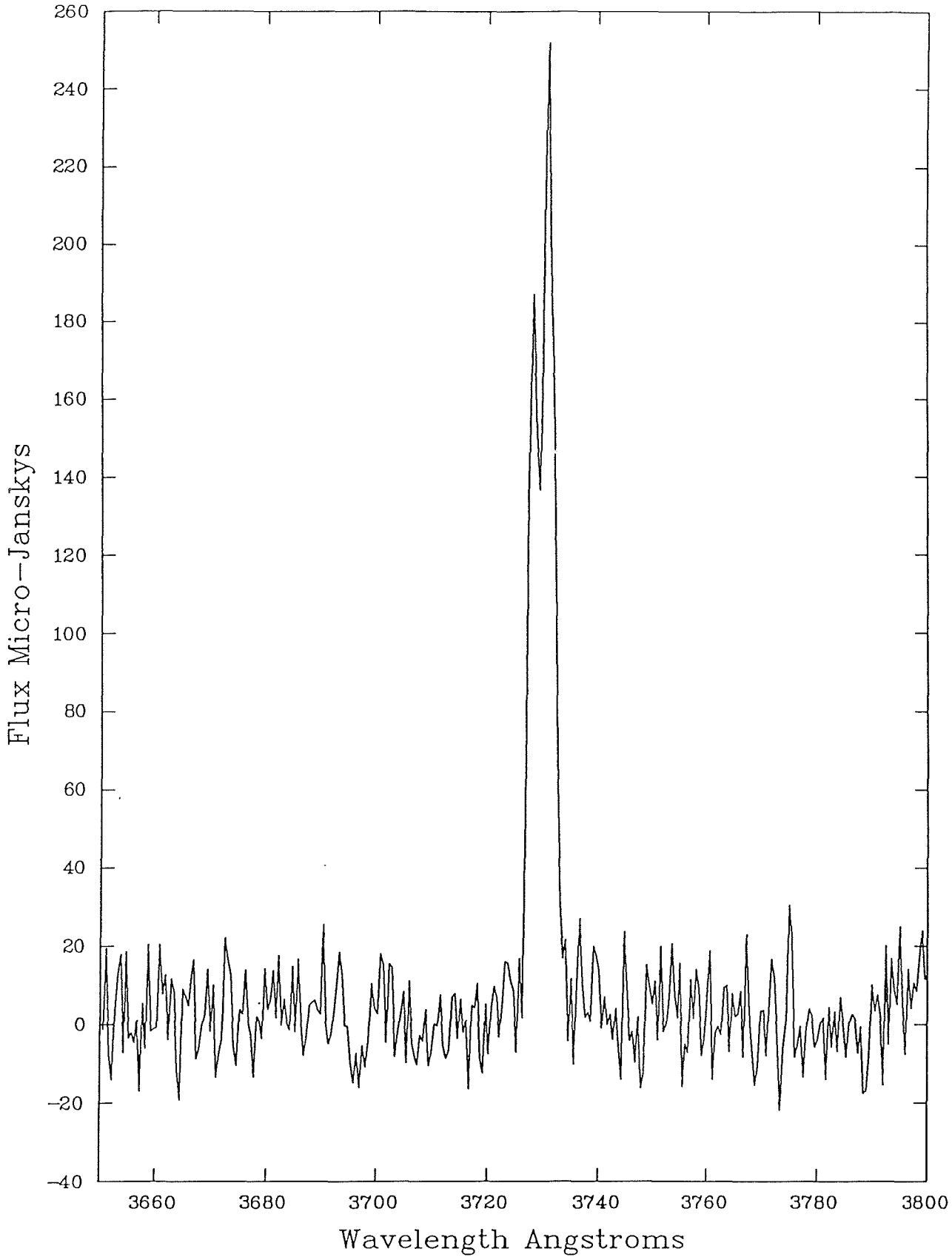

Figure 5.5: The density sensitive [OII] $\lambda\lambda$3726/3729Å lines as observed from the INT on 12/13th September, 1987.

5.6 Abundances in the nebula

Assuming the nebula to be homogeneous with constant T_e and n_e, it is straight forward to derive the abundances from the relative fluxes given in Table 5.1 (AGN, p.97). As discussed earlier, the upper limit on the value of T_e leads to a lower limit for the ionic abundance as determined by their forbidden lines. However, it is important to note that for most forbidden lines, the emission is critically dependent on T_e. (Note, in these calculations the predicted dereddened Hβ flux was used).

In principle, the He^+ abundance can be determined from the He I recombination lines, however, in such a low excitation nebula there is undoubtedly a large fraction of neutral (He^0), and hence unobservable material. Thus the N(He)/N(H) ratio given in Table 5.2 is a lower limit. As these are recombination lines, the ratio of abundances is given by:

$$\frac{N(He)}{N(H)} = \frac{KI_\lambda}{I_{H\beta}} \tag{5.1}$$

where

$$K = \frac{\nu_{H\beta}\alpha_{H\beta}}{\nu_\lambda\alpha_\lambda} \tag{5.2}$$

Here α_λ is the total recombination coefficient from a line of wavelength λ. The values for the constant K (derived at $T_e = 6000\,K$) were taken from Pottasch (1984, p.47) (hereafter PN).

Adopting $T_e = 7000\,K$ for the forbidden line analysis, Table 5.3 shows the relative abundances for the nebula compared with those obtained for an *average* planetary nebula and also NGC 1976—a gaseous nebula (AGN, p.132).

As the nebula is of low excitation it is likely that all the important ions have representative lines in the optical (especially N and O) and so ionization correction factors are not required (for unobserved ionization states). However, for S, it is likely that the near

Table 5.2: Lower limits of relative abundances in nebula.

ion	line Å	N(ion)/N(H) x10^2	Mean relative abundance of ion
[OI]	6300	0.0153	0.0201
[OI]	6363	0.0248	
[OII]	3726	0.0580	0.0545
[OII]	3729	0.0510	
[OIII]	5007	0.0008	0.0008
[NI]	5199	0.0015	0.0015
[NI]	5200	0.0015	
[NII]	6548	0.0081	0.0078
[NII]	6585	0.0075	
[SII]	6720	0.0005	0.0005
[SII]	6731	0.0005	
He I	4471	23	20
He I	5876	16	

Table 5.3: V348 Sgr nebula abundances compared with other objects.

Element	Logarithm of relative abundance		
	V348 Sgr—nebula	*Average* PN	NGC 1976
H	12.00	12.00	12.00
He	11.29	11.23	11.04
O	8.9	8.9	8.79
N	8.0	8.1	7.63
S	5.7	7.9	7.5

IR [SIII] and possibly the far IR [SI] lines are also excited, thus the derived abundance suggests that a large correction factor may be necessary.

5.6.1 The Helium abundance

Although the He I lines are weak the abundance derived from them is of sufficient precision to allow some important conclusions to be drawn:

(i) The He/H number ratio of > 0.195 suggests significant quantities of nuclear processed material has been ejected in the recent past. The He I lines are detectable far out in the nebula so that wind line emission contamination may be ruled out.

(ii) It is extremely unusual to find extended helium emission associated with a nebula and central source of such low ionization.

(iii) As the ionization potential of Hydrogen (13.6 eV) is substantially lower than that of Helium (24.5 eV), it is more fully ionized within the nebula. Helium ionization remains incomplete until central source temperatures of around 35 000 K are reached and so the derived helium abundance is probably a lower limit to the actual abundance as there must be significant fraction of neutral material contained in the nebula.

Because of the uncertainties in the Helium abundance the effects of collision excitation on the helium lines were not corrected for (Clegg, 1987, notes that these effects can reduce the observed Helium abundance by as much as 10% in some cases although the corrections for low density nebulae are generally much less).

5.7 Modelling the nebula

5.7.1 Simple ideas

For a pure hydrogen nebula the volume of gas which a star may ionize is limited to that volume in which the total recombination rate just balances the stellar ionizing flux. The corresponding radius of the sphere is called the *Strömgren Radius* and is given by:

$$R_s = \left(\frac{3Q_{uv}}{4\pi n^2 \alpha_{tot}}\right)^{1/3} \tag{5.3}$$

where n is the hydrogen density ($\sim n_e$), Q_{uv} is the ionizing flux of the star (in photons s^{-1}) and α_{tot} is the total recombination coefficient to $n = 2$ from all higher levels (including the continuum) and is given by the expression:

$$\alpha_{tot} = 2 \times 10^{-16} T^{-\frac{3}{4}} \tag{5.4}$$

The presence of other elements and also dust within the nebula reduces the number of ionizing photons available, thus the Strömgren Radius may be reduced further.

Inserting values for n_e and determining α_{tot} at 7000 K, the Strömgren Radius (in pc) may be determined from:

$$R_s = 6.3 \times 10^{-17} \sqrt[3]{Q_{uv}} \tag{5.5}$$

Table 5.4 shows the results of this calculation for different *main sequence stars.*

The determination of Q_{uv} is fraught with problems, as the behaviour of stellar atmospheres in the extreme UV (EUV) are still not well known. As many central stars of planetary nebula are high gravity objects while some exciting stars in H II regions are supergiants, these results may prove misleading.

As discussed in Chapter 4, the maximum diameter found for the nebula was about 33″, or at a distance of 4.7 kpc (see Chapter 6) a radius of around 0.38 pc is implied. From Table 5.4 this suggests a stellar surface temperature of around 27 000 K. However, given the possible errors in the above procedure this is not conclusive.

As the main purpose of this investigation was to determine if the star in its present state could ionize the nebula, it is important to investigate the nebular ionization more thoroughly.

Table 5.4: Strömgren radius for different spectral types

	T $K/10^3$	M_v	Q_{uv} *log photons* s^{-1}	R_s *pc*
O5	40.3	-5.4	49.9	2.721
O6	39.0	-5.3	49.1	1.473
O7	37.5	-5.1	48.9	1.263
O8	35.6	-4.8	48.6	1.003
O9	33.2	-4.5	48.2	0.738
O9.5	31.6	-4.0	47.9	0.586
B0	29.5	-3.8	47.5	0.431
B1	25.0	-3.2	47.0	0.294
B2	21.5	-2.5	46.0	0.136
B3	19.0	-2.0	45.2	0.074
B4	17.0	-1.6	44.3	0.037
B5	15.4	-1.3	43.6	0.022
B6	14.1	-0.9	42.2	0.007
B7	13.0	-0.5	39.9	0.001

Data for T, M_v and Q_{uv} obtained from: Böhm-Vitense (1981), Balona and Crampton (1974) and Georgelin *et al.* (1975) and extrapolated to the later spectral types.

5.7.2 The Stoy or energy balance temperature

The *forbidden* lines found in the spectrum of a gaseous nebula are caused by electron collisions and are the primary source of heat loss from the system. The heat input to the nebula is by photoionization and the excess photon energy is passed to the ejected electrons. Thus the ratio of the total forbidden line flux to that in a hydrogen recombination line is a direct measure of the excess energy of the original ionizing photon. Hence the stellar temperature may be determined. This technique was originally discussed by Stoy (1933) and extended to more realistic situations in PN (p.179). In an ordinary planetary nebula this method generally serves only to supply lower limits, as forbidden lines not included (ie those in unobservable spectral regions) may have an adverse effect on the value of the final ratio. For very low excitation regions, most of the expected cooling lines are observable in the optical region and hence reliable temperatures may be determined (as discussed earlier it may prove important to include the flux from the IR [SI] and [SIII] lines). For the nebula surrounding V348 Sgr the value of this ratio is:

$$\frac{\sum F_{fl}}{F_{H\beta}} = \frac{510}{100} \tag{5.6}$$

By comparison with Figure VII–9 of PN (p.181) a black body surface temperature of at least 25 000 K is indicated. Correction for unobserved forbidden lines would serve to increase the ratio and hence imply a significantly greater surface temperature.

5.7.3 The Zanstra Temperature

The Zanstra technique enables the number of photons with $\lambda < 912$Å to be determined by observing the stellar continuum (usually in the visual region) and the flux in a recombination line such as Hβ. The theory behind this method has been adequately dealt with by PN (p.166). The fundamental assumption that this is based on is the so-called *on the spot approximation* which requires that the nebula is optically thick to all radiation with $\lambda < 912$Å. Thus all Lyman radiation is absorbed within the nebula, so that the direct measurement of a Balmer recombination line gives an indirect estimate

of the radiation field in the extreme UV (EUV). By comparing the number of EUV photons with those emitted in the optical a surface temperature for the central star may be inferred (with suitable assumptions regarding the continuous energy distribution of the central source).

In the case of V348 Sgr, the situation is complicated by the significant circumstellar reddening incurred by the central star. From a consideration of the C II line intensities (thought to be formed close to the star), DO estimated a circumstellar reddening (when the star was at an intermediate brightness) of $E_{B-V} \sim 0.9$, while Schönberner and Heber (1986) deduced that the observed UV spectrum was consistent with a circumstellar reddening of $E_{B-V} \sim 0.15$ (however, this later result is expected as all IUE spectra of this object were taken when the star was at maximum). The AAT spectra of the central star (Figure 5.6) obtained during this project also indicate $E_{B-V} \sim 0.9$ (from the Balmer decrement), however, the possibility of wind emission contamination from other ionic species is high. For the subsequent analysis it is assumed that at the time of the observations the central star was reddened by $E_{B-V} \sim 0.9$. This is an upper limit for E_{B-V}.

The STARLINK package DIPSO was used to determine the Zanstra temperatures for the H I and the He I lines (T_z(H) and T_z(He) respectively) thus measuring the stellar flux with $\lambda < 912$Å and $\lambda < 504$Å. In each case the stellar flux distribution was assumed to be a black body and the continuum flux was measured in a region around λ4200Å where any emission lines that may be present are weak and so it was assumed to be the true stellar continuum (see Figure 5.6). The calculation also requires an estimate of T_e in the nebula, but is insensitive to the actual value used (7 000 K). Note, variations of several 1 000 K in T_e only produce a change in T_z of several 100 K. The results of this analysis are shown in Table 5.5. Variations of $\pm$ 30% in the line flux produce a variation of only a few 1 000 K in T_z.

Although it is not unusual for T_z(H) and T_z(He) to be in disagreement, this usually only occurs at much higher stellar temperatures, suggesting that the difference may indeed be real. One possible explanation is that the central parts of the nebula are extremely hydrogen-deficient and as this region is also known (Walker, 1986) to contain large quantities of dust (presumably heated by the stellar UV radiation field) the effective

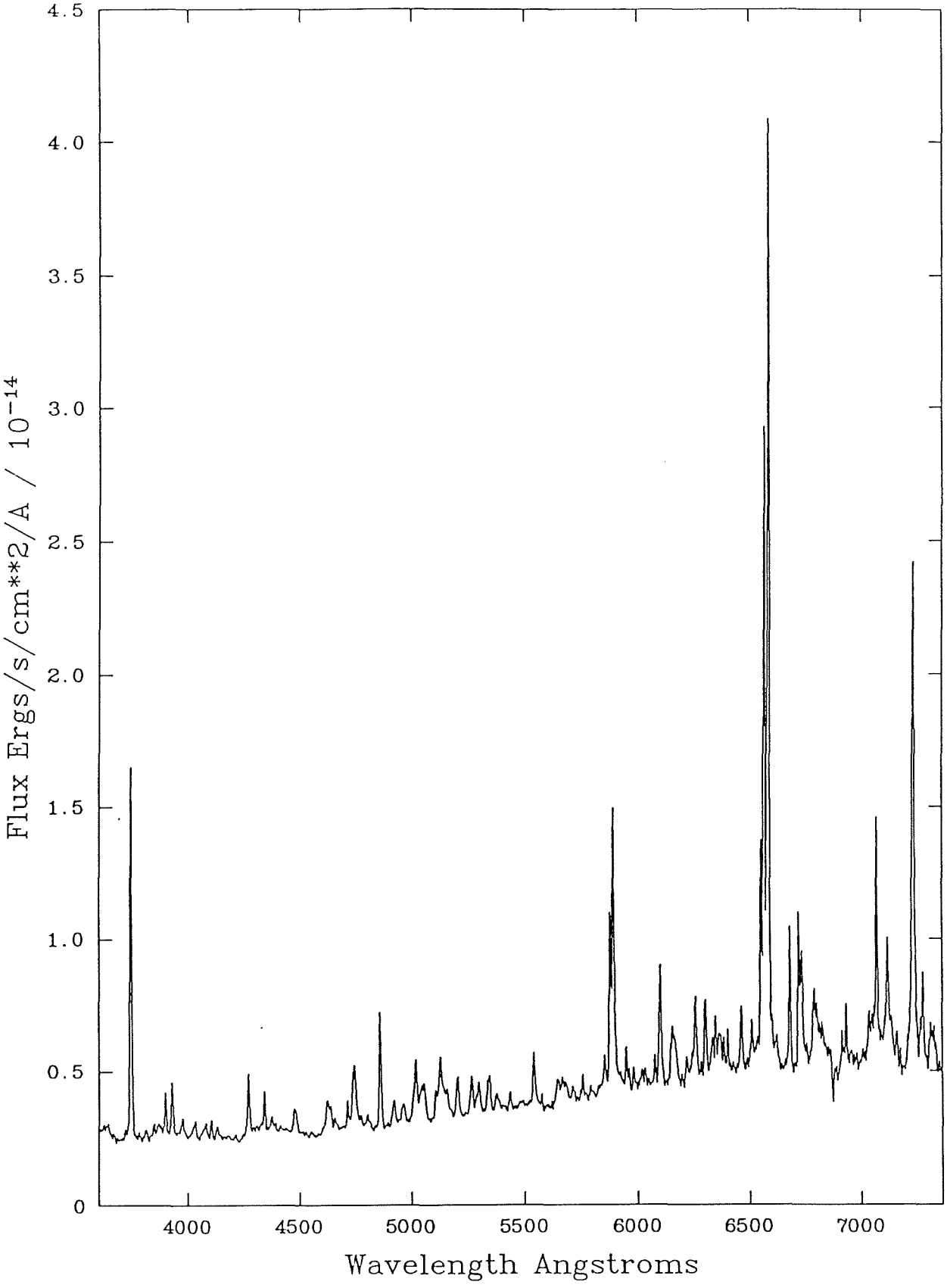

Figure 5.6: AAT spectra of V348 Sgr.

Table 5.5: Zanstra temperatures for star as obtained from H I and He I lines

Stellar Reddening	T_z (in K) obtained from:		
E_{B-V}	Hβ	HeI λ4471Å	HeI λ5876Å
0.4	26 100	34 100	32 500
0.5	24 300	32 500	31 100
0.6	23 000	31 200	29 900
0.7	21 400	29 500	28 400
0.8	20 200	28 400	27 400
0.9	19 000	27 300	26 200
1.0	18 000	26 200	25 000
1.1	17 200	25 100	24 200
1.2	16 300	24 200	23 400
1.3	15 600	23 300	22 600
1.4	14 900	22 600	21 900
1.5	14 200	21 800	21 100
1.6	13 600	21 100	20 400
1.7	13 100	20 400	19 800

temperature of the central source as seen by the bulk of the hydrogen rich material is greatly reduced. The higher T_z(He) is then produced as the Helium is more uniformly distributed throughout the nebula so the central nebula is Helium enriched (relatively). Indeed DO thought the wind region of V348 Sgr to be extremely hydrogen deficient. In this case it may be expected that T_z(He) is the better stellar temperature indicator. At a stellar reddening of $E_{B-V} = 0.9$, T_z(He)$\sim$ 26 500 K—in good agreement with the Strömgren Radius analysis. It is interesting to note that at this reddening T_z(H) = 19 000 K which is approximately the suggested stellar surface temperature!

5.7.4 The nebula ionization equilibrium

The basic ideas behind this technique are reasonably straightforward, however, it is always necessary to make simplifying assumptions, regarding for example:

(i) *physical parameters and flux distribution of the central star,*

(ii) *density distribution of material within the nebula,*

(iii) *relative abundance of elements,*

(iv) *dust and molecular absorption/emission and morphology,* and

(v) *size (hence distance) and geometric structure (usually spherical symmetry) of the nebula.*

In principle the ionization, temperature and emission coefficients can be calculated as a function of radius. Hence the resulting nebular spectra can be calculated at any point within the nebula. In practice, the underlying assumptions often prove unfounded or difficult to implement. For example, (i), stellar flux distributions in the EUV are notoriously unreliable, while (ii), ground-based observations often lack the necessary angular resolution, so density distributions are often theoretically calculated, or just assumed to be uniform. The determination of nebular relative abundances is also unreliable (iii): in many cases *ionization correction factors* are assumed (for important unobserved ionic states). Even in cases when the whole spectrum is well known the lack of precision in the atomic parameters compounded with observational errors may still produce large errors. Dust distributions (iv) are on the whole not well known

for planetary nebulae, although the advent of 2–d IR arrays may soon improve this situation. Possibly the least valid assumption (v) concerns the geometric structure, which for most H II regions and many planetary nebulae can only be speculated upon. The determination of nebular distances is also generally unreliable. Apart from these assumptions there is also the real possibility that some of the governing physics is as yet undiscovered.

Despite these problems, the technique has had considerable success in predicting nebular spectra (eg AGN, p.135). However, care must be taken in choosing the object to be modelled. In the past, NGC 7662 has often been used as it is a bright planetary nebula with a spherical appearance. Much data is available for this object, and the line fluxes obtained from different observations are in good agreement with one another.

5.7.4.1 The Harrington Code

This code was originally described by Harrington (1967, 1968) and later updated and generalised to more realistic planetary nebula situations by Harrington *et al.* (1982). Briefly the program has two segments:

(i) *part 1*; evaluates the thermal structure, ionic equilibrium and distribution,

(ii) *part 2*; determines the observable spectrum as seen by a variety of devices.

For more details of this, see sections 10.1–10.5 of Harrington *et al.* (1982).

5.7.4.2 Starting assumptions

In the case of the nebula surrounding V348 Sgr, many of the initial starting parameters are only poorly known. For instance:

(i) *Abundances.* Lower-limits to the nebular abundances are only available for He, O, N, and maybe S. Ignoring other important elements that are not represented (especially C), is likely to produce unrealistic models, as these elements may have strong lines outside the visual region, although probably not in a nebula of such

low excitation as this. The determination of the Helium abundance represents a major problem; the abundance derived in Section 5.6 is actually the He^+ / H^+ and not the He_{TOT}/H abundance.

(ii) *Electron density.* This was determined from the [SII] lines and assumed to apply to the whole volume of the nebula. This is almost certainly unrealistic.

(iii) *Fudge factors.* All photoionization codes require an estimate of the so-called *filling factor*, which is a measure of the *clumpiness* in a nebula. Observationally, it is impossible to evaluate this quantity directly in a quantitative sense (its value ranges from 0→1). However, for objects that have a uniform appearance on photographic plates the filling factor may be assumed to lie close to 1. The *Harrington Code* also requires an estimate of *the fraction of the nebula that is vacuum*, and again this is not straight-forward to obtain from observational material. As each method outlined in previous sections had suggested that the star is unable to ionize the nebula, these parameters were adjusted to favour the ionization of the nebula by a cool central object (ie the least likely scenario). Thus the filling factor was set as 0.1 (extreme clumpiness) while the fraction of the nebula thought to be vacuum was set to 0.9 (ie most of the nebula is without material).

(iv) *Geometry.* The nebula was assumed to be spherical with a diameter of 33″, corresponding to 0.76 pc at 4.7 kpc—the assumed distance to V348 Sgr (see Chapter 6). We have also assumed that the nebula starts immediately above the photosphere.

(v) *Luminosity.* At a distance of 4.7 kpc the luminosity of the central star is $L_{BOL} \sim$ 3 500 $L_\odot$. This value is typical for other planetary nebula central stars.

(vi) *Dust.* None of the models considered include dust absorption. However, simple considerations suggest that for nebula models at similar temperatures, those that include dust will produce far lower nebular ionization than those without dust.

Figure 5.7 shows a sample nebula parameter input file.

5.7.4.3 Results—black body flux distributions

Using the planetary nebula parameter input file described in the previous section and assuming the energy distribution is defined as a black body, models were run with stel-

```
BLACK BODY   3.20 SL  3500.        1      TYPE,TSTAR,(SL,PL),LUMN,NPRINT
 1550.  4.7           130 122 10 1       WAVE,DIST;   NROW,NCOL,STRT,SCALE
    9    0                              ITERATIONS, NGAP
 0.0000      3.0                          MDUST/MH,  RHO(DUST)
    0    0    0    0    0    0    0     0    0    3    0    0      PRINT CONTRO
    3    3    3    3    3    3    3     3    3    3    3    3      PRINT FREQY
 .0001     .010    3.500E+02    0           R1,RSCALE,DSCALE,IDEN
 1.         1.        1.         1.          1.         1.
 1.         1.        1.         1.          1.         1.
 1.         1.        1.         1.          1.         1.
 1.         1.        1.         1.          1.         1.
 1.         1.        1.         1.          1.         1.
 1.         1.        1.         1.          1.         1.
 1.         0.0/
 0.30       0.50        30% O RESONANCE LINES, 50% BOWEN CONVERSION
 0.90                                          FRACVAC
 0.10                                          FILL
H       1 1.0         HE      2 0.195       C       4 0.00062
N       5 0.00010     O       6 0.000794    NE      6 0.000070
S       6 0.000005    SI      5 0.000006    MG      5 0.0000140
```

Figure 5.6: Sample nebular parameter input file for *Harrington Code.*

lar surface temperatures ranging from 24 000 K to 40 000 K (some of these are shown plotted in Figure 5.8). Although these distributions are probably not very realistic (especially in the EUV) they serve as a useful starting point and lead to several interesting conclusions. The results are shown in Table 5.6.

In general the major forbidden lines are well fitted by the 26 000 K model, however, there are some notably exceptions:

(i) the He I lines are well below the required line flux, but can be fitted using a 32 000 K model. This is an indication that the true Helium abundance in the nebula is far greater than the value used in the input program. Alternatively, a black body flux distribution with an excess emission at 24 eV (corresponding to the He^0 ionisation limit) could selectively strengthen the He I lines.

(ii) *All* the very low excitation lines (which may or may not be contaminated by atmospheric emission) are predicted at far too low a flux. Presumably, the very low excitation lines are either produced by atmospheric contamination or originate far out in the nebula, although, the high excitation required to produce the [OI] $\lambda\lambda$6300, 6363Å lines is usually thought to imply a high temperature region.

The final relative abundances obtained with the 26 000 K model are shown in Table 5.7.

5.7.4.4 Results—Hydrogen model atmospheres

Figure 5.9 shows the relative flux distributions of the *normal* composition Hydrogen rich model atmospheres. All are Kurucz models, with log g = 3.0, 3.5, and 4.0 for the 25 000, 32 000 and 40 000 K models respectively. Table 5.8 shows the resulting nebular spectra except for the 25 000 K model which proved unable to ionize the nebula to its observed extent.

As can be seen from Table 5.8, neither model fits the observed line fluxes very well. Although it is clear that the diminished UV flux of these model atmospheres (compared to black bodies), requires much higher surface temperatures to reach the observed line fluxes. The forbidden line fluxes are poorly fitted by either model, but there are suggestions that a model with surface temperature of around 35 000 K may significantly

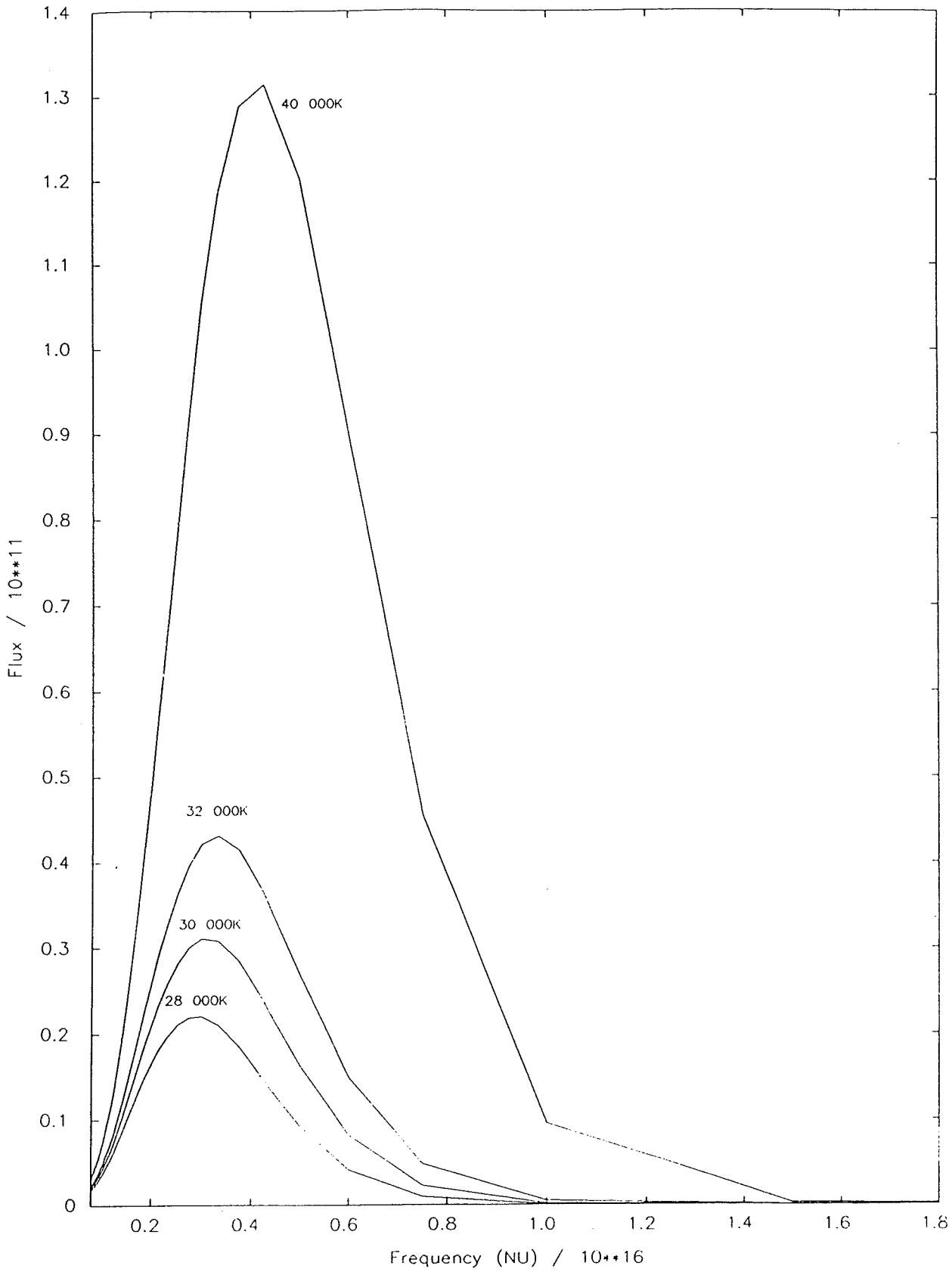

Figure 5.8: 28 000, 30 000, 32 000 and 40 000 K black bodies.

Table 5.6: Line flux as predicted from Black body models.

Ion	Line	Observed	Predicted Line Flux (relative to Hβ)				
	Å	Flux	24 000 K	26 000 K	28 000 K	30 000 K	32 000 K
[OII]	3726	108.5	93.4	109.9	131.7	156.2	179.0
[OII]	3729	113.7	98.3	116.4	138.5	162.9	185.4
Hδ	4101	22.1	26.0	26.0	26.0	26.0	26.0
Hγ	4341	45.3	47.0	47.0	47.0	47.0	47.0
He I	4471	12.1	1.1	2.2	3.7	5.9	8.3
Hβ	4861	100.0	100.0	100.0	100.0	100.0	100.0
[OIII]	5006	5.2	0.7	2.6	7.3	17.2	34.7
[NI]	5197	2.5	0.20	0.14	0.11	0.10	0.10
[NI]	5200	2.9	0.21	0.16	0.12	0.11	0.10
[NII]	5755		0.5	0.6	0.8	0.9	1.0
He I	5876	24.7	3.2	6.2	10.8	16.9	23.4
[OI]	6300	17.0	0.70	0.50	0.42	0.40	0.41
[OI]	6363	9.1	0.20	0.17	0.14	0.13	0.13
[NII]	6548	48.5	43.6	47.7	51.7	55.0	56.8
Hα	6565	302.0	296.6	295.9	295.1	294.3	293.6
[NII]	6584	132.0	128.4	140.4	152.2	162.1	167.3
[SII]	6719	36.6	20.2	18.0	15.7	13.3	11.0
[SII]	6730	33.9	18.7	16.7	14.6	12.4	10.3
[SIII]	9532		9.6	15.1	21.3	27.7	33.8
Total Hβ Flux†		6.75	5.21	5.23	5.26	5.34	5.45

†In this row $1.0 \equiv 1.0 \times 10^{-12}$ erg cm^{-2}s^{-1}.

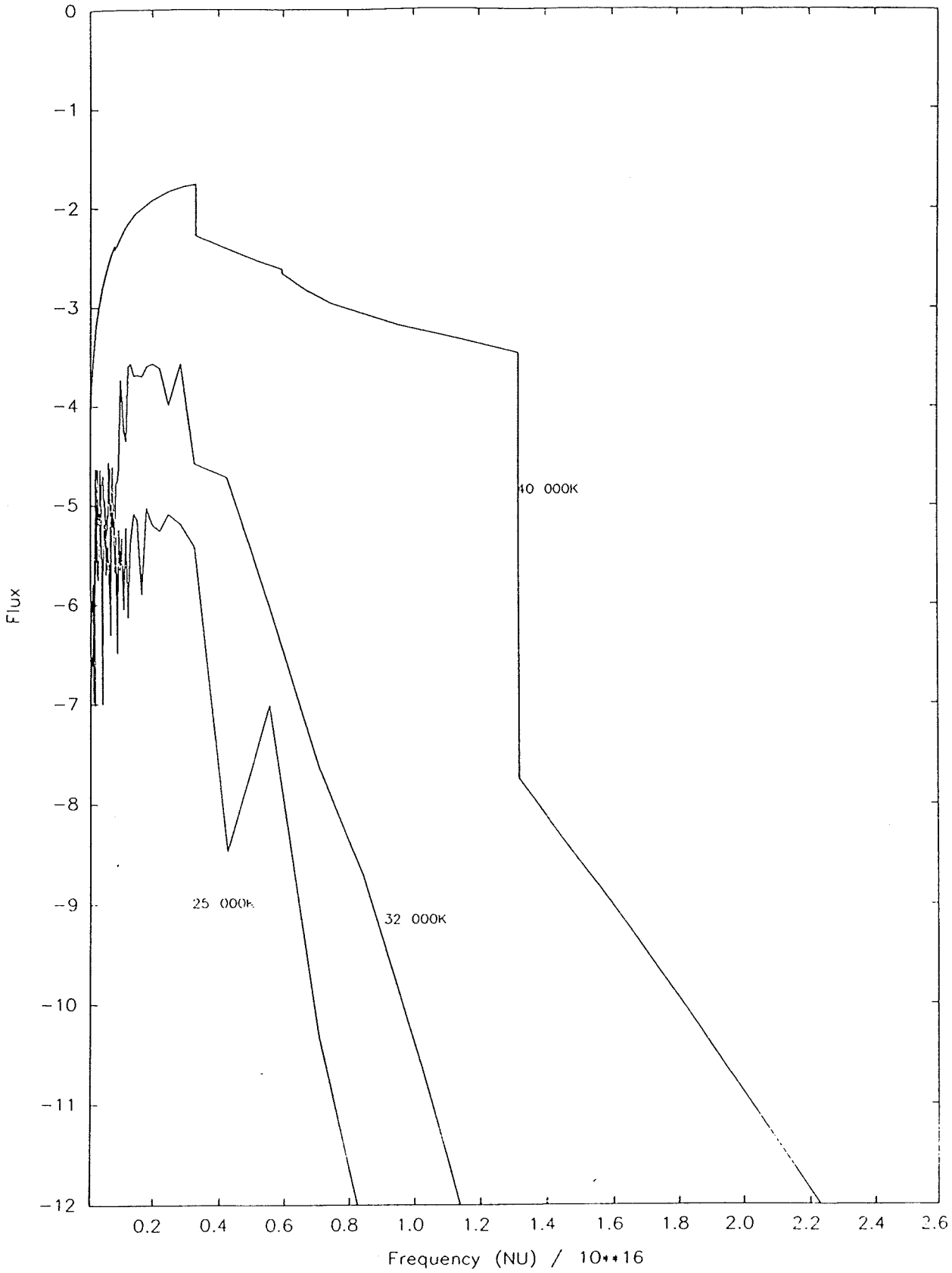

Figure 5.9: Relative flux distributions for 25 000 K ($\log g = 3.0$), 32 000 K ($\log g = 3.5$) and 40 000 K ($\log g = 4.0$) Kurucz atmospheres (with normal solar abundance).

Table 5.7: Relative nebular abundances obtained from 26 000 K black body model.

ELEMENT	I	II	III	IV	V
HYDROGEN	0.936366E-02	0.990636E+00			
HELIUM	0.781363E+00	0.218630E+00	0.740187E-05		
CARBON	0.207143E-02	0.935687E+00	0.622394E-01	0.203480E-05	0.374463E-08
NITROGEN	0.112371E-01	0.963624E+00	0.251367E-01	0.207169E-05	0.189204E-10
OXYGEN	0.759809E-02	0.986794E+00	0.560739E-02	0.713877E-06	0.494194E-11
NEON	0.756992E-01	0.922845E+00	0.145539E-02	0.961124E-08	0.137704E-15
SULPHUR	0.162461E-03	0.592666E+00	0.406805E+00	0.366032E-03	0.663185E-06
SILICON	0.429557E-03	0.824081E+00	0.175306E+00	0.182722E-03	0.694724E-06
MAGNESIUM	0.296111E-02	0.376318E+00	0.620721E+00	0.116406E-09	0.182731E-19

improve the fit, however, the discrepancy in the He I line fluxes would still remain (again possibly attributable to the unknown Helium abundance).

5.7.4.5 Results—EHe model atmospheres

Figure 5.10 shows the relative flux distribution for EHe model atmospheres. As the Schönberner hydrogen-deficient model atmosphere code was not currently operational Dr. C. S Jeffery supplied a BD–9°4395 model atmosphere which has peak flux at a frequency corresponding to approximately 24 500 K. Since this atmosphere was the only one available it was decided to scale and shift the fluxes and frequencies to that corresponding to hotter atmospheres. Although this model is relatively coarse, it should be remembered that as the temperature of the model increases new ionic edges will appear in the EUV. So these models may serve only as a guide until hotter EHe atmospheres become available.

Figures 5.11–5.13 show the relative flux distributions for all types of atmospheres studied. As can be seen the most EUV flux is given by the black body distribution, and the least by the Kurucz model atmospheres. The EHe models lie between the two. Thus at equal temperatures and luminosities, EHe models will produce higher nebula ionization than hydrogen atmospheres. Table 5.9 shows the results of this analysis.

As can be seen, the forbidden line fluxes are best fitted by models of around 32 000 K. At this temperature, the He I line fluxes are still far too low. Again, all the very low excitation lines are far too weak.

Table 5.8: Line flux as predicted from Hydrogen Model Atmospheres.

Ion	Line	Observed	Predicted Line Flux (relative to Hβ)	
	Å	Flux	32 000	40 000
[OII]	3726	108.5	42.2	125.2
[OII]	3729	113.7	44.4	129.5
Hδ	4101	22.1	26.0	26.0
Hγ	4341	45.3	47.0	47.0
He I	4471	12.1	0.11	9.8
Hβ	4861	100.0	100.0	100.0
[OIII]	5006	5.2	0.11	357.9
[NI]	5197	2.5	0.09	0.05
[NI]	5200	2.9	0.10	0.06
[NII]	5755		0.20	0.7
He I	5876	24.7	0.33	28.1
[OI]	6300	17.0	0.25	0.29
[OI]	6363	9.1	0.08	0.10
[NII]	6548	48.5	27.6	32.2
Hα	6565	302.0	299.8	292.6
[NII]	6584	132.0	81.4	94.8
[SII]	6719	36.6	16.4	4.2
[SII]	6730	33.9	15.3	4.0
[SIII]	9532		1.8	43.9
Total Hβ Flux†		6.75	5.72	5.41

†In this row $1.0 \equiv 1.0 \times 10^{-12}$ erg cm^{-2}s^{-1}.

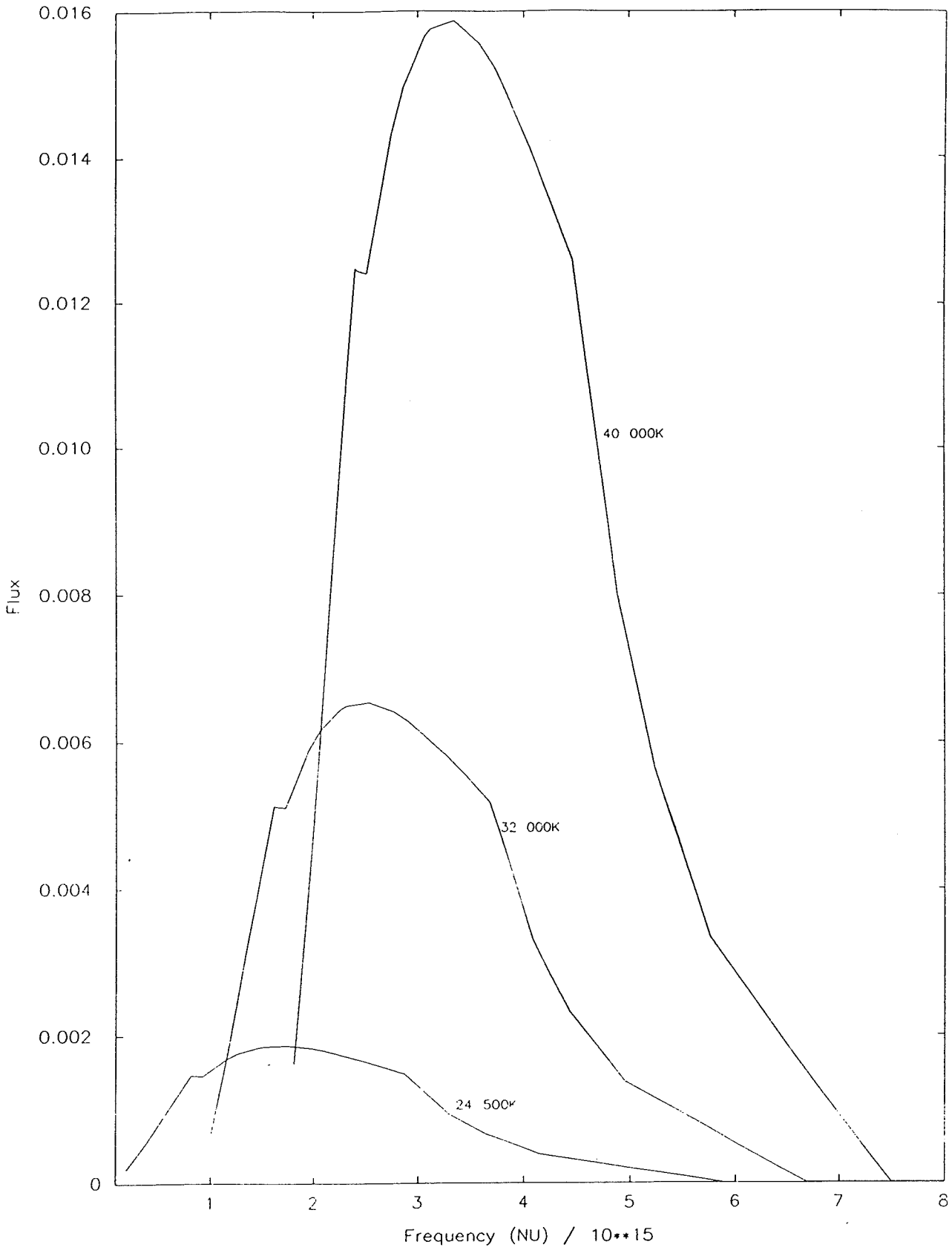

Figure 5.10: Relative flux distributions for 24 500 K, 32 000 K and 40 000 K EHe model atmospheres (based on the BD–9°4395 model atmosphere).

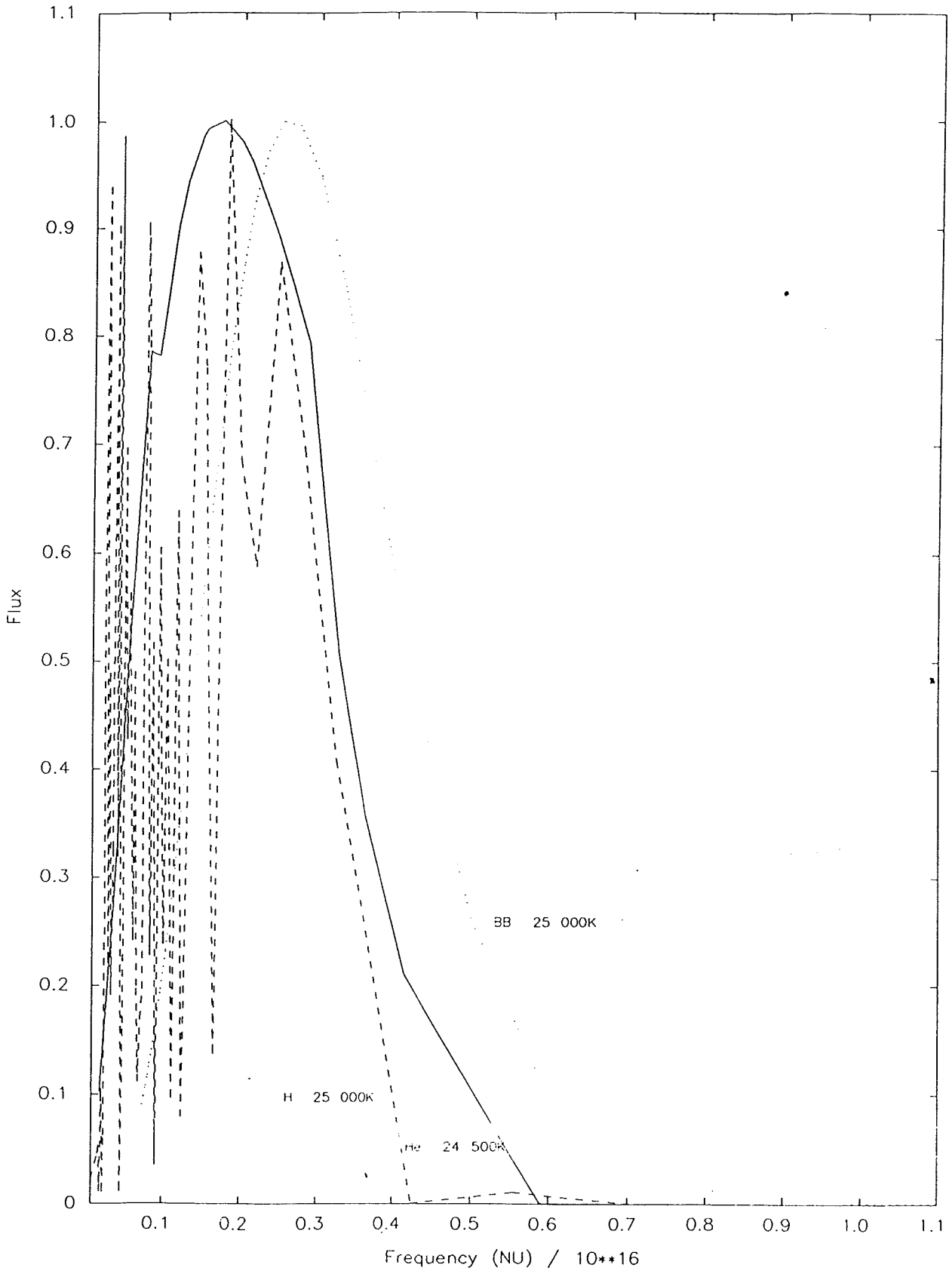

Figure 5.11: 25 000 K relative flux distributions for black body, Kurucz (solar abundances) and EHe (24 500 K) model atmospheres.

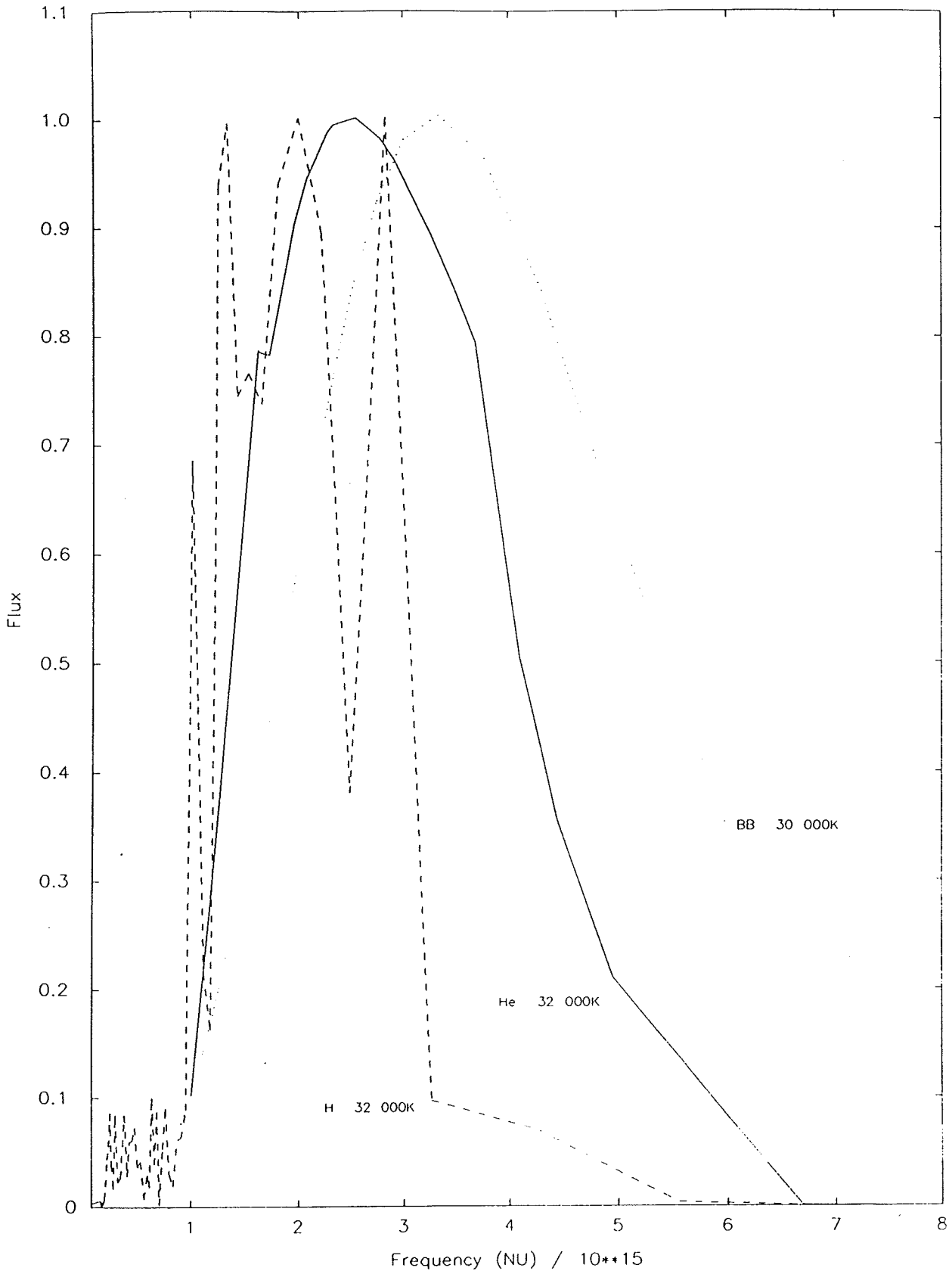

Figure 5.12: 32 000 K relative flux distributions for black body, Kurucz (solar abundances) and EHe (24 500 K) model atmospheres.

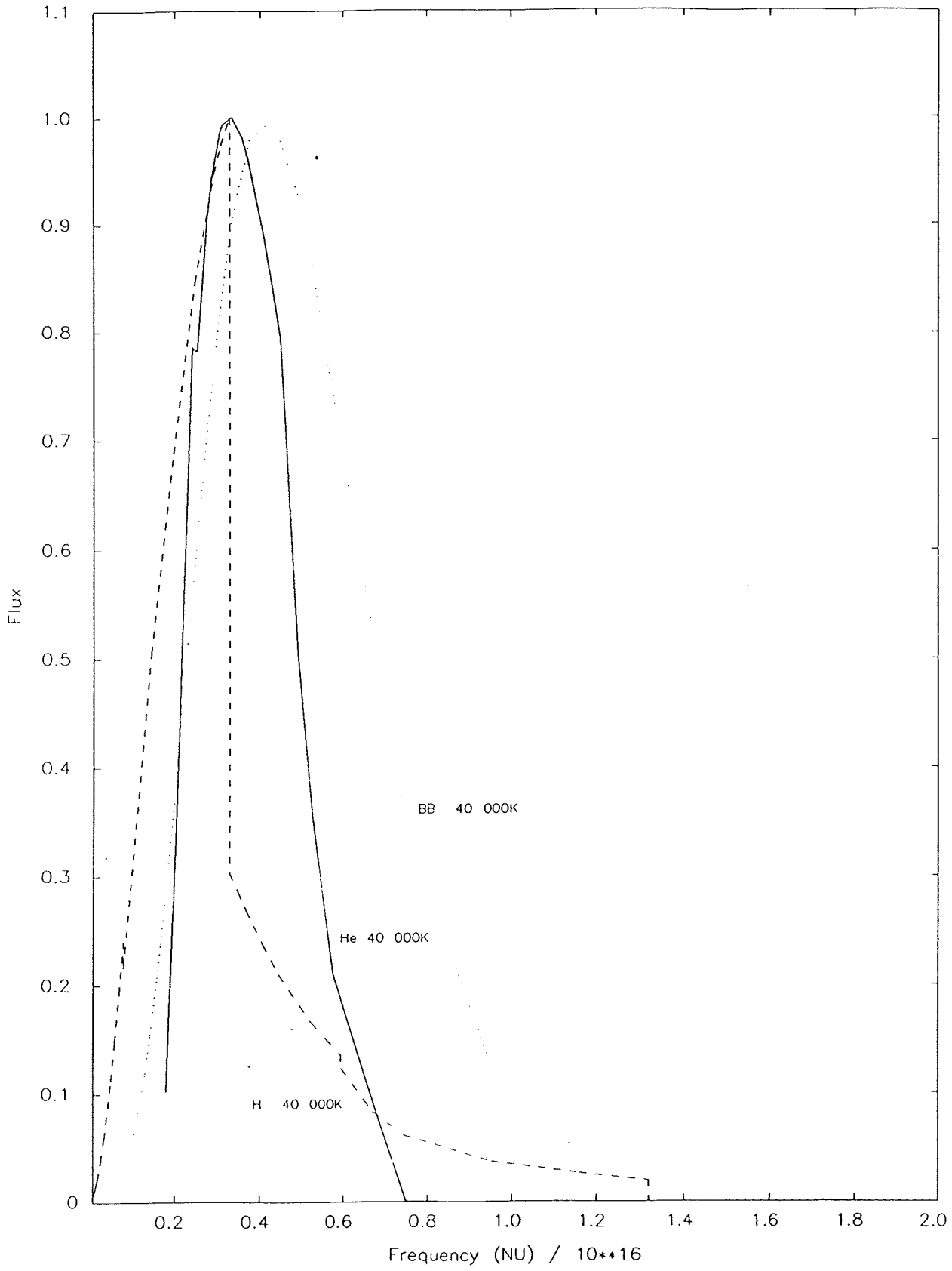

Figure 5.13: 40 000 K relative flux distributions for black body, Kurucz (solar abundances) and EHe model atmospheres.

Table 5.9: Line flux as predicted from Helium Model Atmospheres.

Ion	Line	Observed	Predicted Line Flux (relative to Hβ)			
	Å	Flux	24 500	32 000	40 000	32 000SE ‡
[OII]	3726	108.5	288.7	145.2	263.2	88.4
[OII]	3729	113.7	313.0	152.2	272.1	92.6
Hδ	4101	22.1	26.0	26.0	26.0	26.0
Hγ	4341	45.3	47.0	47.0	47.0	47.0
HeI	4471	12.1	0.04	4.2	9.7	4.0
Hβ	4861	100.0	100.0	100.0	100.0	100.0
[OIII]	5006	5.2	0.01	0.06	0.80	0.04
[NI]	5197	2.5	0.13	0.05	0.05	0.03
[NI]	5200	2.9	0.14	0.06	0.05	0.04
[NII]	5755		2.03	0.89	1.7	0.5
HeI	5876	24.7	0.10	12.03	27.7	11.5
[OI]	6300	17.0	0.60	0.20	0.21	0.14
[OI]	6363	9.1	0.20	0.06	0.07	0.05
[NII]	6548	48.5	87.2	57.4	76.5	43.1
Hα	6565	302.0	291.7	294.7	292.1	296.8
[NII]	6584	132.0	256.7	169.1	225.1	126.9
[SII]	6719	36.6	47.3	7.9	4.2	18.7
[SII]	6730	33.9	42.9	7.4	4.0	17.5
[SIII]	9532		7.2	31.9	49.0	75.8
Total Hβ Flux†		6.75	4.40	5.28	5.35	5.63

†In this row $1.0 \equiv 1.0 \times 10^{-12}$ erg cm^{-2}s^{-1}.

‡sulphur enhanced model.

The last model presented in Table 5.9, is sulphur enhanced, ie the sulphur abundance has been increased to that found in a typical planetary nebula (see Table 5.4). This model has significant differences to others presented in this table.

(i) The [SII] line fluxes are increased by some 250%.

(ii) The line fluxes of other forbidden lines are reduced by around 30–40%.

(iii) The recombination line fluxes are barely affected.

Overall the enhanced sulphur model reduces the He I and forbidden line flux discrepancy.

Table 5.10/11 shows the relative abundances as obtained with the 32 000 K and the 32 000 K sulphur enhanced model.

Table 5.10: Relative nebular abundances obtained from 32 000 K EHe atmosphere model.

ELEMENT	I	II	III	IV	V
HYDROGEN	0.307951E-02	0.996921E+00			
HELIUM	0.582295E+00	0.417705E+00	0.223484E-07		
CARBON	0.872417E-03	0.836749E+00	0.162379E+00	0.146256E-07	0.161555E-13
NITROGEN	0.315753E-02	0.994206E+00	0.263657E-02	0.215900E-07	0.155468E-16
OXYGEN	0.243798E-02	0.997446E+00	0.115684E-03	0.118820E-08	0.415570E-18
NEON	0.147645E-01	0.985226E+00	0.939870E-05	0.276492E-11	0.882652E-25
SULPHUR	0.383964E-04	0.223876E+00	0.776079E+00	0.709208E-05	0.900753E-08
SILICON	0.249801E-03	0.522662E+00	0.477084E+00	0.479776E-05	0.277905E-07
MAGNESIUM	0.128768E-02	0.153401E+00	0.845312E+00	0.219151E-14	0.161935E-30

Table 5.11: Relative nebular abundances obtained from 32 000 K sulphur enhanced EHe atmosphere model.

ELEMENT	I	II	III	IV	V
HYDROGEN	0.325171E-02	0.996748E+00			
HELIUM	0.606860E+00	0.393140E+00	0.201569E-07		
CARBON	0.906681E-03	0.844662E+00	0.154431E+00	0.127699E-07	0.117908E-13
NITROGEN	0.334892E-02	0.994114E+00	0.253711E-02	0.228256E-07	0.157786E-16
OXYGEN	0.257931E-02	0.997312E+00	0.109075E-03	0.122709E-08	0.374404E-18
NEON	0.157360E-01	0.984255E+00	0.889432E-05	0.218359E-11	0.624080E-25
SULPHUR	0.420772E-04	0.233213E+00	0.766738E+00	0.705979E-05	0.811483E-08
SILICON	0.268618E-03	0.527127E+00	0.472600E+00	0.478659E-05	0.240730E-07
MAGNESIUM	0.114712E-02	0.162071E+00	0.836781E+00	0.187390E-14	0.116062E-30

5.7.4.6 Summary of nebular ionization equilibrium models

Several important conclusions have been made by studying the nebular ionization equilibrium:

(i) until a new value of the S abundance can be determined (primarily by studying the [SIII] λ9532Å line), the models are (at least in detail) unrealistic,

(ii) all very low excitation lines are badly fitted by the models,

(iii) there is a significant quantity (possibly $>$ 50%) of unobservable neutral Helium (see tables of relative abundances also Figure 5.14), hence the total Helium abundance must be substantially higher, and

(iv) at least in principle, all models suggest that the surface temperature of the underlying ionizing source must be greater than 26 000 K for a black body distribution, or 32 000 K for a model atmosphere (Hydrogen *or* Helium rich).

5.8 Can V348 Sgr, in its present state, ionize its surrounding nebula ?

All the evidence presented indicate that V348 Sgr *cannot* ionize its nebula. DO estimated a recombination timescale (τ_{rec}) of $\sim$ 1000 years, however, the new data presented here leads to $\tau_{rec}(H^+)$, and $\tau_{rec}(He^o) \sim 200$ years (at $T_e = 5000$ K and $n_e \sim 350\,cm^{-3}$), while $\tau_{rec}(O^{2+}) \sim 5$ years and $\tau_{rec}(O^+) \sim 20$ years (at $T_e = 7500$ K and $n_e \sim 350\,cm^{-3}$). Thus there are four possibilities:

(i) the star was very recently much hotter than it is currently,

(ii) there is an unseen hotter body in the system,

(iii) during decline to minimum, V348 Sgr gets *hotter* (Barlow, 1989). In fact Strömgren photometry, presented by Heck *et al.* (1985), shows that the stellar colours get bluer as the star gets fainter. It is expected that the relative nebular contribution to these colours increases as the star declines in brightness. However, this value is difficult to assess quantitatively.

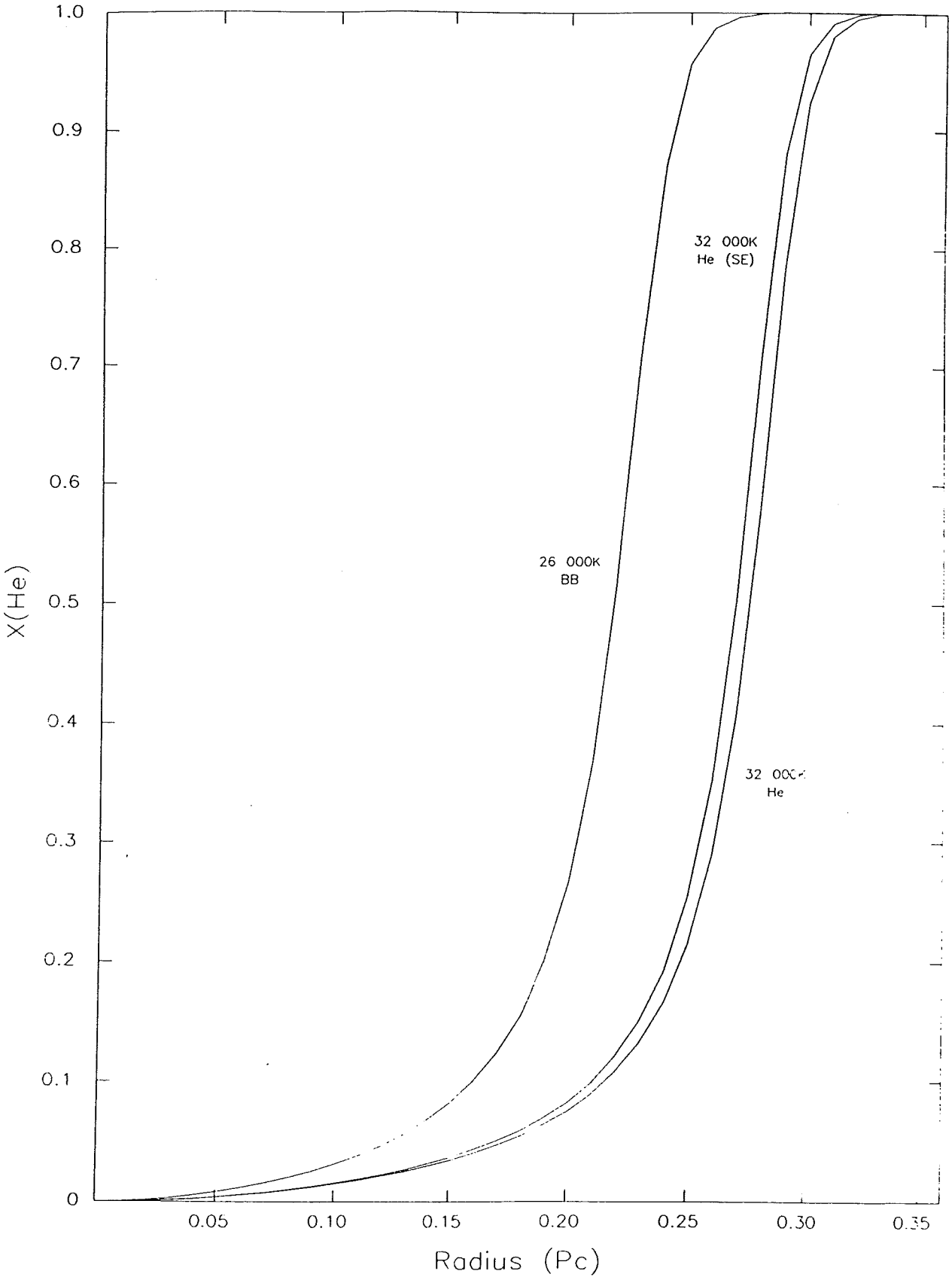

Figure 5.14: The number density of He^0 as a function of radial distance in the nebula, demonstrating the significant quantity of unobservable material (as predicted by all models).

(iv) The Heber and Schönberner (1986) estimate of reddening and surface temperature of this object is *incorrect.* However, it seems highly unlikely that their temperature estimate could be in error by the required amount ($> 8\,000\,\mathrm{K}$).

At present it is impossible to differentiate between these.

5.9 Summary

Several different techniques that have been applied to the forbidden and recombination line fluxes in the nebula prove that it is not possible for a star with $T_{surface} \sim 20\,000\,K$ *and* $L_{BOL} \sim 3500\ L_{\odot}$ *to be able to produce the observed degree or extent of ionization. The models imply that a black body atmosphere with* $T_{surface} \sim 26\,000\,K$ *or a hydrogen-deficient atmosphere with* $T_{surface} > 32\,000\,K$ *is required for a satisfactory fit to the line fluxes. The data suggest that the nebula is substantially Helium enriched and the Zanstra Hydrogen temperature indicates that the bulk of the Hydrogen lies outside the central dusty region.*

Table 5.12: Comparison of predicted star temperature as derived from all methods.

Technique	Stellar Temperature (K)
Strömgren Sphere	27 000
Stoy	> 25 000
Zanstra—H	19 000
Zanstra—He	26 500
†NIE black body	26 000
NIE model atmos.	> 32 000

† NIE = nebular ionization equilibrium method (*Harrington Code*).

5.10 References

1. Balona, L. and Crampton, D., 1974. *Mon. Not. R. astr. Soc.*, **166**, 203
2. Barlow, M. J., 1989. *Private Communication*
3. Böhm-Vitense, E., 1981. *Ann. Rev. of Astron. and Astrophy.*, **19**, 295
4. Boksenburg, A. and Burgess, D. E., 1973. *Proc. Symp. on astronomical observations with TV type sensors*, p21, eds. Glaspey, J. W. and Walker, G. A. H., UBC, Vancouver.
5. Brocklehurst, M., 1971. *Mon. Not. R. astr. Soc.*, **153**, 471
6. Clegg, R. E. S., 1987. *Mon. Not. R. astr. Soc.*, **229**, 31p
7. Dahari, O. and Osterbrock, D. E., 1984. *Astrophys. J.*, **277**, 684 **(DO)**
8. Feast, M. W. and Pollacco, D. L., 1987. *IAU Circ.*, **4399**
9. Georgelin, Y. M., Lortet-Zuckermann, M. C. and Monnet G., 1975. *Astr. Astrophys.*, **42**, 273
10. Harrington, J. P., 1967. *PhD thesis*, Ohio State University
11. Harrington, J. P., 1968. *Astrophys. J.*, **152**, 943
12. Harrington, J. P., Seaton, M. J., Adams, S., and Lutz, J. H., 1982. *Mon. Not. R. astr. Soc.*, **199**, 517
13. Monk, D. J., Barlow, M. J., and Clegg, R. E. S., 1988. *Mon. Not. R. astr. Soc.*, **234**, 583
14. Oke, J. B., 1974. *Astrophys. J. Suppl. Ser.*, **27**, 21
15. Osterbrock, D. E., 1974. *Astrophysics of Gaseous Nebulae* (San Francisco: Freeman) **(AGN)**
16. Pottasch, S. R, 1984. In *Planetary Nebulae: A Study of Late Stages of Stellar Evolution* (Reidel, Dordrecht) **(PN)**
17. Schinckel, A. E., Phillips, M. M. and Hill, P. W., 1982. *AAO Pub. UM-11*
18. Schönberner, D., 1986. *In IAU Coll. No.* **87**, *Hydrogen-Deficient Stars and Related Objects*, p.221, eds. Hunger, K., Schönberner D. and Rao, N. Kameswara., Reidel

19. Stone, Remington P. S. and Baldwin, J. A., 1983. *Mon. Not. R. astr. Soc.*, **204**, 347

20. Stoy, R. H., 1933. *Mon. Not. R. astr. Soc.*, **93**, 588

21. Walker, H. J., 1986. *In IAU Coll. No.* **87**, *Hydrogen-Deficient Stars and Related Objects,* p.407, eds. Hunger, K., Schönberner D. and Rao, N. Kameswara., Reidel

22. Webster, B. L. and Glass, I. S., 1974. *Mon. Not. R. astr. Soc.*, **166**, 491

Chapter 6

V348 Sagittarii—distance

6.1 Introduction

The distance to V348 Sgr has been the source of much controversy. In the past, distance determinations have often been based on flimsy assumptions concerning the nature of the central star. For example, Schönberner (1986) considered the star to be similar to the EHe and R CrB stars and deduced a distance of 9 kpc. Other estimates vary from 2–9 kpc. Because of this uncertainty, and the possible relevance of this object to the understanding of some aspects of the later stages of stellar evolution, a technique was developed to determine the object's distance *not* requiring assumptions regarding the nature of the central star.

6.2 Reddening and reddening-distance relations

As discussed in Chapter 5, the reddening towards V348 Sgr has been found from UV observations of the λ2200Å feature and also optical observations of the Balmer Decrement. Both techniques produce the consistent result of $E_{B-V} = 0.45 \pm 0.10$. By inspection of the galactic reddening maps of Neckel and Klare (1980) we can imply a distance of around 2 kpc, however, large errors may be present as the nearest region studied by them is some 8^o away and towards the galactic plane. It is likely that this

estimate is very much a lower limit as the reddening is generally expected to diminish with distance away from the plane.

Even a cursory glance at the blue and red Schmidt Survey plates for this region shows that the field surrounding V348 Sgr is particularly devoid of unreddened early type stars. As a consequence, the Q technique (which is the unaffected by reddening) obtained from UBV photometry (as applied by Neckel and Klare) is not applicable. So a different method must be sought.

Dean *et al.* (1980) have described a technique using the *Cape-Kron* BVI photometric system to obtain Cepheid reddenings through their pulsation cycle. This technique can be modified to allow the determination of stellar reddening and hence intrinsic colour. Thus the spectral type can be estimated. It is first necessary to express the intrinsic main-sequence in the $(V-I),(B-V)-(V-I)$ plane, with the values taken from Cousins (1980) (see Figure 6.1). With these colour indices the reddening lines are inclined at their greatest angle to the intrinsic main-sequence, so confusion between spectral types may be minimized.

From Dean *et al.* the reddening for a particular spectral type can be determined from the following relations:

$$\frac{E_{V-I}}{E_{B-V}} = X[1 + 0.06(B-V)_o + 0.014E_{B-V}] \tag{6.1}$$

and

$$E_{B-V} = E_o[1 - 0.08(B-V)_o] \tag{6.2}$$

where, E_o is the colour excess a star with $(B-V) = 0$ would suffer when observed through the same quantity of material, and X is given by $X = \frac{E_{V-I}}{E_{B-V}}$ for a star with $E_{B-V} \rightarrow 0$ and $(B-V) = 0$.

Dean *et al.* derived these equations empirically by observing early type stars, and then determining the corrections to be applied for later spectral types. The second

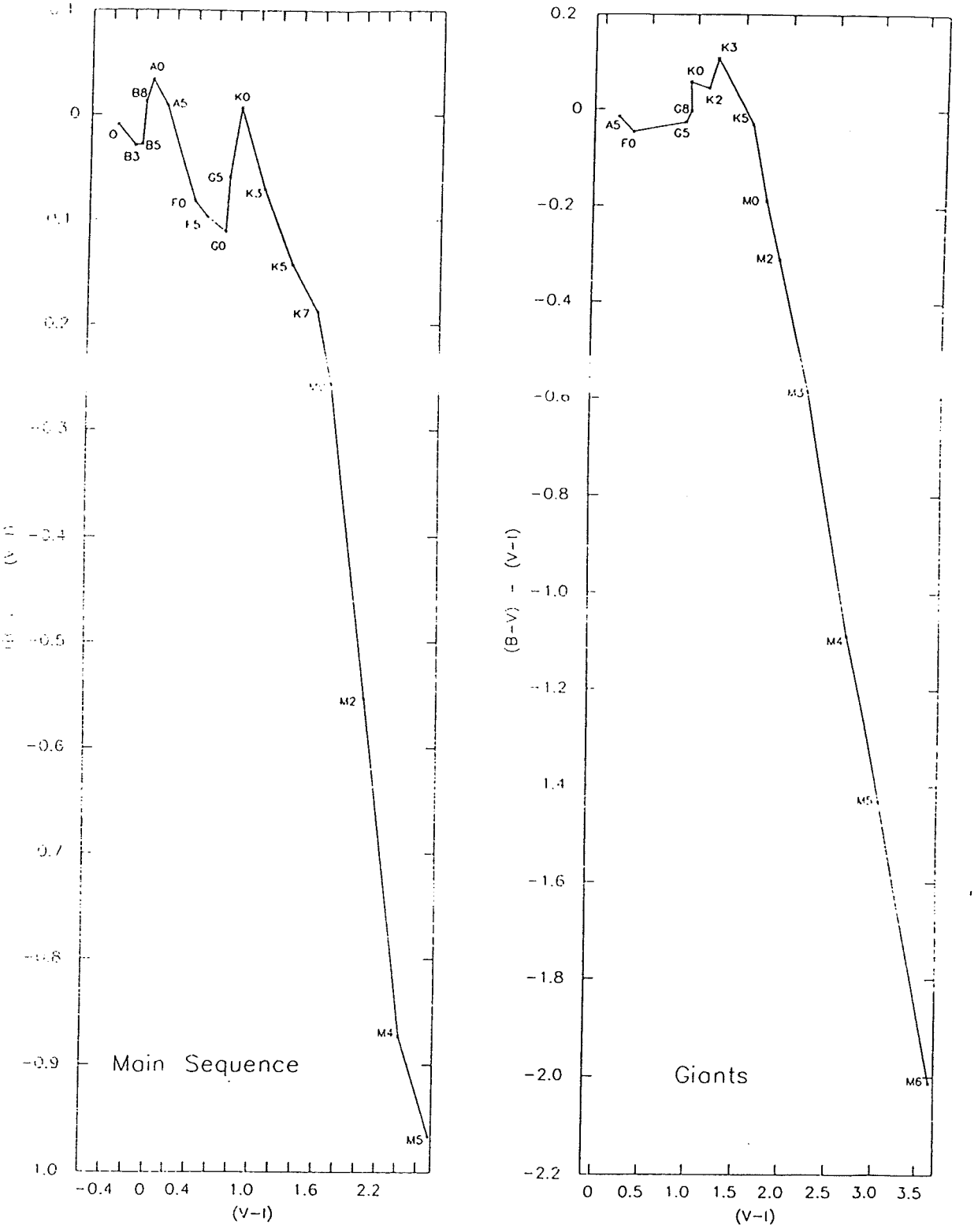

Figure 6.1: The main-sequence and giant branch in the $(V-I),(B-V)-(V-I)$ plane.

equation was an implication of Schmidt-Kaler's (1961) analysis, but a slight discrepancy exists between the observed and predicted values of X. Dean *et al.* chose to use their observationally determined value of 1.250. Figures 6.2–6.4 show the reddening lines for main-sequence, giant and supergiant luminosity classes.

Cousins (1978) has found that observations of unreddened standard stars lie along the intrinsic lines but appeared slightly scattered by an amount that is large compared to the internal errors of the photometry used. He suggests a number of possible causes.

(i) *Colour excess.* It is expected that giants and supergiants will be affected to a larger extent than dwarfs, as they have more circumstellar material.

(ii) *Duplicity.*

(iii) *Line emission.* It is well known that some late type stars display line emission in their spectra.

(iv) *Metallicity.* Catchpole *et al.* (1977) found that barium-enhanced stars followed different intrinsic lines.

(v) *Luminosity effects.*

Although the Q method results in less confusion amongst early spectral types, the BVI_{KC} technique is applicable over a greater range of types. With this technique spectral confusion may arise from late B to late F, and therefore stars of these types have greater uncertainty in their absolute magnitude calibration. Objects with extremely high reddening may also cause confusion. For the giants the situation is less severe, with problems only occurring for highly reddened stars, while for supergiants confusion may occur for early types and also for highly reddened objects.

Close inspection of Figures 6.2–6.4 shows that there is a certain amount of overlap between the different luminosity classes. At these points, it is not possible using ordinary broadband photometry to identify the stellar type. Therefore it is necessary to use a less direct approach, invoking a statistical argument based on the number density of different luminosity classes. Although selection effects may be important, we can, in the first instance, assume that all stars that lie near main-sequence reddening curves are indeed of luminosity class V. Those that are left were first assumed to be giants

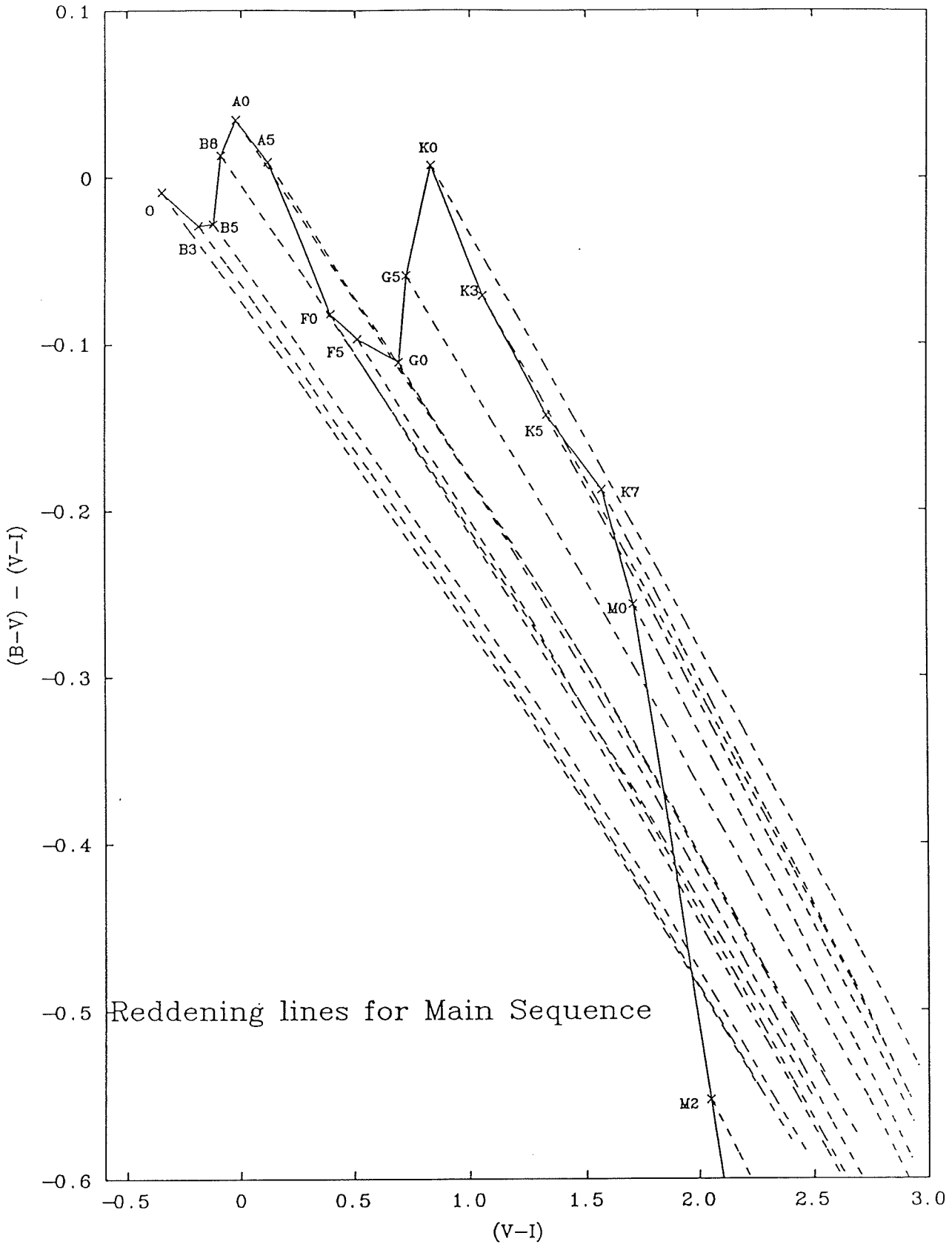

Figure 6.2: Reddening lines for luminosity class V.

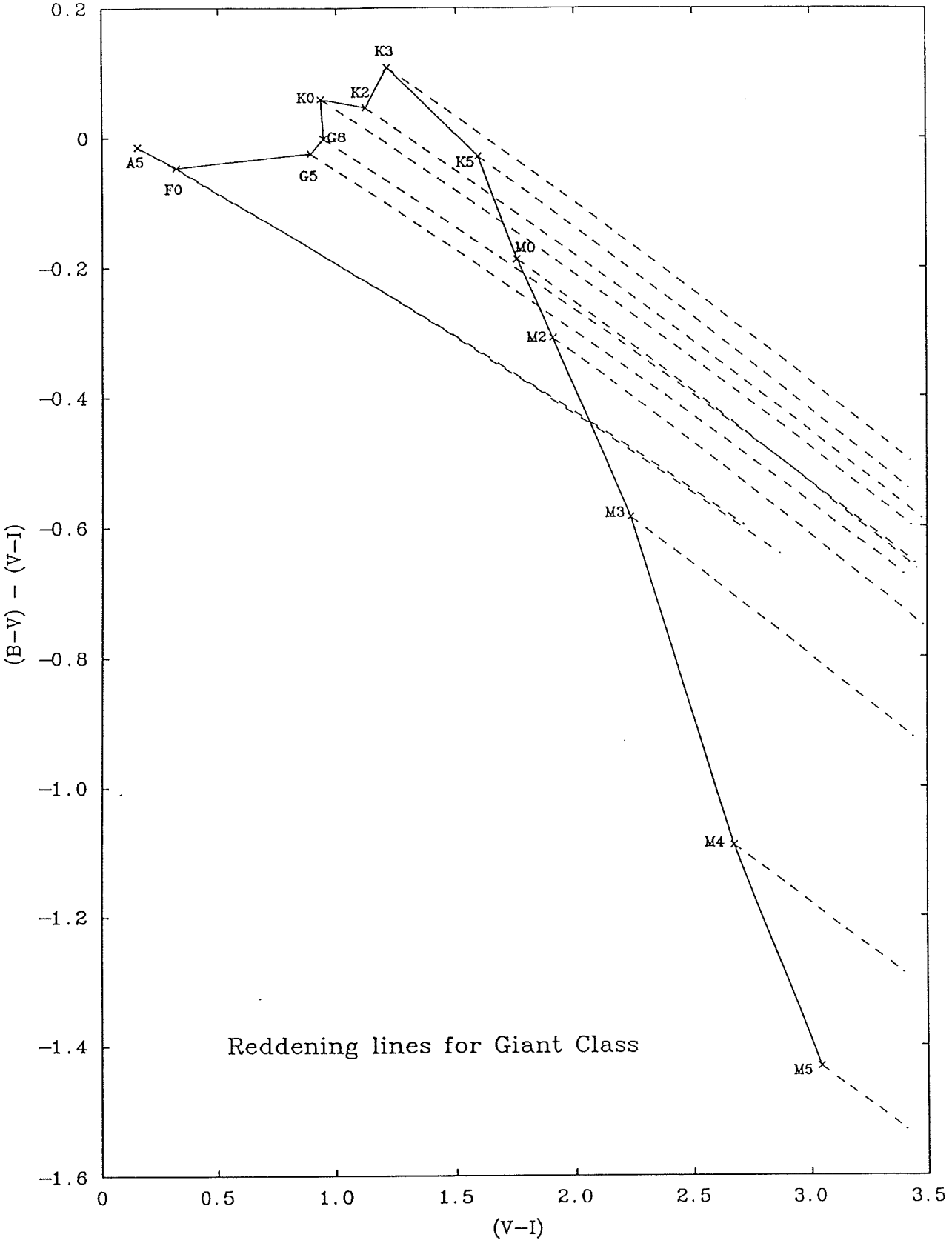

Figure 6.3: Reddening lines for luminosity class III.

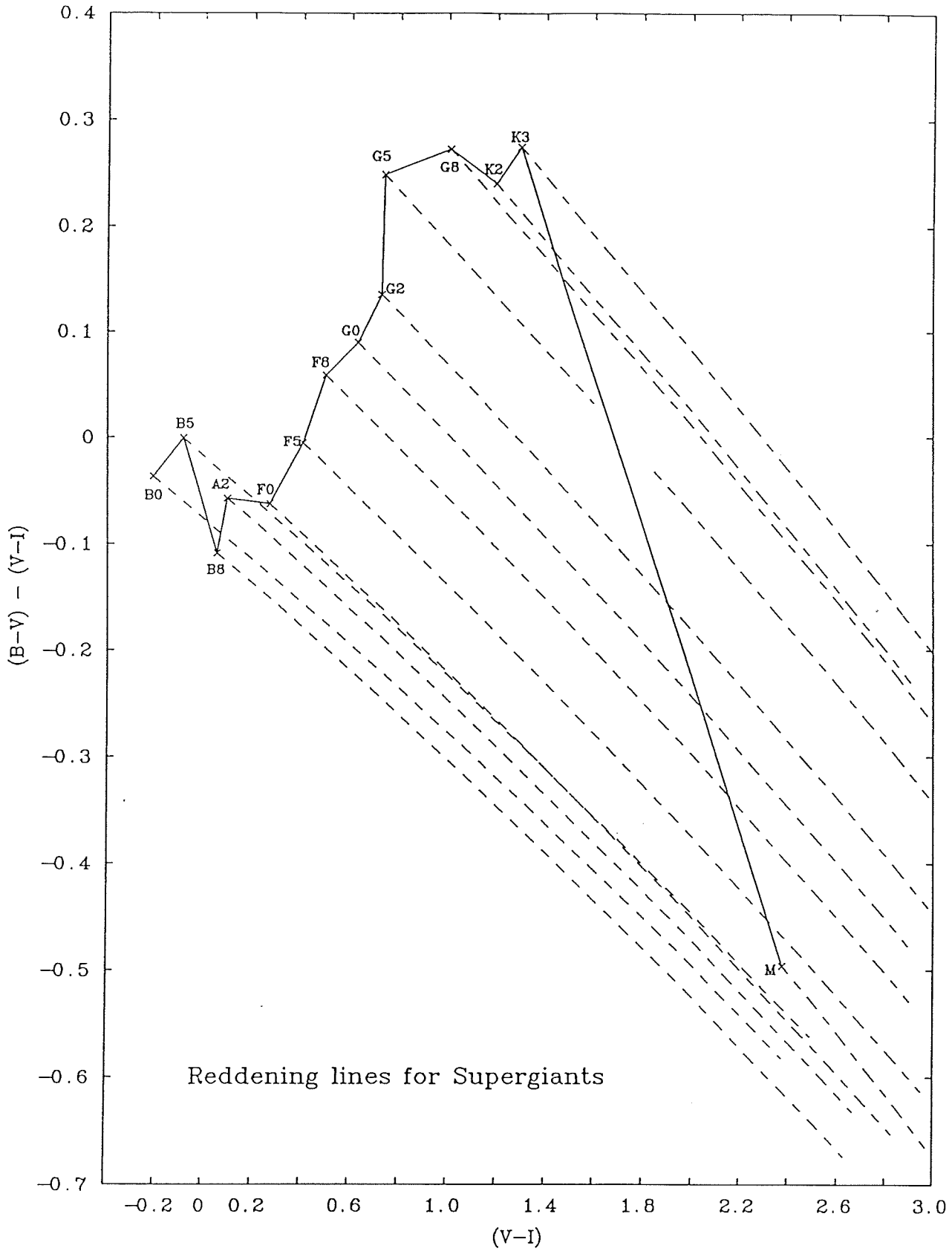

Figure 6.4: Reddening lines for luminosity class I.

and then supergiants (with giants the more likely).

As there can be considerable confusion in spectral type this technique is undoubtedly less certain than the Q method. However, the advent of CCD detectors has allowed simultaneous photometry of hundreds of stars in a field so the errors produced by the classification can be considerably reduced.

6.3 Application to the galactic direction of V348 Sgr

6.3.1 SAAO CCD observations

CCD observations were obtained at SAAO on 12^{th} June 1986, using the 1.0m telescope and RCA CCD. SAAO filter set #2 was used for all the observations. The night was completely photometric, however, the moon was close to full consequently enhancing the sky background. Standards were observed throughout the night. The images of V348 Sgr were obtained as the star approached the zenith. No *fringing* was apparent on any of the frames. The seeing during the night varied from 2–3″. Flat-field frames were secured on the twilight and dawn skies, with the telescope put out of focus.

6.3.2 Reduction of the E-Region standard star images

All object frames were flat-fielded and dark frame subtracted at SAAO under the guidance of Dr. P. Mack using the standard SAAO reduction package. Only flat-field frames with a reasonable number of counts and free from cosmic ray blemishes were used. Using SAAO versions of ASPIC programs that allow aperture photometry to be performed, the standard stars were reduced to the instrumental $UBVRI$ system (the standard SAAO colour coefficients for Filter set #2 were used, see Walker, 1984). This package ran as a batch job, requiring no interaction. The derived zero-points for transforming from the instrumental to standard magnitudes are shown in Table 6.1.

Table 6.2 shows the final derived standard star magnitudes. The quoted errors are the difference between their derived and accepted magnitudes.

Table 6.1: Zero-point corrections from the instrumental to the standard system.

Magnitude	Std error	Number
V : 0.555	0.0023	8
B-V: 0.186	0.0041	8
U-B: -2.570	0.0237	7
V-R: -0.272	0.0045	8
V-I: 0.460	0.0068	8

Table 6.2: Derived standard star magnitudes.

Star	V	B-V	U-B	V-R	V-I
1 E520	7.528 -0.010	0.560 0.009	-0.048 0.030	0.326 0.009	0.650 -0.015
2 E523	8.378 0.002	0.652 0.008	0.180 0.046	0.350 0.000	0.680 -0.016
3 E534	8.534 0.009	1.529 0.005	0.000 9.999	0.816 0.013	1.560 0.012
4 E517	8.788 0.000	0.524 0.005	0.114 0.038	0.314 -0.011	0.620 -0.005
5 E572	8.940 0.000	0.670 0.001	0.141 0.000	0.368 -0.021	0.723 -0.005
6 E568	9.476 -0.001	0.254 -0.009	0.142 -0.008	0.138 0.007	0.286 0.011
7 E506	8.537 -0.007	0.170 0.006	0.106 -0.135	0.096 -0.009	0.204 -0.018
8 E710	8.837 0.006	0.014 -0.026	-0.386 0.030	0.035 0.013	0.067 0.037

Table 6.3: Broadband images of V348 Sgr obtained on $14/15^{th}$ June, 1987.

Run no.	Filter	Seeing *arcsecs*	Dwell time *secs*
102-2-54	R	2.5	1100
102-2-55	I	2.5	1400
102-2-56	B	2.1	2000
102-2-57	V	2.4	1400
102-2-58	U	2.2	5500

6.3.3 Measuring the colours and magnitudes of the program stars

The broadband images of V348 Sgr obtained are tabulated in Table 6.3. Although a U frame was obtained, the CCD efficiency at this wavelength is only a few percent, and only the brightest stars were detectable.

The V frame was used to identify 121 relatively unblended objects that could be used in the subsequent analysis. Figure 6.5 is a contour plot of this frame with the chosen stars indicated. The six most isolated stars (9, 21, 34, 61, 92, 101) were then designated *local standards* and were used via aperture photometry to derive the necessary corrections to the standard system. The procedure consisted of firstly determining a zero-point (say FZP) which is dependent on the integration time (Int), extinction coefficient (k_λ) for the given filter, and airmass ($sec(z)$) at the time of observation (although not strictly correct, this was assumed to be the airmass at the central point of the integration). FZP for any filter is given by:

$$X_{FZP} = 20 + 2.5\log(Int) - k_\lambda sec(z) \tag{6.3}$$

This procedure was repeated for all filters used to obtain $V_{FZP}, B_{FZP}, R_{FZP}$, and I_{FZP}. If the actual local standard magnitudes are given by M_{frame}, the instrumental magnitudes (M_{instru}) can be expressed as:

$$M_{instru} = M_{frame} - X_{FZP} \tag{6.4}$$

After forming the required colour indices, the magnitudes can be transformed to the standard system using (see Walker, 1984):

$$V = V_{instru} + V_{zp} \tag{6.5}$$

$$B - V = 1.090(B - V)_{instru} + (B - V)_{zp} \tag{6.6}$$

$$V - R = 1.030(V - R)_{instru} + (V - R)_{zp} \tag{6.7}$$

$$V - I = 0.975(V - I)_{instru} + (V - I)_{zp} \tag{6.8}$$

ASPIC routines were then used to measure the magnitudes (as given by the actual program used) for all the identified stars *via* Lorentz profile fitting. The zero-point of the program magnitude scale was then shifted so the magnitudes of the local standards agreed with the magnitudes of these stars when placed on the standard system. Table 6.4 shows the magnitudes and colours for all the stars measured.

It is not straight forward to estimate the errors in the these quantities as they are strongly dependent on the brightness of the star in question and its degree of blending with neighbouring objects. However, the brightest stars should have photometric errors of around $0^{m}.01$, while the faintest stars may have errors as large as $0^{m}.2$. V348 Sgr (star #41) appears to display very unusual colours.

In Table 6.4 the symbols S and H in the first column refers to stars used as *local standards* and those having their *V magnitude measured by Heck et al. (1985)* respectively.

6.3.3.1 Comparison with the work of Heck et al

Heck *et al.* (1985) observed the V348 Sgr field and produced a photometric sequence to aid photographic photometry of the region. There are some stars in common between their list and those measured with the CCD observations. Table 6.5 compares the two sequences.

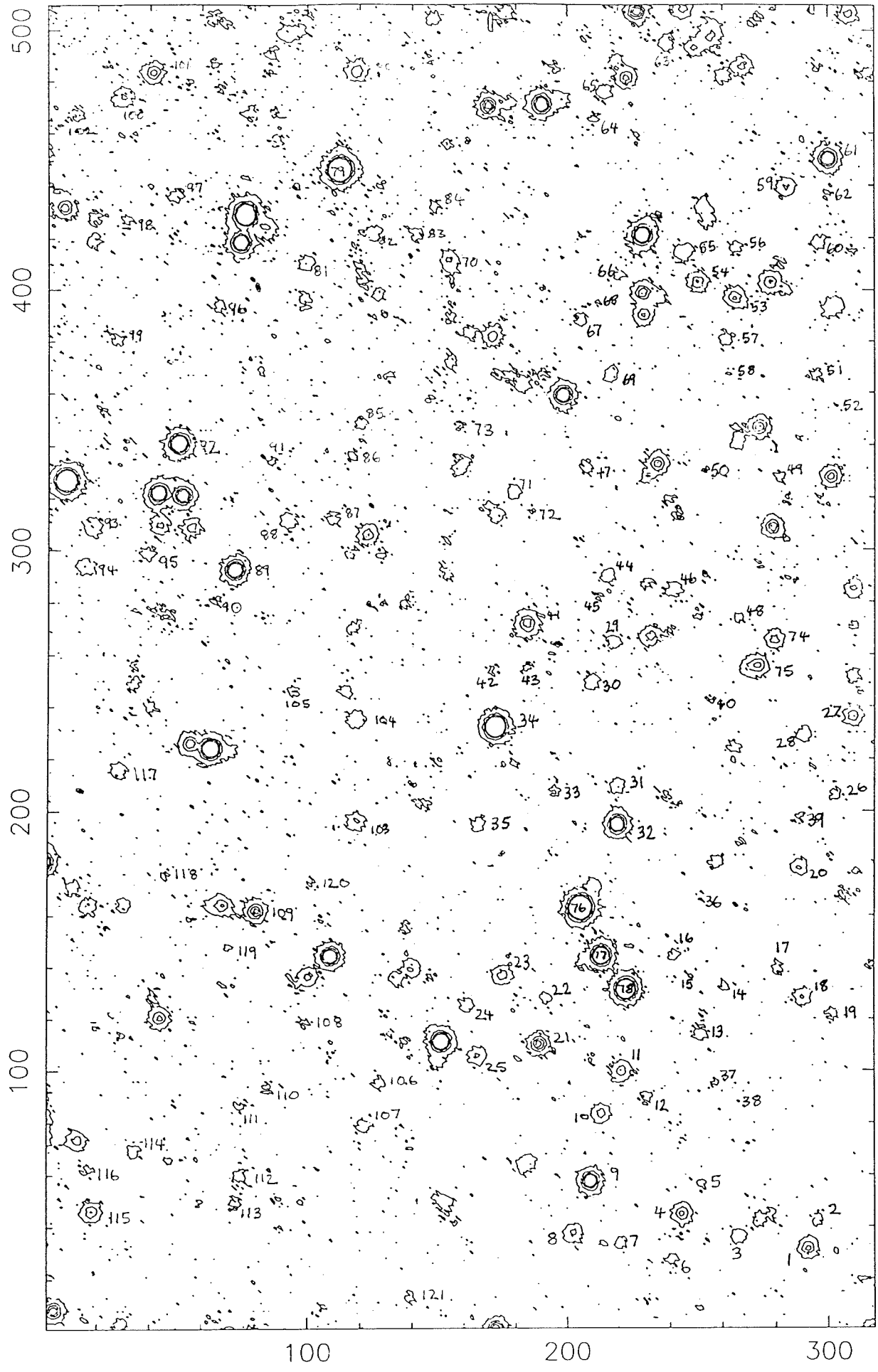

Figure 6.5: Identifications for stars used in reddening determination.

Table 6.4: Magnitudes and colours for stars identified in Figure 6.5.

Star	V	$B-V$	$V-R$	$V-I$	$R-I$	$(B-V)-(V-I)$	$(V-R)-(R-I)$
#1H	17.21	0.99	0.53	1.08	0.55	-0.09	-0.02
#2	18.92	0.80	0.54	1.01	0.46	-0.21	0.08
#3	18.41	0.91	0.35	0.99	0.64	-0.08	-0.29
#4	17.14	1.08	0.55	1.16	0.61	-0.08	-0.06
#5	19.07	0.91	0.48	1.34	0.86	-0.43	-0.38
#6	19.17	0.70	0.18	0.78	0.60	-0.08	-0.42
#7	18.71	1.11	0.57	1.31	0.74	-0.20	-0.16
#8	17.61	1.11	0.56	1.12	0.56	-0.01	0.00
#9S	15.97	1.27	0.65	1.35	0.69	-0.08	-0.04
#10	17.70	0.89	0.46	1.00	0.54	-0.10	-0.08
#11	17.45	1.04	0.58	1.11	0.53	-0.08	0.05
#12	18.86	0.93	0.46	0.97	0.51	-0.04	-0.05
#13	18.73	0.87	0.48	1.07	0.59	-0.20	-0.11
#14	19.02	1.05	0.60	1.28	0.68	-0.23	-0.07
#15	19.23	1.45	0.19	1.30	1.11	0.15	-0.92
#16	18.90	0.95	0.43	1.02	0.59	-0.07	-0.16
#17	18.50	1.16	0.57	1.25	0.68	-0.09	-0.10
#18	17.84	1.09	0.52	1.10	0.58	-0.01	-0.06
#19	18.31	1.45	0.72	1.42	0.70	0.03	0.02
#20	17.96	0.93	0.46	1.05	0.59	-0.12	-0.13
#21S	16.84	0.94	0.48	1.04	0.56	-0.10	-0.08
#22	18.78	1.13	0.62	1.33	0.70	-0.19	-0.08
#23	17.46	1.05	0.55	1.15	0.60	-0.11	-0.05
#24	18.31	1.19	0.56	1.26	0.70	-0.07	-0.13
#25	17.75	1.10	0.44	1.10	0.66	0.00	-0.23
#26	18.80	1.12	0.56	1.14	0.58	-0.02	-0.02
#27	17.78	0.63	0.41	0.85	0.44	-0.22	-0.03
#28	18.25	1.05	0.51	1.11	0.60	-0.07	-0.09
#29	18.68	0.77	0.39	1.04	0.65	-0.26	-0.26
#30	18.25	0.88	0.45	1.10	0.65	-0.22	-0.21
#31	18.17	1.00	0.52	1.10	0.58	-0.10	-0.06
#32	16.14	0.92	0.47	1.00	0.53	-0.08	-0.06
#33	19.10	0.96	0.58	1.22	0.64	-0.26	-0.05
#34SH	14.85	1.27	0.65	1.34	0.68	-0.07	-0.03
#35	18.51	0.98	0.43	1.00	0.57	-0.01	-0.14
#36	19.48	0.89	0.51	1.11	0.60	-0.22	-0.09
#37	19.27	0.76	0.43	0.92	0.49	-0.15	-0.06
#38	19.20	1.48	0.70	1.52	0.83	-0.04	-0.13
#39	18.98	1.05	0.42	1.03	0.61	0.02	-0.19
#40	19.63	1.06	0.44	1.17	0.73	-0.11	-0.29
#41	17.18	0.76	0.76	2.01	1.25	-1.25	-0.49
#42	19.18	1.11	0.48	1.10	0.62	0.01	-0.14
#43	19.21	1.07	0.24	1.07	0.83	-0.01	-0.59
#44	18.40	0.97	0.46	1.05	0.60	-0.08	-0.14
#45	19.29	1.05	0.41	1.05	0.65	-0.01	-0.24
#46	18.59	1.69	0.37	0.95	0.58	0.74	-0.21
#47	18.58	1.09	0.61	0.81	0.20	0.28	0.42
#48	19.07	0.95	0.68	1.19	0.52	-0.24	0.16
#49	18.97	1.05	0.53	1.48	0.95	-0.44	-0.42
#50	19.31	1.23	0.57	1.39	0.81	-0.15	-0.24
#51	18.80	1.03	0.59	1.18	0.59	-0.16	0.00
#52	19.60	1.28	0.63	1.11	0.48	0.16	0.16
#53	16.97	1.38	0.69	1.42	0.73	-0.03	-0.04
#54	17.38	0.98	0.47	1.05	0.58	-0.06	-0.11
#55	18.11	1.01	0.51	1.08	0.57	-0.07	-0.06
#56	18.77	1.09	0.41	1.03	0.64	0.05	-0.23
#57	18.80	0.83	0.54	1.07	0.53	-0.25	0.01
#58	19.48	1.00	0.60	1.24	0.64	-0.24	-0.03
#59	17.94	0.85	0.49	1.03	0.54	-0.17	-0.05

Star	V	$B-V$	$V-R$	$V-I$	$R-I$	$(B-V)-(V-I)$	$(V-R)-(R-I)$
#60	18.25	1.23	0.70	1.36	0.66	-0.12	0.04
#61S	16.34	0.79	0.41	0.88	0.47	-0.09	-0.06
#62	19.19	1.24	0.68	1.28	0.60	-0.04	0.07
#63	18.05	1.38	0.60	1.49	0.89	-0.11	-0.29
#64	19.15	1.03	0.36	1.24	0.88	-0.21	-0.53
#65	18.90	0.96	0.15	1.12	0.97	-0.16	-0.82
#66	19.87	0.77					
#67	18.50	1.22	0.58	1.37	0.78	-0.15	-0.20
#68	19.10	1.37	0.56	1.35	0.78	0.03	-0.22
#69	18.34	1.15	0.56	1.09	0.53	0.05	0.03
#70	17.67	1.07	0.64	1.25	0.61	-0.18	0.04
#71	18.55	1.03	0.33	0.97	0.64	0.06	-0.32
#72	19.34	0.99	0.39	1.19	0.80	-0.20	-0.42
#73	19.03	1.21	0.64	1.34	0.69	-0.13	-0.05
#74	17.63	1.00	0.54	1.07	0.53	-0.07	0.01
#75	16.84	1.28	0.71	1.30	0.59	-0.02	0.11
#76H	14.46	1.18	0.59	1.20	0.61	-0.02	-0.01
#77	14.86	1.88	1.06	2.17	1.11	-0.29	-0.05
#78	15.47	0.77	0.38	0.83	0.45	-0.06	-0.08
#79H	14.36	1.35	0.70	1.37	0.67	-0.01	0.03
#80	17.31	1.07	0.56	1.17	0.61	-0.10	-0.05
#81	18.09	1.19	0.60	1.23	0.63	-0.04	-0.02
#82	18.64	0.93	0.47	1.10	0.63	-0.18	-0.16
#83	18.80	1.01	0.63	1.21	0.58	-0.20	0.06
#84	18.99	0.99	0.43	1.00	0.57	0.00	-0.14
#85	18.55	1.22	0.57	1.11	0.54	0.11	0.03
#86	18.88	1.09	0.66	1.22	0.57	-0.13	0.09
#87	18.83	0.87	0.16	1.05	0.89	-0.18	-0.73
#88	18.09	1.10	0.50	1.03	0.52	0.08	-0.02
#89	15.19	1.90	1.15	2.51	1.36	-0.61	-0.21
#90	19.08	1.06	0.45	0.97	0.52	0.09	-0.07
#91	19.12	1.06	0.49	1.09	0.60	-0.04	-0.11
#92SH	15.89	0.91	0.44	0.96	0.52	-0.05	-0.08
#93	17.65	1.45	0.72	1.41	0.69	0.04	0.03
#94	18.01	1.17	0.58	1.14	0.56	0.02	0.02
#95	18.64	0.99	0.46	1.05	0.60	-0.06	-0.14
#96	18.62	1.18	0.59	1.22	0.63	-0.04	-0.03
#97	18.74	0.87	0.53	1.03	0.49	-0.15	0.04
#98	19.10	0.97	0.46	1.16	0.70	-0.19	-0.24
#99	18.75	1.22	0.92	2.07	1.15	-0.85	-0.22
#100	17.71	1.06	0.47	1.04	0.57	0.02	-0.10
#101S	16.67	1.53	0.79	1.55	0.76	-0.03	0.03
#102	18.96	1.03	0.53	1.10	0.57	-0.08	-0.04
#103H	18.19	0.65	0.35	0.77	0.43	-0.12	-0.08
#104	17.81	1.31	0.66	1.40	0.74	-0.09	-0.09
#105	18.97	1.04	0.44	1.06	0.63	-0.03	-0.19
#106	18.69	0.96	0.45	1.02	0.57	-0.06	-0.12
#107	18.37	1.09	0.56	1.19	0.63	-0.10	-0.07
#108	19.58	0.59	0.77	1.33	0.56	-0.74	0.21
#109	16.78	1.04	0.49	1.06	0.57	-0.03	-0.08
#110	18.93	1.08	0.61	1.08	0.47	0.00	0.14
#111	18.98	1.01	0.38	1.02	0.64	0.00	-0.26
#112	18.59	0.92	0.49	0.99	0.50	-0.07	-0.01
#113	18.57	1.18	0.57	1.08	0.51	0.09	0.06
#114	18.27	1.38	0.70	1.33	0.63	0.06	0.06
#115	17.38	1.01	0.50	1.05	0.54	-0.03	-0.04
#116	19.23	0.95	0.21	1.10	0.89	-0.15	-0.68
#117	18.27	1.04	0.46	0.99	0.53	0.05	-0.07
#118	19.21	0.94	0.61	1.00	0.38	-0.06	0.23
#119	19.16	1.07	0.42	1.05	0.64	0.01	-0.22
#120	19.11	1.12	0.44	1.06	0.63	0.06	-0.19
#121	18.94	1.00	0.44	1.03	0.59	-0.02	-0.15

Table 6.5: Comparison of CCD results with those of Heck *et al.*

Heck *et al.* #	R.A. 1950	Dec. 1950	$V_{Heck et al.}$	CCD #	V_{CCD}	$V_{Heck et al.} - V_{CCD}$
8	18 37 13	-22 56 52	14.31±0.02	79	14.36	-0.05
10	18 37 16	-22 56 27	15.90±0.08	92	15.89	0.01
12	18 37 19	-22 57 13	14.83±0.03	34	14.85	-0.02
13	18 37 20	-22 56 45	17.92±0.14	103	18.19	-0.27
14	18 37 21	-22 57 25	14.37±0.10	76	14.46	-0.09
20	18 37 25	-22 57 55	17.20±0.36	1	17.21	-0.01

As can be seen, the residuals between the two sets of measurements are well within the observational errors. For the brighter stars the agreement is good, while for fainter stars the CCD magnitudes are to be preferred, being less affected by sky measurement problems etc.

6.3.4 Spectral types of the program stars

The objects were then plotted in the $(V-I),(B-V)-(V-I)$ plane (Figure 6.6) and their spectral types determined using the classification criteria established in Section 6.2. These results are given in Table 6.6 along with the corresponding absolute magnitude (M_V) found using the relationship given by Allen (1973). For some stars of uncertain spectral type, two possible types may be determined by adopting both high and low reddening estimates.

Table 6.7 lists the remaining stars, along with their corresponding distance estimates. The last column describes the degree of uncertainty in the classification (3 indicates the least certain, and 1 the most). Figure 6.7 is a plot of reddening *vs* distance for all the objects in Table 6.7 and demonstrates that considerable scatter may result if objects of dubious spectral type are included. However, it is interesting to note that to a first approximation two groups of stars appear to be present.

(i) *Stars with low reddening, but apparently high distance.* These objects were generally classified as luminosity group III, but were not thought to be reddened appreciably. It is likely that these objects have all been misclassified.

(ii) *Stars having a linear increase of reddening with distance.* It is expected that the spectral type classification for these objects is at least approximately correct, and it is these stars that will define the final reddening-distance relationship.

Using the objects in Table 6.7 that were assessed to have the most reliable spectral type, the reddening-distance relation was redrawn (see Figure 6.8). The relationship is best defined up to $E_{B-V} \sim 0.5$. Beyond this distance (about 5kpc) late type dwarfs are no-longer detectable (improved images may change this), and we are forced to rely on highly-reddened early type stars. The increase in scatter in the relationship at high reddening values is caused by:

(i) confusion produced by spectral type uncertainty for early type stars,

(ii) the predicted distances for these objects place them in the galactic halo and as already discussed metallicity effects may be important to intrinsic colours,

(iii) the number of objects defining the relationship at high reddening is small,

6.4 Implications of the new reddening—distance relation for V348 Sgr

The reddening-distance relation obtained suggests that V348 Sgr is at a distance of (4.7 $\pm$ 1.0)kpc. However, the small number of reliable candidate stars defining the most distant parts of the relation imply that some error in the upper limit may be present, although unlikely. Without deeper images of this field it is difficult to ascertain the magnitude (if present) of this error. However, if we assume that 4.7kpc is indeed the object's distance and that the apparent magnitude is $m_v \sim 12^m.2$ with $E_{B-V} = 0.45$, then using a bolometric correction suitable for a 20 000 K helium atmosphere (BC $\sim$ 1.7: Schönberner, 1986) we can derive a luminosity of $L_{BOL} \sim 3\,500\ L_\odot$. This value is slightly lower than luminosities usually derived for EHe and R CrB stars ($L_{BOL} \sim 10^4\ L_\odot$).

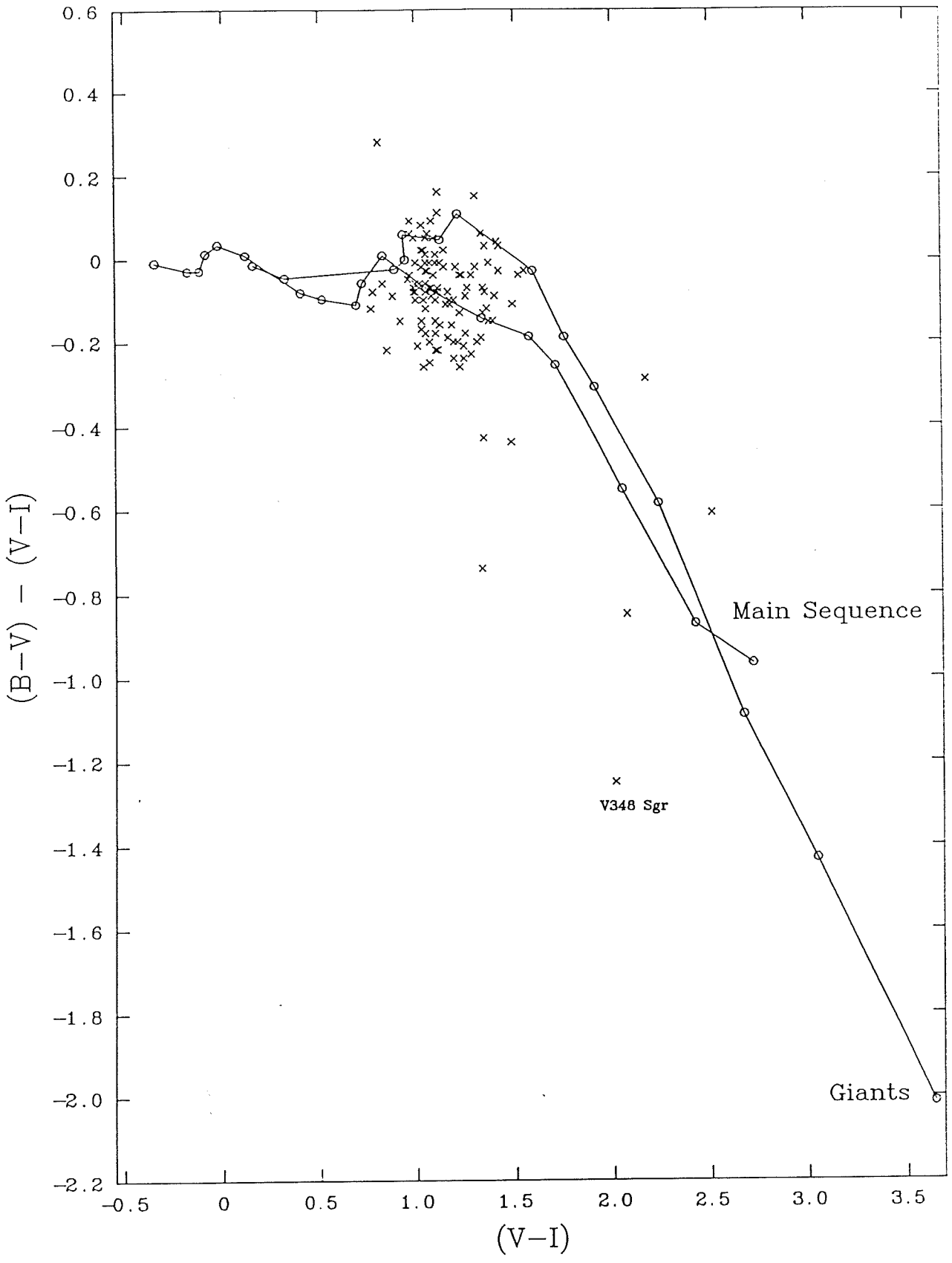

Figure 6.6: The positions of the program stars in the $(V-I),(B-V)-(V-I)$ plane.

Table 6.6: Spectral types as determined from Figure 6.6.

Star	Spectral Type if:		M_V range	$E(B-V)$	m_V reddening corrected
	High Reddening	Low Reddening			
#1	G5-K0 V		5.1—5.9	0.24	16.44
#2	B8-F5 V	A0-A5 V	-0.25—3.5	0.40—0.90	16.04—17.64
#3	G5-K0 V		5.1—5.9	0.18	17.83
#4	G5-K0 V		5.1—5.9	0.28	16.24
#5	?				
#6	G5 V		5.1	0.48	18.98
#7	G5 V		5.1	0.06	17.17
#8	G8-K0 III		0.7—0.8	0.15	17.13
#9	G8-K0 III		0.7—0.8	0.33	14.91
#10	G5-K0 V		5.1—5.9	0.20	17.06
#11	G5-K0 V	K0-K3 V	5.1—6.65	0.24	16.68
#12	G5-K0 V	K0-K3 V	5.1—6.65	0.12	18.48
#13	A0-A5V,F5-G0V		0.65—4.4	0.38—0.86	15.98—17.51
#14	G0-G5 V		4.4—5.1	0.51	17.39
#15	?				
#16	G5-K0 V	K0-K3 V	5.1—5.9	0.19	18.29
#17	K0 V		5.9	0.33	17.44
#18	G8-K0 III		0.7—0.8	0.12	17.46
#19	K3-K5 III	K4 III	-0.2—0.3	0.00—0.19	17.70—18.31
#20	G5-K0 V		5.1—5.9	0.24	17.19
#21	G5-K0 V		5.1—5.9	0.22	16.14
#22	G5-K0 V		5.1—5.9	0.48	17.24
#23	G5-K0 V	K0-K3 V	5.1—6.65	0.30	16.50
#24	G8-K0 III		0.7—0.8	0.26	17.48
#25	G8-K0 III		0.7—0.8		
#26	G8-K0 III		0.7—0.8	0.18	18.22
#27	B5-B8 V		-1.2—-0.25	0.77	15.32
#28	G5-K0 V		5.1—5.9	0.23	17.51
#29	B5-B8 V		-1.2—-0.25	0.91	15.77
#30	F5-G0 V		3.5—4.4	0.46—0.95	15.21—16.78
#31	G5-K0 V	K0-K3 V	5.1—6.65	0.26	17.34
#32	G5-K0 V	K0-K3 V	5.1—6.65	0.18	15.56
#33	B3-B8V,F0-F5V		-1.6—3.5	0.55—1.05	15.74—17.34
#34	G8-K0 III		0.7—0.8	0.32	13.83
#35	K0V,G8-K0III		0.7—5.9	0.05—0.11	18.16—18.35
#36	B8-A0V,F5-G0V		-0.25—4.4	0.47—0.94	16.46—17.98
#37	G0-G5 V		4.4—5.1	0.22	18.57
#38	K2-K3 III		0.3—0.5	0.32	18.18
#39	G8-K0 III		0.7—0.8	0.09	18.69
#40	G5-K0 V	K0-K3 V	5.1—6.65	0.31	18.64
#41	V348 Sgr				
#42	G8-K0 III		0.7—0.8	0.14	18.73
#43	G8-K0 III		0.7—0.8	0.10	18.89
#44	G5-K0 V	K0-K3 V	5.1—6.65	0.21	17.73
#45	G8-K0 III		0.7—0.8	0.10	18.97
#46	?				
#47	?				
#48	B8-A0V,F5-G0V		-0.25—4.4	0.52—1.02	15.81—17.41
#49	?				
#50	G5-K0V,K3-K5V	K5-K9 V	5.1—8.7	0.00—0.47	17.81—19.31
#51	G5-K0 V		5.1—5.9	0.37	17.62
#52	?				
#53	K2-K3 III		0.3—0.5	0.24	16.20
#54	G5-K0 V	K0-K3 V	5.1—6.65	0.19	16.77
#55	G5-K0 V	K0-K3 V	5.1—6.65	0.22	17.41
#56	K0-K2 III	K1 III	0.5—0.7	0.00—0.05	18.61—18.77
#57	B5-B8 V		-1.2—-0.25	0.89	16.73
#58	B8-A0V,F5-G0V		-0.25—4.4	0.55—1.01	16.25—17.72
#59	G0-G5 V		4.4—5.1	0.30	16.98

Star	Spectral Type if:		M_V range	$E(B-V)$	m_V reddening corrected
	High Reddening	Low Reddening			
#60	K0 V		5.9	0.43	16.87
#61	G5-K0 V		5.1—5.9	0.12	15.96
#62	G8-K0 III		0.7—0.8	0.29	18.26
#63	G8-K0 III		0.7—0.8	0.46	16.58
#64	G0-G5 V		4.4—5.1	0.43	17.77
#65	G0-G5 V		4.4—5.1	0.32	17.88
#66	?				
#67	G5-K5 V	K5-K7 V	5.1—8.1	0.00—0.46	17.03—18.50
#68	K2-K3 III		0.3—0.5	0.15	18.62
#69	K0-K3 III	K1 III	0.3—0.7	0.00	18.34
#70	G5-K0 V		5.1—5.9	0.42	16.33
#71	K0-K2 III	K0 III	0.5—0.7	0.00	18.55
#72	G0-G5 V		4.4—5.1	0.42	18.00
#73	G5-K0V,K0-K5V		5.1—7.35	0.42	17.69
#74	G5-K0 V		5.1—5.9	0.21	16.96
#75	K0-K2 III		0.5—0.7	0.36	15.69
#76	G8-K0 III		0.7—0.8	0.21	13.79
#77	G8-K0III,K5-M0III		-0.4—0.8	0.35	13.74
#78	G5-K0 V		5.1—5.9	0.06	15.28
#79	K2-K3 III		0.3—0.5	0.20	13.72
#80	G5-K0 V	K3 V	5.1—6.65	0.00—0.30	16.35—17.31
#81	G8-K0 III		0.7—0.80	0.25	17.29
#82	G0-G5 V		4.4—5.1	0.31	17.65
#83	G0-G5 V		4.4—5.1	0.41	17.49
#84	?				
#85	?				
#86	G5-K0 V	K4 V	5.1—7.0	0.36	17.73
#87	G0-G5 V		4.4—5.1	0.28	17.93
#88	?				
#89	M2-M3 III		-0.6	0.31	14.20
#90	?				
#91	K0 V		5.9	0.20	18.48
#92	G5-K0 V	K0-K3 V	5.1—6.65	0.00—0.12	15.51—15.89
#93	K2-K3 III	K4 III	0.0—0.5	0.00—0.18	17.07—17.65
#94	K0-K2 III		0.5—0.7	0.12	17.63
#95	G5-K0 V	K0-K3 V	5.1—6.65	0.00—0.19	18.03—18.64
#96	G8-K0 III		0.7—0.8	0.33	17.56
#97	G0-G5 V		4.4—5.1	0.24	17.97
#98	G0-G5 V		4.4—5.1	0.35	17.98
#99	?				
#100	G8-K0 III		0.7—0.8	0.09	17.42
#101	K2-K3 III	K5 III	-0.2—0.5	0.38	15.45
#102	G5-K0 V	K3 V	5.1—6.65	0.00—0.23	18.22—18.96
#103	G0-G5 V		4.4—5.1	0.05	18.03
#104	G8-K0 III		0.7—0.8	0.38	16.59
#105	K0V,G8III		0.8—5.9	0.10—0.17	18.43—18.65
#106	G5-K0 V	K0-K3 V	5.1—6.65	0.00—0.18	18.11—18.69
#107	G5-K0 V	K3-K5 V	5.1—6.65	0.00—0.31	17.38—18.37
#108	?				
#109	K0V,G8III		0.8—5.9	0.10—0.18	16.20—16.46
#110	?				
#111	?				
#112	G5-K0 V	K0-K3 V	5.1—6.65	0.00—0.17	18.05—18.59
#113	?				
#114	K2-K3 III	K4 III	0.0—0.4	0.00—0.11	17.92—18.27
#115	K0V,G8III		0.8—5.9	0.09—0.16	16.87—17.09
#116	G5 V		5.5	0.30	18.27
#117	K0-K2 III	K1 III	0.5—0.7	0.00—0.02	18.21—18.27
#118	G5-K0 V	K0-K3 V	5.1—6.65	0.17	18.67
#119	G8-K0 III		0.7—0.8	0.09	18.87
#120	K0-K2 III	K1 III	0.5—0.7	0.0	19.11
#121	G8 III		0.8	0.15	18.46

Table 6.7: Final values of distance and reddening for program objects.

Star	$\overline{m_V}$	$\overline{M_V}$	Average distance Pc.	$\overline{E(B-V)}$	Degree of Confusion
#1	16.44	5.5	1542	0.24	1
#2	16.84	1.6	11015	0.65	3
#3	17.83	5.5	2924	0.18	1
#4	16.24	5.5	1406	0.28	1
#5					
#6	18.98	5.1	5970	0.48	1
#7	17.17	5.1	2594	0.06	2
#8	17.13	0.8	18450	0.15	3
#9	14.91	0.8	6637	0.33	2
#10	17.06	5.5	2051	0.20	1
#11	16.68	5.9	1432	0.24	1
#12	18.48	5.9	3281	0.12	3
#13	16.75	2.5	7079	0.62	1
#14	17.39	4.8	3266	0.51	3
#15					
#16	18.29	5.5	3614	0.33	1
#17	17.44	5.9	2032	0.19	1
#18	17.46	0.8	21478	0.12	3
#19	18.01	0.1	38194	0.10	3
#20	17.19	5.5	2178	0.24	1
#21	16.14	5.5	1343	0.22	1
#22	17.24	5.5	2228	0.48	2
#23	16.50	5.9	1318	0.30	1
#24	17.48	0.8	21677	0.26	3
#25					
#26	18.22	0.8	30478	0.18	3
#27	15.32	-0.5	14588	0.77	1
#28	17.51	5.5	2523	0.23	1
#29	15.77	-0.5	17947	0.91	1
#30	16.00	4.0	2511	0.71	3
#31	17.34	5.9	1940	0.26	1
#32	15.56	5.9	855	0.18	1
#33	16.54	1.1	12246	0.80	1
#34	13.83	0.8	4036	0.32	1
#35	18.26	5.9	2965	0.08	3
#36	17.22	2.0	11066	0.71	1
#37	18.57	4.8	5675	0.22	2
#38	18.18	0.4	35975	0.32	3
#39	18.69	0.8	37844	0.09	3
#40	18.64	5.9	~~0.31~~ 352	0.31	1
#41					
#42	18.73	0.8	38548	0.14	3
#43	18.89	0.8	41495	0.10	3
#44	17.73	5.9	2323	0.21	1
#45	18.97	0.8	41495	0.10	3
#46					
#47					
#48	16.61	2.0	8356	0.77	1
#49					
#50	18.56	7.0	2051	0.24	1
#51	17.62	5.5	2654	0.37	1
#52					
#53	16.20	0.4	14454	0.24	3
#54	16.77	5.9	1493	0.19	1
#55	17.41	5.9	2004	0.22	1
#56	18.69	0.6	45499	0.03	3
#57	16.73	-0.7	30620	0.89	3
#58	16.99	2.0	9954	0.78	1
#59	16.98	4.8	2729	0.30	1

Star	$\overline{m_V}$	$\overline{M_V}$	Average distance Pc.	$\overline{E(B-V)}$	Degree of Confusion
#60	16.87	5.9	1563	0.43	2
#61	15.96	5.5	1236	0.12	1
#62	18.26	0.8	31046	0.29	3
#63	16.58	0.8	14322	0.46	3
#64	17.77	4.8	3926	0.43	1
#65	17.88	4.8	4130	0.32	1
#66					
#67	17.77	7.0	1426	0.23	3
#68	18.62	0.4	44056	0.15	3
#69	18.34	0.5	36983	0.00	3
#70	16.33	5.5	1466	0.42	2
#71	18.55	0.6	38905	0.00	3
#72	18.00	4.8	4365	0.42	1
#73	17.69	6.2	1986	0.24	1
#74	16.96	5.5	1959	0.21	1
#75	15.69	0.6	11803	0.36	3
#76	13.79	0.8	3963	0.21	1
#77	13.74	0.2	5105	0.35	1
#78	15.28	5.5	904	0.06	1
#79	13.72	0.4	4613	0.20	1
#80	16.83	5.9	1535	0.15	1
#81	17.29	0.8	19861	0.31	3
#82	17.65	4.8	3715	0.31	1
#83	17.49	4.8	3451	0.41	1
#84					
#85					
#86	17.73	6.2	2036	0.36	1
#87	17.93	4.8	4228	0.28	1
#88					
#89	14.20	-0.6	9120	0.31	2
#90					
#91	18.48	5.9	3281	0.20	1
#92	15.70	5.9	912	0.06	1
#93	17.36	0.4	24660	0.09	3
#94	17.63	0.6	25468	0.12	3
#95	18.34	5.9	3076	0.09	3
#96	17.56	0.8	22491	0.33	3
#97	17.97	4.8	4305	0.24	1
#98	17.98	4.8	4325	0.35	1
#99					
#100	17.42	0.8	21086	0.09	3
#101	15.45	0.1	11749	0.38	3
#102	18.59	5.9	3451	0.12	3
#103	18.03	4.8	4426	0.05	3
#104	16.59	0.8	14388	0.38	3
#105	18.54	3.4	10666	0.13	3
#106	18.40	5.9	3162	0.09	3
#107	17.88	5.9	2489	0.15	1
#108					
#109	16.33	3.4	3855	0.14	3
#110					
#111					
#112	18.32	5.9	3048	0.09	3
#113					
#114	18.10	0.2	38019	0.06	3
#115	16.98	3.4	5200	0.13	2
#116	18.27	5.5	3581	0.30	1
#117	18.24	0.6	33728	0.01	3
#118	18.67	5.9	3581	0.17	3
#119	18.87	0.8	41115	0.09	3
#120	19.11	0.6	50350	0.00	3
#121	18.46	0.8	34041	0.15	3

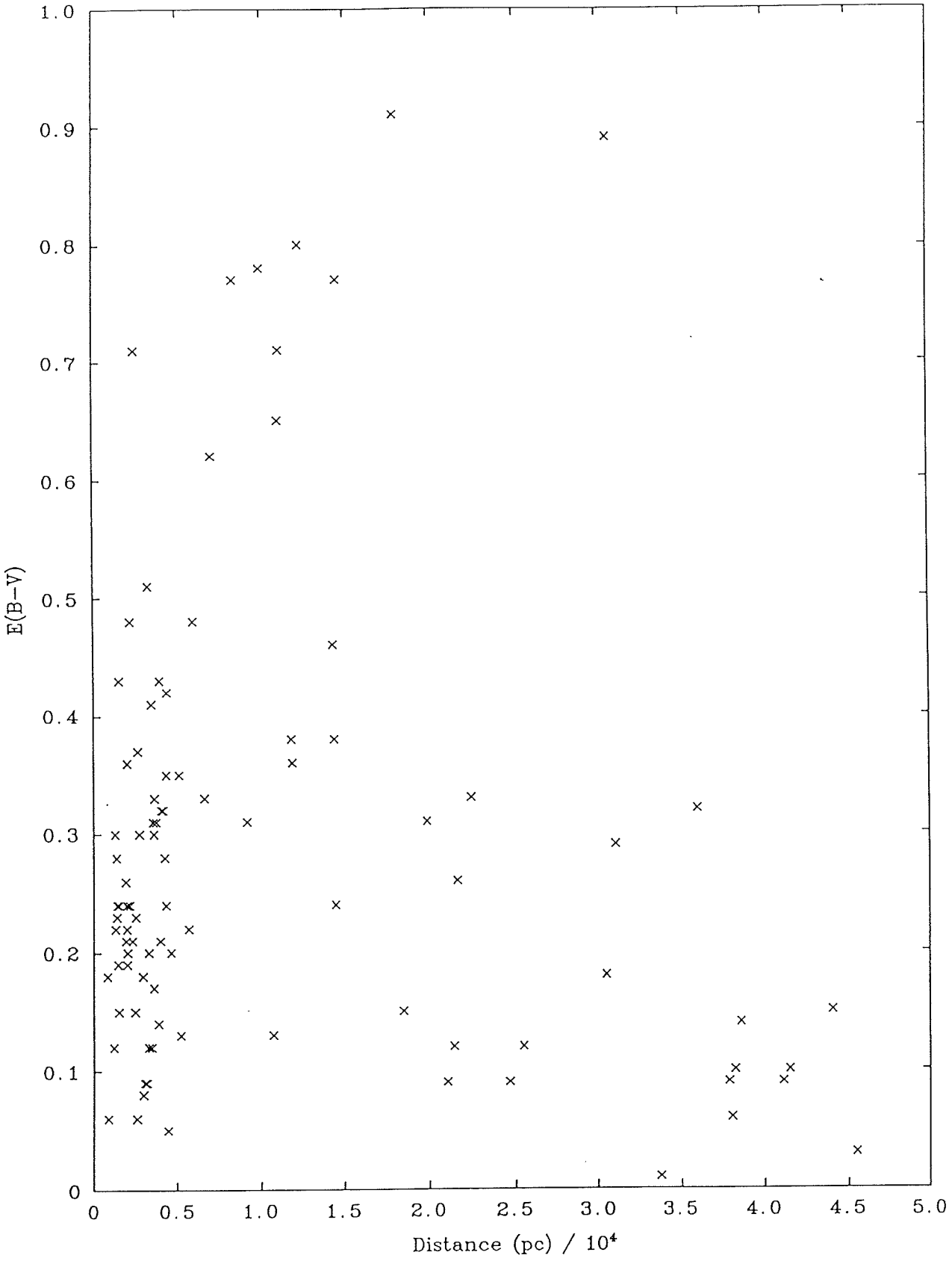

Figure 6.7: The reddening-distance relation defined using all the stars measured.

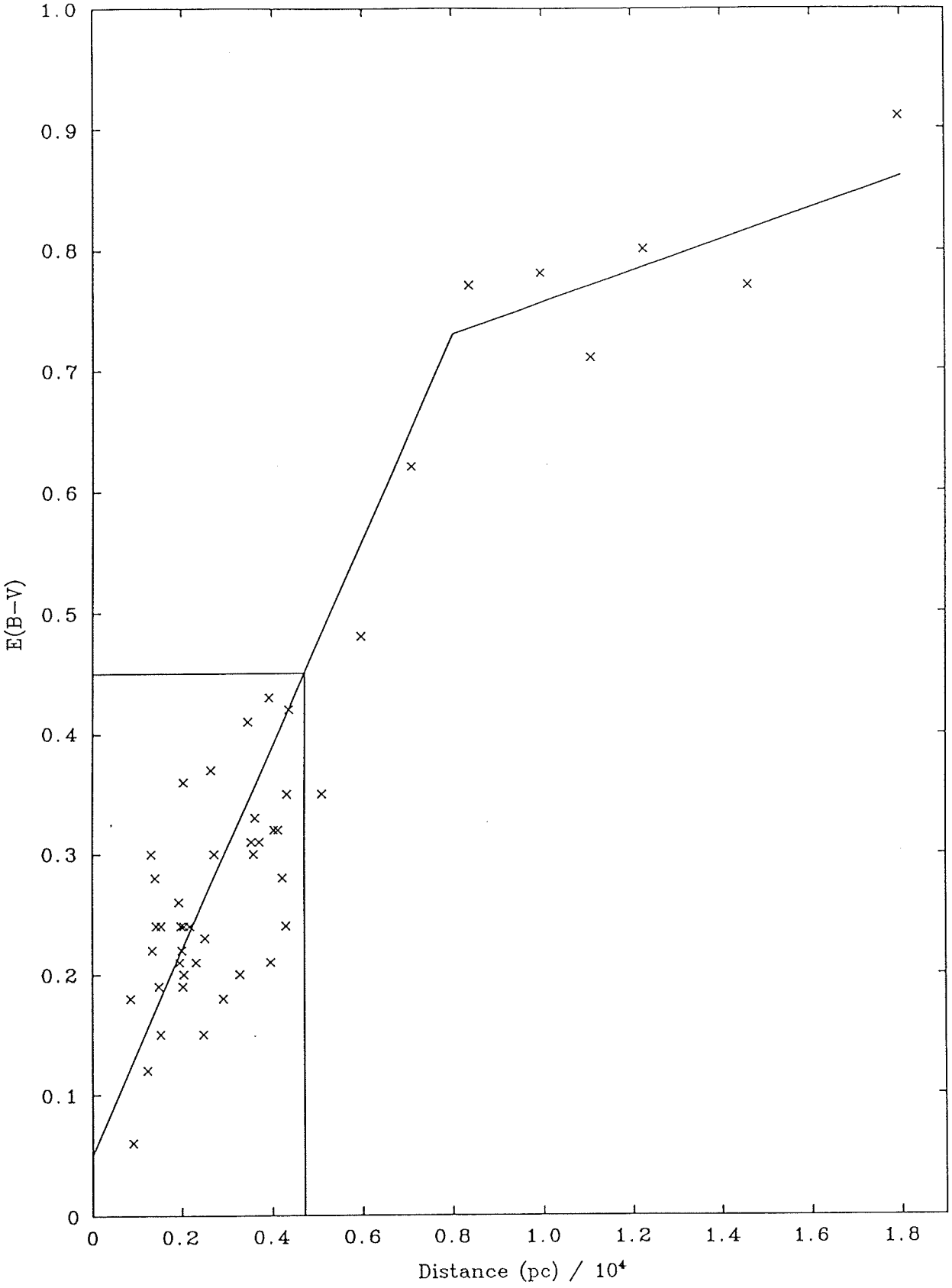

Figure 6.8: The reddening-distance relation defined by those stars with the most certain spectral type classification. At the reddening of V348 Sgr the implied distance is (4.7 ± 1.0) kpc.

6.5 Summary

The BVI_{KC} colours have been used to derive a distance of (4.7 ± 1.0) kpc for V348 Sgr. This distance implies a luminosity of $L_{BOL} \sim 3500\ L_{\odot}$. The method used provides a powerful new technique for obtaining distances for objects where the interstellar reddening may be separated from any circumstellar component.

6.6 References

1. Allen, C. W., 1973. In *Astrophysical Quantities*, p.200 (Athlone Press)
2. Catchpole, R. M., Robertson, B. S. C. and Warren, P. R., 1977. *Mon. Not. R. astr. Soc.*, **181**, 391
3. Cousins, A. W. J., 1978. *Mon. Not. astro. Soc. South Africa*, **37**, 62
4. Cousins, A. W. J., 1980. *SAAO Circ.*, **6**, 4
5. Dean, J. F., Warren, P. R. and Cousins, A. W. J., 1980. *Mon. Not. R. astr. Soc.*, **183**, 569
6. Heck, A., Houziaux, L., Manfroid, J., Jones, D. H. P. and Andrews, P. J., 1985. *Astr. Astrophys. Suppl. Ser.*, **61**, 375
7. Neckel, Th. and Klare, G., 1980. *Astr. Astrophys. Suppl. Ser.*, **42**, 251
8. Schmidt-Kaler, Th., 1961. *Astr. Nachr.*, **286**, 113
9. Schönberner, D., 1986. *In IAU Coll. No.* **87**, *Hydrogen-Deficient Stars and Related Objects*, p.221
10. Walker, A., 1984. SAAO manual *CCD Photometry using the ASPIC Programs.*

Chapter 7

The evolutionary status of the hot R CrB stars

7.1 Do the hot R CrB Stars constitute a homogeneous group?

Before it is possible to answer this question it is necessary to define the characteristics of the class more stringently. The usual criteria are:

(i) the stellar photosphere is extremely hydrogen-deficient,

(ii) the stellar photosphere must have a temperature comparable to the EHe stars (> 9 000 K),

(iii) the visual light curve displays R CrB variations, and

(iv) the star must have an IR excess (indicative of circumstellar material).

With these definitions in mind, let us briefly discuss the supposed membership of each of the candidate stars.

7.1.1 DY Cen

Is the photosphere of this star extremely hydrogen-deficient? The results of the *quick* hydrogen abundance analysis (Chapter 3) are not decisive and leave room for doubt. The recent long-term visual light curve of this object is reasonably well known and there are very few reliable observations describing possible deep minima, so in order to avoid detection these minima must occur very infrequently. The main observational material is the discovery work (Harvard patrol plates) described by Hoffleit (1930), who found well-defined minima in 1897, 1901, 1924, and 1927 from 257 observations. No minima have been recorded by the Variable Star Section of the Royal Astronomical Society of New Zealand since their members started observing it on a regular basis (around 1958). Bateson (1978) pointed out that the visual light curve suggests a gradual fading in maximum light over that period. DY Cen is a weak IR source (Glass, 1978). IRAS observations have indicated the presence of a 350 K (black body fit) dust shell (Walker, 1986).

7.1.2 MV Sgr

The photosphere of this star in many ways resembles the EHe star HD 124448 (Jeffery *et al.* , 1988), but the presence of emission lines suggests matter is still in the process of being ejected. There can be no doubt as to the hydrogen-deficient nature of this star's photosphere. Although MV Sgr was discovered by Woods (1928), she published relatively few observations but was able to determine the magnitude range of the variation. Hoffleit (1959) presents some 25 years of photometric observations for this star, within which two minima are apparent. The period required for recovery of the star to maximum appears to be relatively long by R CrB standards—around 3 years. MV Sgr is known to have a strong IR excess (Feast and Glass, 1974 and Walker, 1986).

7.1.3 V348 Sgr

At low resolution the spectrum of this star at maximum light is dominated by stellar wind and nebular emission. Observations at high resolution are extremely rare

(Houziaux, 1968) and indicate that the photosphere may be hydrogen-deficient although higher quality data are required to determine to what extent this is so. Heber *et al.* (1984) found the UV spectrum strongly resembles that of extreme helium stars. Photometrically the star is extremely active. Bateson and Dodson (1982) analysed 26 years of visual observations and found that the star to have spent only 55% of that period close to maximum light. Hoffleit (1958) suspected that the star undergoes semi-regular variations with periods of around 200 days at some epochs of its light curve. Heck *et al.* (1985) have compiled all the available photometry (from amateur and professional sources), and again found extremely erratic behaviour. For example, the maximum of August 1981 (which was partially followed with a 1.0 m telescope at ESO) required no more than 6 days to fall from $12^{\rm m}.2$ to $> 17^{\rm m}.0$, but had recovered to approximately maximum brightness 8 days later. As with DY Cen, Heck *et al.* suggest a possible gradual fading in maximum brightness has taken place over the last 80 years. V348 Sgr has been found to be a strong IR source (Feast and Glass, 1974, Rao and Nandy, 1986, and Walker, 1986).

7.1.4 Discussion

Consider a scenario whereby a cool R CrB star (typically 7 000 K) is warmed up to temperatures comparable to EHe stars. According to the *period-temperature law* for hydrogen-deficient stars, the pulsation period should rapidly diminish from 40 days at 7 000 K to just a few days at 19 000 K. It has been suggested that the ejection mechanism in R CrB stars is in some way related to the pulsation phase (Pugach, 1977). If this is so it is reasonable to expect more *puffs* of material at shorter pulsation periods. If the star remains at *constant luminosity* then dust condensation may only occur at great distances from the central star. According to Fadeyev (1986) at luminosities comparable[1] to cool R CrB stars, the radial distance at which dust condensation occurs increases rapidly with temperature. Therefore obscuration by ejected material would only be observable if the puffs were orientated directly towards us. The decline to minimum and recovery to maximum brightness would both be rapid (the opaque dust

[1]DY Cen has a comparable luminosity to R CrB stars (see Chapter 2) while according to Jeffery *et al.* (1988) MV Sgr has $M_c \sim 0.6$ implying $L \sim 3\,000\,L_\odot$ (Jeffery, 1988)—significantly less than R CrB stars.

would disperse faster because of the large distance involved), but with the number of minima greatly reduced. In agreement with this model, minima in DY Cen and MV Sgr are very rare. Insufficient minima of these stars have been well enough observed to say anything quantitative about their duration. As the dust is thought to be carbon rich it is expected that the photospheres of these stars will have strong carbon lines, however, Jeffery *et al.* find a severe underabundance (2 dex) in carbon for MV Sgr (this may be the result of wind/chromospheric contamination of the absorption lines). DY Cen is known to have strong carbon lines in its spectra (Chapter 3).

For V348 Sgr the situation is less clear. In Chapter 6 we obtained a bolometric luminosity of $L_{BOL} \sim 3\,500\ L_{\odot}$ (similar to many PN central stars and MV Sgr) which is significantly less than the luminosity estimated for R CrB stars (Schönberner, 1986). V348 Sgr must also be physically much smaller than a typical R CrB star. In the scenario described above, this would have the affect of reducing the dust condensation distance from the photosphere. Thus, as the direction of dust ejection is less crucial (and the angular diameter of the star as seen from the dust cloud is smaller) the star may be expected to vary erratically.

Now consider the effect in physical appearance of cooling V348 Sgr to lower temperatures. Provided the thermal evolution time scale of the star is substantially longer than the recombination time scale of the nebula $\tau_{rec}(H^+) \sim 200$ years, see Chapter 5) then at 16 000 K, V348 Sgr would show a resemblance to MV Sgr, except the carbon absorption lines would be much stronger. The nebula would no longer be detectable at optical wavelengths. On further cooling to 14 000 K V348 Sgr may show a striking optical resemblance to DY Cen (depending on the hydrogen abundance). The situation in the IR is different as V348 Sgr is a strong source while DY Cen is not. Unless large quantities of cool dust are discovered around DY Cen, confusion between the two objects would not be likely.

On the strength of the evidence presented here it seems very *unlikely* that the class is homogeneous.

7.2 The evolutionary status of the individual stars

Although at first glance V348 Sgr and MV Sgr do not appear very similar, closer inspection shows that they do share many observational properties. Table 7.1 list all three stars and some important physical parameters.

Table 7.1: Physical parameters for suspected hot R CrB stars.

Star	Mass $M_\odot$	Luminosity $L_\odot$	IR Excess
DY Cen	0.75[a]	15 000[a]	weak
MV Sgr	0.6[b]	3 000[c]	strong
V348 Sgr	0.6[c]	3 500[d]	strong

[a]This thesis—Chapter 2

[b]From Jeffery *et al.* (1988)

[c]Using Jeffery (1988)

[d]This thesis—Chapter 6

Although it is difficult to quantify the associated errors attached to each of the parameters in Table 7.1, if we take the parameters at face value we may draw some important conclusions:

(i) DY Cen is more massive than the others,

(ii) DY Cen has a very low IR excess compared to the others, and

(iii) DY Cen has a significantly larger luminosity than the other two members, which have similar luminosities,

If we also assume that V348 Sgr and MV Sgr are both extremely hydrogen-deficient while DY Cen has appreciable quantities of hydrogen at its surface, then we can infer that V348 Sgr and MV Sgr are closely related and are in a similar evolutionary state, while for DY Cen the situation remains unresolved.

7.2.1 The final thermal pulse scenario of Renzini (1979, 1981)

Stars that have reached the white dwarf configuration may suffer a final thermal pulse bringing them back to cooler temperatures and higher luminosities (see Figure 7.1). The time scale for re-ignition of the helium-burning shell during the thermal pulse to reaching the red supergiant region is strongly dependent on the initial stellar mass. Thus stars with M $\sim$ 0.9 $M_{\odot}$ take only a few tens of years, while those with M $\sim$ 0.6 $M_{\odot}$ may take a few thousand years. Due to mixing processes occurring during the thermal pulse these objects are expected to show significant enhancement of *s-process* elements. However, the low excitation of the spectral lines from these elements means that they will only be observable in cool objects. U Aqr is a cool R CrB star that does show large enhancements of s-process elements in its photosphere (Bond *et al.* , 1979). Other classical R CrB stars that have been investigated in sufficient detail show normal metal abundances (Lambert, 1986).

If the derived positions of V348 Sgr and MV Sgr are plotted in the HR diagram (Figure 7.1) it can be seen that both stars lie close to the predicted Renzini's loop trajectory. The suggested thermal evolution timescale (Chapter 5) is also consistent with this scenario.

7.2.2 The confused evolutionary status of DY Cen

Older evolutionary theories required R CrB stars to evolve by contraction to become EHe stars somehow loosing their circumstellar shells along the way (EHe stars do not appear to have IR excesses—Drilling, 1984 and Walker, 1986). Due to the relatively short time scales involved it has proved difficult to understand the mechanism by which the shell is dissipated; DY Cen may be a key to our understanding of this. The derived position of DY Cen is also plotted on Figure 7.1 and as can be seen it appears to be closely related to both the R CrB and EHe stars. Indeed, we have already found the object to display observational qualities reminiscent of both groups.

At present we have no indication as to DY Cen's direction of evolution.

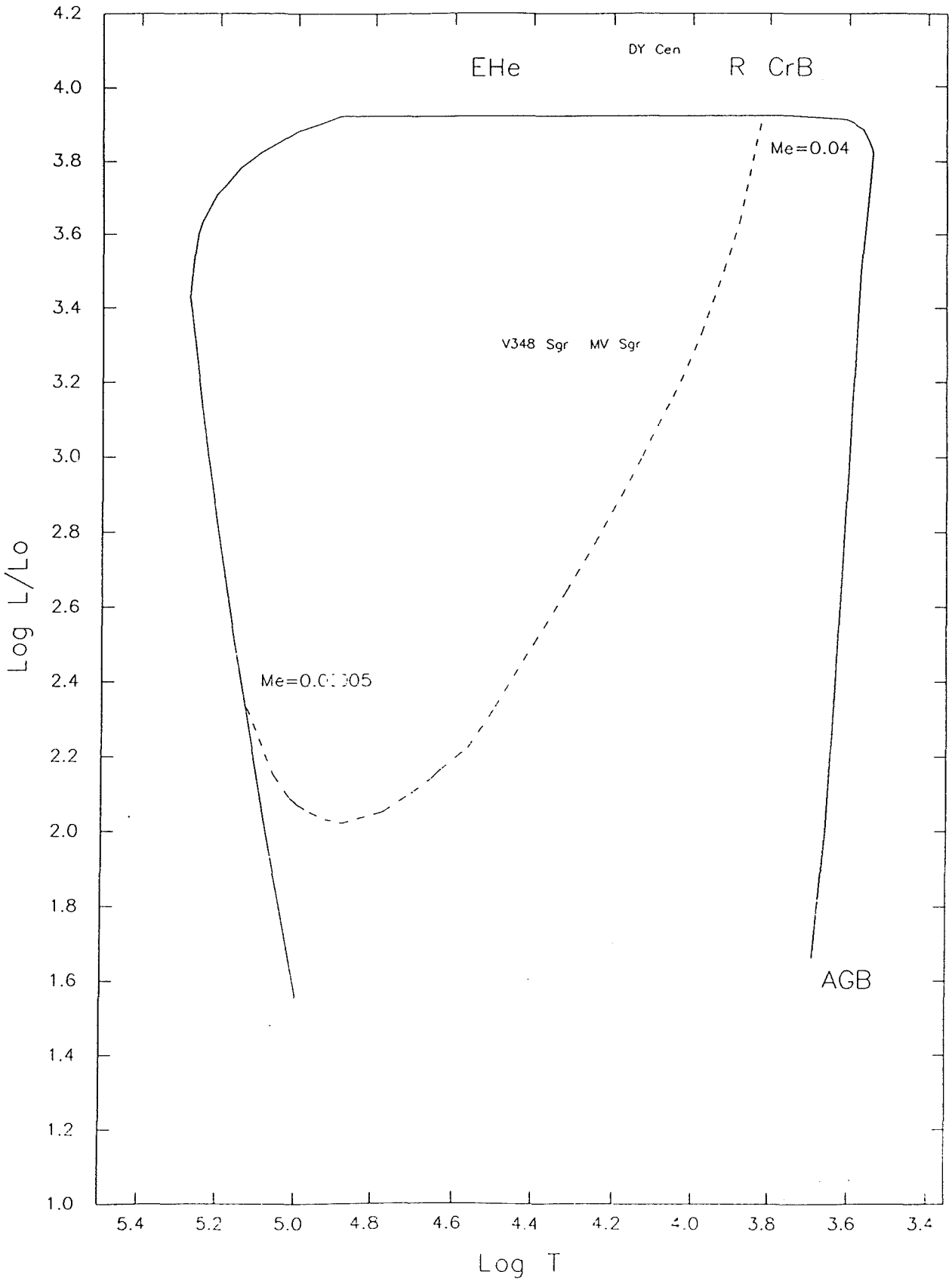

Figure 7.1: Evolution of 0.[illegible] $M_\odot$ star after the last thermal pulse. The positions of DY Cen, MV Sgr and V348 Sgr are marked.

7.2.3 Other evolutionary scenarios

In many ways the photometric behaviour of MV Sgr and DY Cen are similar to that observed in Be stars during the shell ejection phase (eg Underhill and Doazan, 1982). The self absorption in the metal lines observed in the wind/chromospheric spectra of MV Sgr (Jeffery *et al.* , 1988) is also similar to that observed in Be stars. In this case, these objects could simply represent the helium analogue of the classical Be stars.

Schönberner (1986) has studied the UV extinction in V348 Sgr and deduced that spectra taken of the object when bright require a dereddening by a circumstellar component of $E_{B-V} \sim 0.15$ in addition to the interstellar component of $E_{B-V} \sim 0.45$. However, by comparing the UV flux distribution (dereddened) with those produced from combinations of black bodies it is apparent that a 30 000 K object with low visual luminosity cannot be ruled out (see Figure 7.2).

To a certain extent it is possible to place constraints on the luminosity of any second body in the system. To excite the nebula it must have a surface temperature of $>$ 30 000 K. This places the object amongst the O-type stars. A main-sequence star of this type would dominate the visual and UV spectrum to a large extent and could not avoid detection in this system. However, these constraints may be reconciled if the nature of the secondary were a *sub-dwarf (sdO)*. These stars are underluminous for their temperature and its long UV and visual flux could be hidden by the flux from a luminous but relatively cool EHe star.

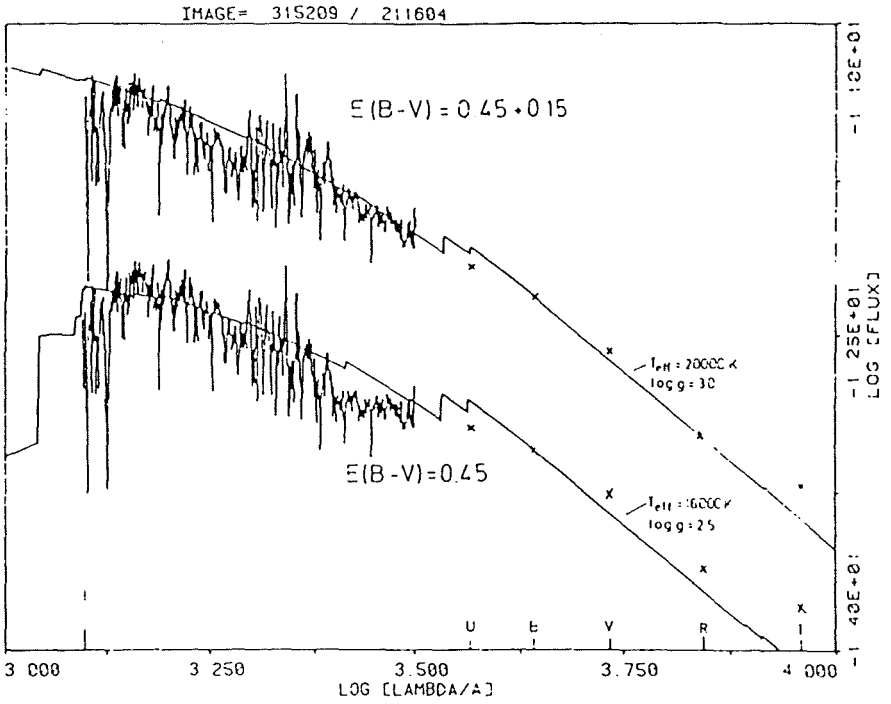

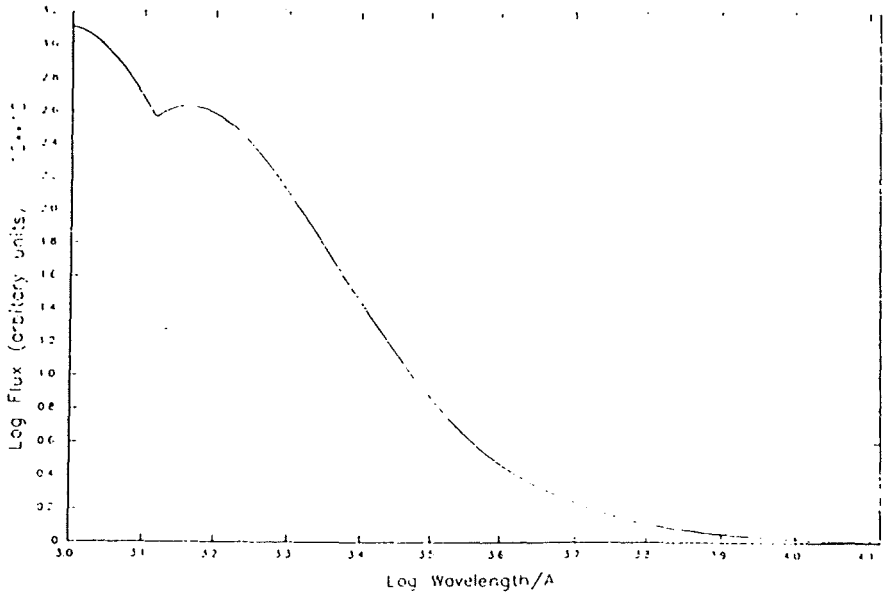

Figure 7.2: *Above*: the dereddened UV spectrum of V348 Sgr (from Schönberner and Heber, 1986), and *below*: 20 000 and 30 000 K black body distributions.

7.3 References

1. Bateson, F., 1978. *Pub. of the Variable Star Section R. astr. Soc. N. Zealand*, **6**, 39
2. Bateson, F. and Dodson, A.W., 1982. *Pub. of the Variable Star Section R. astr. Soc. N. Zealand*, **10**, 1
3. Bond, H.E., Luck, R.E. and Newman, M.J., 1979. *Astrophys. J.*, **233**, 205
4. Dahari, O. and Osterbrock, D.E., 1985. *Astrophys. J.*, 277, 648
5. Drilling, J.S., Landolt, A.U. and Schönberner, D., 1984. *Astrophys. J.*, **279**, 748
6. Fadeyev, Y.A., 1986. *In IAU Coll. No.* **87**, *Hydrogen-Deficient Stars and Related Objects*, p.441, eds. Hunger, K., Schönberner D. and Rao, N. Kameswara., Reidel
7. Feast, M.W. and Glass, I.S., 1973. *Mon. Not. R. astr. Soc.*, **161**, 293
8. Glass, I.S., 1978. *Mon. Not. R. astr. Soc.*, **185**, 23
9. Heber, U., Heck, A., Houziaux, L., Manfroid, J. and Schönberner, D., 1984. In *Proc. 4th European IUE Conf.*, Rome, Italy, p.367
10. Heck, A., Houziaux, L., Manfroid, J., Jones, D.H.P. and Andrews, P.J., 1985. *Astr. Astrophys. Suppl. Ser.*, **61**, 375
11. Hoffleit, D., 1930. *Harvard Bull.*, **874**, 1
12. Hoffleit, D., 1959. *Astronomical J.*, **64**, 241
13. Hoffleit, D., 1958. *Astronomical J.*, **63**, 78
14. Houziaux, L., 1968. *Bull. Astron. Inst. Czechoslowakia*, **19**, 265
15. Jeffery, C.S., 1988. *Mon. Not. R. astr. Soc.*, **235**, 1287
16. Jeffery, C.S., Heber, U., Hill, P.W. and Pollacco, D.L., 1987. *Mon. Not. R. astr. Soc.*, **226**, 317
17. Lambert, D.L., 1986. *In IAU Coll. No.* **87**, *Hydrogen-Deficient Stars and Related Objects*, p.127, eds. Hunger, K., Schönberner D. and Rao, N. Kameswara., Reidel
18. Pugach, A.F., 1977. *Inf. Bull. Variable Stars*, **1277**
19. Rao, N. Kameswara and Nandy, K., 1986. *Mon. Not. R. astr. Soc.*, **222**, 357

20. Renzini, A., 1979. In *Stars and Star Systems*, p.155, Ed. Westerlund, B.E. (Reidel)

21. Renzini, A., 1981. In *Effects of Mass loss on Stellar Evolution*, p.319, Eds. Chiosi, C. and Stalio, R. (Reidel)

22. Schönberner, D., 1986. *In IAU Coll. No.* **87**, *Hydrogen-Deficient Stars and Related Objects,* p.471, eds. Hunger, K., Schönberner D. and Rao, N. Kameswara., Reidel

23. Schönberner, D., and Heber, U., 1986. *In IAU Coll. No.* **87**, *Hydrogen-Deficient Stars and Related Objects,* p.217, eds. Hunger, K., Schönberner D. and Rao, N. Kameswara., Reidel

24. Underhill, A. and Doazan, V., 1982. In *B Stars With and Without Emission Lines*, p.342, NASA SP-456

25. Walker, H. J., 1986. *In IAU Coll. No.* **87**, *Hydrogen-Deficient Stars and Related Objects,* p.407, eds. Hunger, K., Schönberner D. and Rao, N. Kameswara., Reidel

26. Woods, I. E., 1928. *Harvard Bull.*, **838**

Chapter 8

Summary of results and recommended future work

8.1 DY Cen

From the new data presented in this thesis DY Cen was found to display small amplitude photometric variations with a period of around 3.8–5.5 days. An estimate of $(14\,000\pm1\dot{5}00)$ K was obtained for the stellar photospheric temperature by comparison with other EHe stars. Using these values a pulsational mass of M$\sim$ 0.71–0.78 $M_{\odot}$ was derived corresponding to a luminosity of L$\sim$ 13 000–18 000 $L_{\odot}$. These values are substantially higher than those found for the other hot R CrB stars (this thesis) implying that this object may belong on a different evolutionary sequence. The stellar spectra show weak hydrogen lines (which may be blended with those of other ionic species) and indicate an upper limit of $n_H / n_{He} \sim 0.9$. *Thus the hydrogen-deficient nature of this star has been established quantitatively for the first time.*

The heliocentric radial velocity of the star was found to be $(15.1\pm2.5)\,km\,s^{-1}$.

8.2 V348 Sgr

The nebula surrounding V348 Sgr has been shown to be similar in morphology to type 1 planetary nebulae. Thus the controversy over the nature of this nebula has been *established beyond doubt.* Herbig's *curious* neighbouring nebula has been found to be a distant spiral galaxy and therefore not physically related to the system as had been suspected by some workers.

Lower limits for the nebular abundances have been established. They demonstrate that the helium abundance (number ratio: He / H > 0.195) is *far higher* than previously thought. There is also substantial evidence of a *hydrogen abundance gradient* within the nebula. If the currently accepted value of the stellar surface temperature is correct then it is *not* possible for the star to ionize the nebula to the observed degree or extent. A black body temperature of $\sim 27\,000$ K is required for a satisfactory fit to the forbidden line fluxes. This leads to the exciting possibility that either one (or a combination) of the following may obtain.

(i) The star was recently (within the last few hundred years) much hotter.

(ii) There is an unseen, hotter second body in the system (the UV data do not rule out such a body).

(iii) During decline to minimum the surface temperature of V348 Sgr *increases.*

(iv) There is an excess flux at 24 eV causing the observed He ionization.

The distance to V348 Sgr was derived, using a *new* reddening distance technique (developed by the author), as (4.7±1.0) kpc implying $L_{BOL} \sim 3\,500\ L_{\odot}$. From this a mass of $M \sim 0.6\ M_{\odot}$ was obtained. The luminosity is typical of the central stars of many planetary nebulae. The BVI_{KC} reddening technique is *not* dependent on the sole use of early type stars as is the Q method of UBV phtometry. After more development the BVI_{KC} technique may become an important method of obtaining stellar distances for many different types of object.

8.3 Future work

In order to determine the relevance of Renzini's final thermal pulse model it is important to test its theoretical evolutionary implications against observationally derived constraints. As the evolutionary timescales involved are relatively short, variations in stellar parameters should be detectable over a period of years (depending on the stellar mass). There are several areas that require immediate attention.

- *Fine analyses of V348 Sgr and MV Sgr.* When using optical data, chromospheric contamination of photospheric absorption lines render abundance analysis unreliable in these objects. It is therefore desirable to obtain high resolution, good S/N UV spectra (with the Hubble Space Telescope) as the contamination in this part of the spectrum is known to be reduced (from IUE data). By fitting line profiles to the *wind lines* an estimate of the mass loss rates from these systems will also be possible. Any hotter companions will also be detectable.
- *Spectrophotometry of V348 Sgr during decline.* This will enable the stellar temperature to be determined at all points of the light curve.
- *Examination of MV Sgr and DY Cen for surrounding nebulae.* If Renzini's scenario is correct then it may still be possible to detect a recombining nebula around MV Sgr.
- *Long term monitoring of carbon lines in the spectra of V348 Sgr, MV Sgr and DY Cen.* If these objects are indeed closely related to classical R CrB stars then they are expected to eject clouds of carbon rich material on a timescale of days. Photometrically this can only be seen when the direction of ejection is orientated towards the observer and a minimum results. High resolution spectra of some carbon lines may enable individual *puffs* of material to be detected even when not in the line of sight. A recent high-resolution spectrum of V348 Sgr (Dr. C. S. Jeffery, private communication) has shown the C II λ4267Å line (which is in emission) to be composed of several components at different radial velocities. It is tempting to associate the separate components with individual puffs; however more observational material obtained on a daily basis is required to be certain. Observations of MV Sgr and DY Cen could also reveal variations in absorption

line profiles for the same reasons (these stars only show carbon absorption lines as they are substantially cooler than V348 Sgr).

- *Fine analysis of U Aqr.* As discussed in the previous section this star is the only known R CrB star to show a significant enhancement of s-process elements. It is important to obtain accurate abundances for these elements for comparison with envelope mixing mechanisms. A determination of the stellar mass is needed in order to confirm the validity of the final thermal pulse scenario for this object.

- *Dedicated short term photometric monitoring of V348 Sgr and MV Sgr.* It is important to look for pulsational instabilities in these objects. They are known to be variable over a short timescale but observations have not been thorough enough to determine periodicity. Detection of radial pulsation will enable accurate photometric masses to be deduced using the period-temperature law.

- *Fine analysis of DY Cen.* Our understanding of this object is severely affected by our ignorance of conditions and abundances within its photosphere. High resolution optical and low resolution UV data are required.

- *Long term photometric monitoring of DY Cen.* This may provide important evidence as to the evolutionary status of this star. Unfortunately the long time base required renders the object suitable for only amateur or automatic photometric telescopes.